DEVELOPMENT OF SURFACE PLASMON RESONANCE SPECTROSCOPY AS A BIOLOGICAL SENSOR

JARUPAT DISRATTAKIT

A THESIS SUBMITTED IN PARTIAL FULFILLMENT
OF THE REQUIREMENTS FOR
THE DEGREE OF MASTER OF SCIENCE (PHYSICS)
FACULTY OF GRADUATE STUDIES
MAHIDOL UNIVERSITY
2005

ISBN 974-04-6321-5
COPYRIGHT OF MAHIDOL UNIVERSITY

Thesis
Entitled

DEVELOPMENT OF SURFACE PLASMON RESONANCE SPECTROSCOPY AS A BIOLOGICAL SENSOR

……
Mr. Jarupat Disrattakit
Candidate

……
Assist. Prof. Toemsak Srikhirin,
Ph.D. (Polymer Science and Engineering)
Major-Advisor

……
Assist. Prof. Srisuda Varamit,
Ph.D. (Physics)
Co-Advisor

……
Assoc. Prof. Galayanee Doungchawee,
M.Sc. (Pathobiology)
Co-Advisor

……
Mr. Boonsong Sutapun,
Ph.D. (Electrical Engineering and Applied Physics)
Co-Advisor

……
Assoc. Prof. Rassmidara Hoonsawat,
Ph.D.
Dean
Faculty of Graduate Studies

……
Assist. Prof. Wannapong Triampo,
Ph.D. (Biophysics)
Chair
Master of Science Programme in Physics
Faculty of Science

Thesis
Entitled

DEVELOPMENT OF SURFACE PLASMON RESONANCE SPECTROSCOPY AS A BIOLOGICAL SENSOR

was submitted to the Faculty of Graduate Studies, Mahidol University
for the degree of Master of Science (Physics)
on
June 9, 2005

……
Mr. Jarupat Disrattakit
Candidate

……
Assist. Prof. Toemsak Srikhirin,
Ph.D. (Polymer Science and Engineering)
Chair

……
Assoc. Prof. Vijittra Leardkamolkarn,
Ph.D. (Cell Biology and Anatomy)
Member

……
Assist. Prof. Srisuda Varamit,
Ph.D. (Physics)
Member

……
Assoc. Prof. Galayanee Doungchawee,
M.Sc. (Pathobiology)
Member

……
Mr. Boonsong Sutapun,
Ph.D. (Electrical Engineering and Applied Physics)
Member

……
Assoc. Prof. Rassmidara Hoonsawat,
Ph.D.
Dean
Faculty of Graduate Studies
Mahidol University

……
Prof. Amaret Bhumiratana,
Ph.D. (Microbiology)
Dean
Faculty of Science
Mahidol University

ACKNOWLEDGEMENT

This thesis can been succeeded by the extensive support and assistance from my major advisor, Asst. Prof. Toemsak Srikhirin and my co-advisor, Assoc. Prof. Galayanee Doungchawee, Asst. Prof. Srisuda Varamit, and Lect. Boonsong Sutapun. I am grateful to them for their valuable advice and guidance on this research.

I wish to thank Lect.José H. Hodak for suggestion on an apparatus improves. Moreover, he counsels me about some statistical concepts.

I wish to thank Ms.Yodsoi Kanintronkul for advice on the test results analyze by using the clinical biostatistics.

I would like to thank the Electro-Optics Section, National Electronics and Computer Technology Center (NECTEC) for supporting a surface plasmon resonance spectroscope and financial about this research. Thank Mr.Ratthasart Amarit for programming on the Labview 6.0i program.

I would like to thank the Capability Building Unit in Nanoscience and Nanotechnology for supporting the atomic force microscope and office accessories. Thank Mr.Sompon Maneetoon for the mechanical working.

I would like to express my gratitude to everyone at the Department of Pathobiology who helped and taught me. They had the courtesy to prepare the antibody, antigen, and other chemicals that were applied to experiments.

Ultimately, I really appreciated to my family. I deeply thank my first and second elder sister who had a portion of thoughts on a research. I wish to thank especially Ms.Pranee Changkev for giving the time and ideas on everything. I am thankful for all the teachers who have taught me.

Jarupat Disrattakit

DEVELOPMENT OF SURFACE PLASMON RESONANCE SPECTROSCOPY AS A BIOLOGICAL SENSOR

JARUPAT DISRATTAKIT 4436203 SCPY/M

M.Sc. (PHYSICS)

THESIS ADVISOR : TOEMSAK SRIKHIRIN, Ph.D. (POLYMER SCIENCE AND ENGINEERING), SRISUDA VARAMIT, Ph.D. (PHYSICS), GALAYANEE DOUNGCHAWEE, M.Sc. (PATHOBIOLOGY), BOONSONG SUTAPUN, Ph.D. (ELECTRICAL ENGINEERING AND APPLIED PHYSICS)

ABSTRACT

Surface plasmon resonance (SPR) is an optical phenomenon where reflected light from a metal surface is diminished at a specific angle. SPR is a sensitive technique for detecting a change in refractive index and thickness of a sample. The main objective of this research work was to apply the SPR technique in determining the binding of leptospiral bacteria on a surface.

An experimentally developed biosensor model allowed attachment of specific anti-Leptospiral (*L. interrogans* serovar Canicola) antibodies to the sensor surface via electrostatic attraction (positively charged surface) and covalent binding. The unreacted sites were blocked by ethanolamine or bovine serum albumin to prevent a non-specific binding. It was found that the covalent binding is a more effective method for detecting the leptospiral bacteria.

KEY WORDS : SURFACE PLASMON RESONANCE / BIOSENSOR / LEPTOSPIRAL BATERIA

95 P. ISBN 974-04-6321-5

การพัฒนา surface plasmon resonance spectroscopy เป็นเครื่องมือตรวจวัดทางชีวภาพ (DEVELOPMENT OF SURFACE PLASMON RESONANCE SPECTROSCOPY AS A BIOLOGICAL SENSOR)

จารุภัทร ดิษรัฐกิจ 4436203 SCPY/M

วท.ม. (ฟิสิกส์)

คณะกรรมการควบคุมวิทยานิพนธ์ : เติมศักดิ์ ศรีคิรินทร์, Ph.D. (Polymer Science and Engineering), ศรีสุดา วรามิตร, Ph.D. (Physics), กัลลยานี ดวงฉวี, M.Sc. (Pathobiology), บุญส่ง สุตะพันธ์, Ph.D. (Electrical Engineering and Applied Physics)

บทคัดย่อ

Surface Plasmon Resonance (SPR) เป็นปรากฏการณ์เชิงแสง ซึ่งเกิดขึ้นเมื่อแสง ตกกระทบลงบนผิวของโลหะ ซึ่งไวต่อการเปลี่ยนแปลงของคุณสมบัติเชิงแสง และความหนาของฟิล์มบาง บนผิวทองที่เคลือบอยู่บนปริซึม ซึ่งทำจากแก้วชนิด BK7 ในงานวิจัยนี้ ได้ศึกษาความเป็นไปได้ของการประยุกต์ใช้ SPR ในงานตรวจวัดเชิงชีวภาพ (biosensing) และรูปแบบการเตรียมผิวสำหรับงานตรวจจับเชื้อแบคทีเรีย Leptospiral ด้วยเทคนิค SPR

งานวิจัยนี้ อาศัยเทคนิค surface plasmon resonance spectroscopy ในการตรวจวัดความเปลี่ยนแปลงของฟิล์มบาง บนผิวทอง ซึ่งประกอบชั้นของสารเคมี ที่ถูกเตรียมขึ้น 2 ลักษณะ คือ อาศัยพันธะโควาเลนซ์ และไม่อาศัยพันธะโควาเลนซ์ (อาศัยแรง Van der Waals) อาศัยเพื่อควบคุมการจัดเรียงตัวของชั้น antibody และผิวของตัวตรวจจับ ถูกทำให้มีความเจาะจงต่อเชื้อโรค (antigen) โดยใช้ ethanolamine หรือ bovine serum albumin ป้องกันการเกาะติดของสารอื่นที่ไม่ใช่คู่ของ antibody

จากผลการทดลองพบว่า หลังจากหยดส่วนของเชื้อเลปโตสไปรา (เซลล์ตาย) ที่ทำหน้าที่เป็น antigen ลงบนผิวของแผ่นตรวจจับ ซึ่งมีผิวที่เตรียมขึ้นในการจับ antibody ด้วยพันธะโควาเลนซ์ไว้ ตรวจพบความแตกต่างของสัญญาณ ซึ่งพิจารณาได้จากมุมที่ทำให้เกิดปรากฏการณ์ SPR มากกว่าผิวที่เตรียมโดยวิธีที่แตกต่าง ซึ่งเป็นแบบแรง ionic ในการยึด antibody

95 หน้า. ISBN 974-04-6321-5

CONTENTS

CONTENTS (cont.)

CONTENTS (cont.)

CONTENTS (cont.)

LIST OF TABLES

LIST OF FIGURES

LIST OF FIGURES (cont.)

LIST OF FIGURES (cont.)

LIST OF FIGURES (cont.)

LIST OF FIGURES (cont.)

LIST OF FIGURES (cont.)

LIST OF FIGURES (cont.)

CHAPTER I
INTRODUCTION

Biosensors are analytical devices that convert biological actions into detectable signals. The detection mechanism makes use of specific biological processes such as

- Enzymes for their substrates or other ligands,
- Antibodies for their antigens,
- Lectins for carbohydrates and
- Nucleic acids for their complementary sequences antibodies.

A biological reaction usually takes place in close contact with a signal transducer. The resulting signal is compared with a reference signal, the signal which is usually produced by a similar system without the biologically active material. The difference between these two signals, which optimally is proportional to the material being analyzed, is amplified, processed and displayed or recorded. The primary advantage of using biologically active molecules as part of a biosensor is due to their high specificity and high discriminatory power [1].

Optical biosensors (also called optodes) are currently generating a considerable interest, particularly with respect to the use of fiber optics and optoelectronic transducers. These allow a safe non-electrical remote sensing of materials in hazardous or sensitive environments. Surface plasmon resonance (SPR), is an optical biosensor technology, and highly versatile for measuring real-time binding of proteins of interest to the surface immobilized ligands. This technique has been widely explored in numerous applications [1, 2].

1.1 Surface Plasmon Resonance Spectroscopy

The introduction of commercial instruments, such as BIAcore, that are capable of measuring SPR and simplified the study of macromolecular interactions by providing a useful format at real time measurement with small analytical quantity of

material. Several SPR instruments are available, ranging from simple and inexpensive model to more sophisticated instruments with attendant robotics, optical interfaces and software. The simplest device, called a Spreeta chip, was developed by Texas Instruments [3]. It maintains an in formative Web Site with an interesting description of the physical basis of SPR. A more sophisticated instrument is the IBIS Biosensor by XanTec Instruments [4]. The IBIS Biosensor uses cuvettes, but it is also compatible with BIAcore sensor chips. Two instruments utilize cuvettes rather than chips. One is a programmable biosensor called Plasmon, which is manufactured by BioTul [5]. The other, Iasys, is an optical biosensor that uses a stirred cuvette [6].

For SPR spectroscopy, light is reflected from the internal surface of a prism that has been coated with a thin metal film (i.e., gold). At a specific angle of reflection, the incident light creates a resonant oscillation of electrons in the surface of the metal film (i.e., plasmon resonance). The SPR response is extremely sensitive to any change in the dielectric constant, that relate to reflective index of the medium adjacent to the gold surface of a sensor chip. Changes in the SPR signals are monitored by the angular changes where the reflected light is minima [2, 7].

1.2 *Leptospira* Bacteria and Background

Leptospira spp. is the causative agent of Leptospirosis, which is an acute febrile illness occurring as zoonosis. The organisms can spread via urine of reservoir animals into the environment. The sources of infection are variable wild and domestic animals, rodents, marsupials, cattle, dogs and digs [8]. Human usually acquires infection by pathogenic *Leptospira* via skin abrasion or cracks in the feet, especially when walking through contaminated water, and by penetrating into mucous membranes of the eyes, nose or mouth.

After incubation period (usually 7-12 days, with a range of 2-20 days) the leptospiral bacteria initiate septicaemic or leptospiraemic may follow by complete or apparent recovery (about 3-4 days). During this first stage which loots about 4-7 days, the patient develops a non specific flu like illness of varying severity [9].

After a few day periods, the fever seems and followed by immune or leptospiruric stage, which circulating antibodies. This may be detected and the organism may be isolated from urine. Nonspecific symptoms involved are fever,

headache, muscle pains, tenderness and sometimes with rigors, accompanied by nausea or with vomiting, conjunctiva suffusion, a transient skin and mucosal rash, photophobia and other signs of meningitis. At the time of onset it is not possible to clinically identify immediately whether mild, severe nor how severe illness would be used be for early diagnosis [9]. Diagnosis of the leptospirosis is made by detecting organism or antibodies in serum [8]. Following table shows some available diagnostic tools used:

Table 1.1 Variable of antigen and antibody based assays [9].

Implement	**Method**	**Period of detection**	**Results obtained**	**Sampling**
Antigen detection	Microscopy	1-10days (later)	Immediate	Single sample
	Culture	1-10 days	2-8 weeks	Single sample
	DNA techniques	1-10 days (later)	1-2 weeks	Single sample
	PCR	1-10 days (later)	Few days	Single sample
Antibody detection	Serology	>10 days	Few days	Paired samples 7-10 days apart

The most useful and definite diagnosis of leptospirosis is based on the detection of leptospires, either circulating in the blood or recovered by cultivation of blood, urine and cerebrospinal fluid specimens. However, detection of antibodies specific to leptospiral can be used as alternative diagnostic tool, but need longer time period of investigation [91].

1.3 Objective

- To develop biosensor for determining the presence of biological materials using antigen-antibody model and SPR spectroscopy.
- To evaluate the capability of laboratory prepared biosensor for detecting leptospiral organism in liquid medium.

CHAPTER II
SUEFACE PLASMON RESONANCE TECHNIQUE

2.1 Surface Plasmon Resonance

The surface plasmon resonance (SPR) is a quantum optical-electrical phenomenon arising from the interaction of light with a metal surface. Under certain conditions the energy carried by photons of light is transferred to packets of conduction electron gas, called plasmons (plasma oscillation in metal), on a metal's surface. Energy transfer occurs only at a specific resonance wavelength of light. That is, the wavelength where the quantum energy carried by the photons exactly equals the quantum energy level of the plasmons [10].

A plasma oscillation in metal is a collective longitudinal excitation of the conduction electron gas. The surface plasmons (SPs) is quantum of the plasma oscillations propagating along a metal surface that are changed by thin dielectric coatings [11] as shown in Figure 2.1.

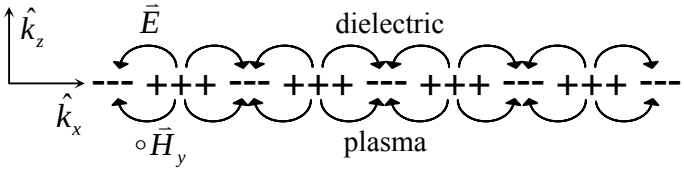

Figure 2.1 The charges and the electromagnetic filed of SPs propagating on a surface in the *x* direction are shown schematically. $\vec{H}_y$ shows the magnetic filed in the *y* direction of this *p*-polarized wave.

The choice of metal used is critical, since the metal must exhibit free electron behavior as described by the free electron model. Suitable metals include silver, gold, copper and aluminium of which silver and gold are more commonly used. Silver is used as it provides a sharp SPR resonance peak and gold due to its stability [12].

The SPs may be excited by passing an electron through a thin metallic film or by reflecting an electron or a photon from a film [13]. The resonance condition that permits energy transfer from photons to plasmons depends upon a quantum mechanical criterion related to the energy and momentum of the photons and plasmons. Both the energy and momentum of the photons must match exactly the energy and momentum of the plasmons. There are three general configurations of SPR devices that alter the momentum of photons in a way that fulfills the resonance criterion, namely,

-prisms,

-gratings and optical, and

-optical waveguide-based SPR system

as shown in Figure 2.2 [10].

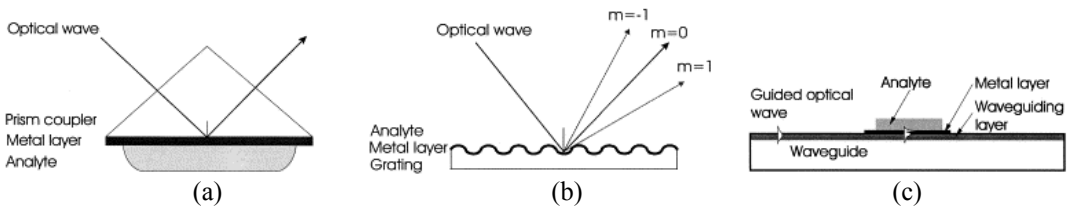

Figure 2.2 Most widely used configurations of SPR sensors: (a) prism coupler-based SPR system (attenuated total reflectance method), (b) grating coupler-based SPR system, (c) optical waveguide-based SPR system.

2.1.1 Attenuated Total Reflectance Configurations

The system of SPR can be applied in different configurations. In the Otto arrangement there is a distance between the metal and the total internal reflection (TIR) surface. The space is filled with a lower refractive index medium. This configuration is useful in the study of SPR in solid phase media [14] as shown in Figure 2.3.

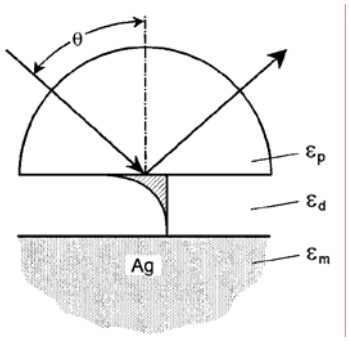

Figure 2.3 The Otto configuration is based on the total internal reflection of a plane wave incident at an angle θ at the base of a prism. The evanescent tail of this inhomogeneous wave can excite PSP states at an Ag-dielectric interface, provided the coupling gap is sufficiently narrow.

However since the distance between metal and TIR surface reduces the SPR efficiency, it is less useful for applications with solutions. In the Kretchmann configuration, the metal layer is directly on top of the TIR surface enabling a more efficient plasmon generation [15] as shown in Figure 2.4.

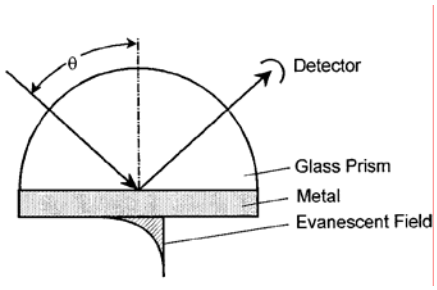

Figure 2.4 Attenuated total internal reflection (ATR) construct for PSP excitation in the Kretschmann geometry. A thin metal film ($d \approx 50$ nm) is evaporated onto the base of the prism and acts as a resonator driven by the photon field incident at an angle θ.

2.1.2 Analysis of Surface Plasmon Resonance Spectroscopy

The practical and commonly used method by which to excite surface plasmon was initially investigated by Kretschmann and Raether [16]. In the Kretschmann configuration, the incident light, wavelength λ, falls on through a prism under total reflection condition and onto a metal film evaporated onto the base of the prism. The SPR system is composed of a prism, a gold film and a sample. The

sequences of the optical media from prism to buffer are denoted by medium 1, 2, 3, 4 and 5. The symbols *x* and *z* are the directions of the coordinate system for the optical system as shown in Figure 2.5.

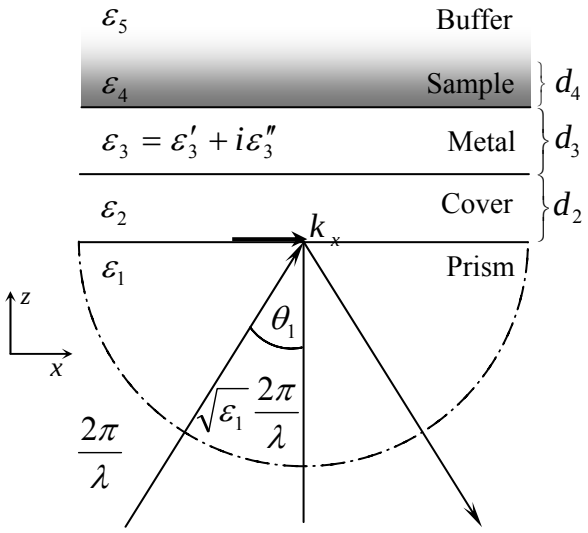

Figure 2.5 In Kretschmann configuration, the light is reflected at a metal surface (ε_3). The medium below the metal is a dielectric medium (ε_1) as glass or quartz; above the metal are the sample (ε_4) and the buffer (ε_5).

2.1.2.1 Principle of SPR Spectroscopy

When a beam of light passes from material with a high refractive index (e.g. glass) into material with a low refractive index (e.g. water) some light is reflected from the interface. When the angle at which the light strikes the interface (the angle of incidence or θ_0) is greater than the critical angle (θ_c), the light is completely reflected (total internal reflection). Although the fully reflected beam does not lose any net energy across the TIR interface, the light beam leaks an electrical field intensity called an evanescent field wave into the low refractive index medium. The amplitude of this evanescent field wave decreases exponentially with distance from the interface, decaying over a distance of about one light wavelength from the surface (Figure 2.4). The wave vector of the evanescent field or incident light in the interface surface direction (k_x) is given by

$$k_x = \frac{2\pi}{\lambda}\sqrt{\varepsilon_1}\sin\theta_0 \tag{2.1}$$

where λ is the wave length of incident light, ε_1 is dielectric constant of prism (glass). If the surface of the glass is coated with a thin film of a noble metal (e.g. gold), this reflection is not total; some of the light is lost into the metallic film. There is a second angle greater than the critical angle at which this loss is greatest and at which the intensity of reflected light reaches a minimum or dip. This angle is called the surface plasmon resonance angle (θ_{SPR}). It is a consequence of the oscillation of mobile electrons (or plasma) at the surface of the metal film. These oscillating plasma waves are called surface plasmons (SP). The wave vecetor of the surface plasmons is be approximated to

$$k_{SP} = \frac{2\pi}{\lambda}\left(\frac{\varepsilon_3'\varepsilon_4}{\varepsilon_3' + \varepsilon_4}\right)^{1/2} \tag{2.2}$$

where ε_3' is the real part of dielectric constant of the metal film and ε_4 is the dielectric constant of sample layer.

When the wave vector of the incident light matches the wave vector of the surface plasmons, the electrons resonate, hence the term surface plasmon resonance. The coupling of the incident light to the surface plasmons results in a loss of energy which causes a reduction in the intensity of the reflected light. It is because the amplitude of the wave vector in the plane of the metallic film depends on the angle at which it strikes the interface that an θ_{SPR} is observed [17].

$$k_x = k_{sp}$$

$$\sqrt{\varepsilon_1}\sin\theta_{SPR} = \sqrt{\frac{\varepsilon_3'\varepsilon_4}{\varepsilon_3' + \varepsilon_4}} \tag{2.3}$$

The efficiency of SPR spectroscopy is limited by the evanescent wave. In TIR, the reflected photons create an electric field on the opposite site of the interface. The plasmons create a comparable field that extends into the medium on either side of the film. This field is called the evanescent wave because it decays with distance.

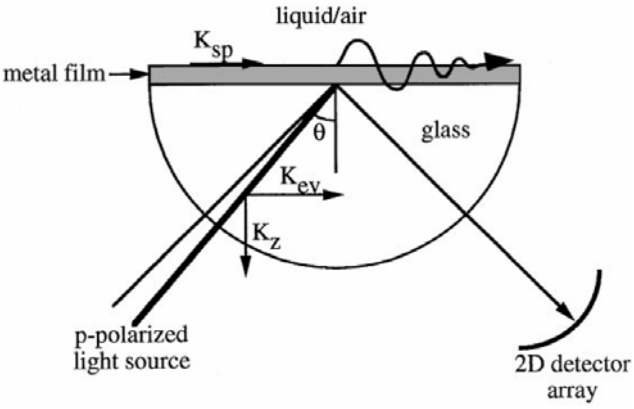

Figure 2.6 The Kretchmann configuration for SPR: resonance of a surface plasmon is excited at the metal/air interface when the angle of incidence of light is such that the evanescent component of its wave vector (k_{ev}) is equal to the wave vector of the propagating surface plasmon (k_{sp}) [12].

Equations, which describe how electric fields travel through a medium, include a term for the properties of the medium as shown in Table 2.1. For light, this term is the refractive index. The light is seen as refracted because the photons have a different velocity in different media [14].

Table 2.1 Formulae of property of evanescent wave (see detail in Chapter III).

Quantities	Formulae
Decay length	$l = \frac{1}{2k_x''} = \frac{c}{\omega}\left(\frac{\varepsilon_3'\varepsilon_4}{\varepsilon_3' + \varepsilon_4}\right)^{-3/2} \frac{\varepsilon_3'^2}{\varepsilon_3''}$ (2.4)
Skin depth	
in the metal with ε_1	$\hat{z}_1 \approx \frac{c}{\omega}\left(\frac{\varepsilon_3' + \varepsilon_4}{\varepsilon_3^2}\right)^{1/2}$ (2.5)
in the medium with ε_2	$\hat{z}_2 \approx \frac{c}{\omega}\left(\frac{\varepsilon_3' + \varepsilon_4}{\varepsilon_4^2}\right)^{1/2}$ (2.6)

In the same way the velocity (and therefore the wave vector) of the plasmons is changed when the composition of the medium changes. Because of the change in wave vector, that related to momentum, the angle of incident light at which

the resonance changes. This can be measured very precise. On the other hand, at a fixed angle of incident light, the wavelength can be varied until resonance occurs.

2.1.2.2. Limitation of Surface Plasmon Resonance Spectroscopy

The system, which consists of the layers of prism, metal, and dielectric, is presented in Figure 2.6. The efficiency is limited by the range of evanescent wave, as shown in Table 2.2,

Table 2.2 For 632.8 nm of wavelength, gold surface (dielectric constant is -10.9318+ 1.46075i, thickness = 50 nm), prism is Schott glass type BK7 (dielectric constant is 2.2955).

	Air	Water	Ethanol
Reflective index	1.000	1.333	1.362
Decay Length (um)	7.135	2.666	2.467
Skin depth (nm)			
In Sample layer (nm)	317.395	171.496	163.568
In metal layer (nm)	29.034	27.876	27.756
SPR Angle (Degrees)	44.0029	73.2405	78.4183

2.2 Surface Plasmon Resonance Analytical Application

The phenomenon of SPR is completely non-specific. It cannot distinguish various chemical changes. This appears to be a limitation, but it is really a powerful advantage. Specificity depends upon selection of pairs of molecules which react to each other. One of the pair is called detector and the other is the target to be analyzed or detected. Any complementary pair of interested molecules which having specific binding such as and antibody, a DNA probe and complementary strand, an enzyme and substrate, oil and gas or liquid phase that is soluble in the oil, and chelating agent and metal ion.

SPR can be modified into a sensor for both qualitative and quantitative measurement with high sensitivity toward a broad spectrum of chemical and biological entities. It offers a number of important practical advantages over current analytical techniques. The procedure time required varies with the specific chemistry

but can be as short as 5 minutes. In most cases, there is no need to pretreat the sample before applying onto the sensor. A single sensor format (i.e. size, storage and protocol, reader, etc.) may be applicable for a variety of assay system including immunological, nucleic acid binding, enzymatic, chemical, and gas adsorption. Some of the potential areas of application include medical diagnostics, environmental monitoring, agriculture pesticide and antibiotic monitoring, food additive testing, military and civilian airborne biological and chemical agent testing, and real time chemical and biological production process monitoring [10].

2.2.1. Situations Suit Surface Plasmon Resonance Technique

2.2.1.1. Estimation of Macromolecules

Most laboratories studying biological problems at the molecular or cellular level dialed with recombinant proteins. The structure of the recombinant protein had been found compatible to its native counterpart. Except enzymes that involve multiple residues in their interaction with the natural ligands. Of which the primary amino acid sequence require a correctly folded protein without natural ligands. The monoclonal antibodies are developed specifically to bind to the most native proteins as an excellent means in assessment of the structural integrity of some recombinant protein [17].

2.2.1.2. Adsorption Kinetics Measurements

Chemical kinetics is the study of the rates of chemical reactions, the factors that interferes reaction rates and mechanisms. Rates of reactions are usually expressed in units of moles per liter per unit time. If we know the chemical equation of a reaction, its rate can be determined quantitatively, according to the change of concentration of any product or reactant involving [18]. This change is measured continuously to form a sensorgram, which provides a complete record of the progress of association or dissociation of the reactants.

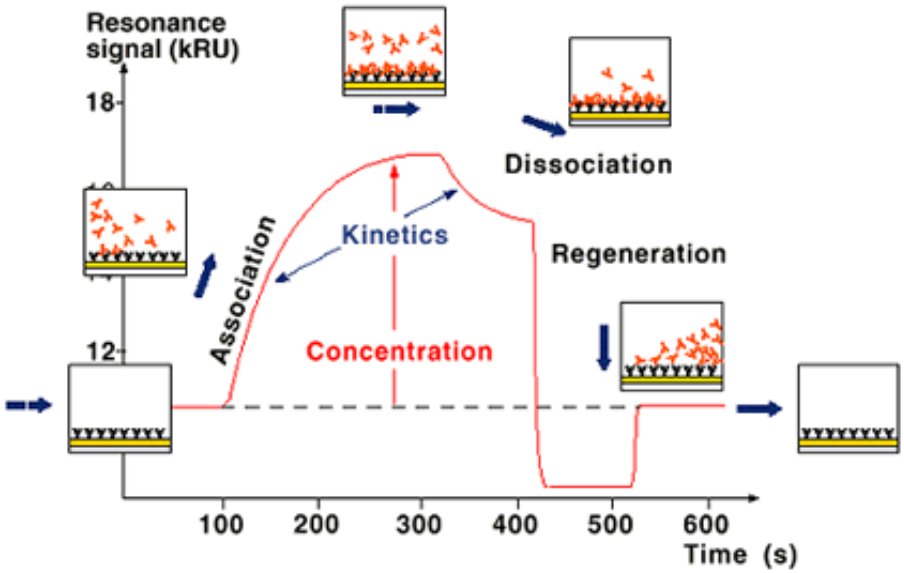

Figure 2.7 The progress of an interaction is monitored as a sensorgram. Analyte binds to the surface-attached ligand during sample injection, resulting in an increase in signal. At the end of the injection, the sample is replaced by a continuous flow of buffer and the decrease in signal now reflects dissociation of interaction from the surface-bound complex.

When molecules in the test solution bind to a target molecule the mass increases, when they dissociate the mass falls. This simple principle forms the basis of the sensorgram - a continuous, real-time monitoring of the association and dissociation of the interacting molecules (see Figure 2.7). The sensorgram provides quantitative information in real-time on specificity of binding, active concentration of molecule in a sample, kinetics and affinity. The change is quantified in resonance units or response units (RUs).

Table 2.3 Comparison of SPR units in resonance unit (RU) and other units.

SPR Angle shift [17]	1 RU = 10^{-4} Degrees
Surface concentration (Empirical measurements) [19]	1 RU = 10^{-12} g/mm^2

As the concentrations of reactants change at constant temperature, the rate of reaction depends on concentrations. The reaction rate is given by followings:

$$\text{Reaction rate} = \underbrace{\text{Number of collisions per unit time}}_{\substack{\text{This factor depends on reactant concen - tration and so can be manipulated. When concentration increases, so does this factor.}}} \times \underbrace{\text{Fraction of collisions with energy equal to or greater than activation energy } (E_a) \times \text{Fraction of collisions in which molecules have proper orientation}}_{\text{These factors are inherent. They depend on bond strength and molecular shape (not on concentration).}}$$

Chemists like to simplify equations. In that case, we symbolize the two inherent factors

$$K = \text{Fraction of collisions with energy equal to or greater than } E_a \times \text{Fraction of collisions in which molecules have proper orientation} \qquad (2.7)$$

The K is called the rate constant for a reaction. Each reaction has its own value of K. If K is large, the reaction is fast. If K is small, the reaction is slow. The value of K depends on both the E_a value of a reaction and the shapes (orientations) of the reactant molecules [20].

In any chemical reaction at a fixed temperature, the number of collisions per unit time is proportional to the product of the concentration of the reactants, each concentration value raised to some power (exponent) called an order. For the general reaction $A+B \rightarrow P$, we express this relationship in the form

$$\text{Reaction rate} = K[A]^x[B]^y \qquad (2.8)$$

The powers to which the concentrations are raised, x and y, are usually small integers or zero but are occasionally fractional or even negative. A power of one means the rate is directly proportional to the concentration of which reactant. A power of two means the rate is directly proportional to the square of that concentration. A power of zero means that the rate does not depend on the concentration of which reactant, so long as some of the reactant is present. The overall of the reaction is $x+y$. The units of K depend on the overall order of the reaction.

For the application of SPR as biosensor, the kinetics of binding of the ligate solution (*A*) to the free ligand (*B*) may be followed by monitoring the time dependence of the SPR signal, denoted by *R*, which typically the shift in resonance angle. The system normally allowed to reach equilibrium, which is denoted by the plateau in the sensorgram. The equilibrium constant for formation of the ligate-ligand complex (*AB*) can be measured directly from data of the type displayed in the sensorgram (see Figure 2.7). Consider the equilibrium

$$A+B \rightleftharpoons AB$$

$$K_{eq} = \frac{K_{on}}{K_{off}} = \frac{[AB]_{eq}}{[A]_{eq}[B]_{eq}} \quad \text{only at equilibrium.} \qquad (2.9)$$

Where K_{on} and K_{off} are the rate constants for formation and dissociation of the ligate-ligand complex, and K_{eq} is the equilibrium constant for formation of the ligate-ligand complex. It follows that

$$\frac{\mathrm{d}[AB]}{\mathrm{d}t} = K_{on}[A][B] - K_{off}[AB] \qquad (2.10)$$

where the brackets [ ] are read as concentration. The maximum change in SPR angle (R_{max}) is proportional to the total ligand concentration ([*B*]+[*AB*]), R_{max}-*R* is proportional to the free ligand concentration [*B*] and [*A*] may be considered as a constant (a_0) since the free ligate is constantly replenished under flow condition [12]. We can also write [*B*]=b_0-[*AB*] from mass-balance considerations, where b_0 is the total concentration of ligand. Finally, the SPR signal is often observed to be proportional to [*AB*]. The maximum value that *R* can have is $R_{max} \propto b_0$, which would be measured if all ligand molecules were adsorbed onto the free ligate. We may then write

$$\frac{\mathrm{d}R}{\mathrm{d}t} = K_{on}a_0(R_{\max} - R) - K_{off}R$$

$$= k_{on}a_0R_{\max} - (K_{on}a_0 + K_{off})R \qquad (2.11)$$

Rate constants are then determined by plotting d*R*/d*t* vs.*R* for a range of ligate concentrations. The gradient of each concentration plot (k_s) is then plotted against the ligate concentration (a_0) to produce a straight line where $-k_s=K_{on}a_0-K_{off}$. From this graph, K_{on} is the gradient and K_{off} the y-axis intercept. A more accurate measurement of the dissociation constant can be determined if the bound [*AB*] complex is in a

buffer only solution, where the concentration of analyte in solution falls to zero and the Equation (2.11) can be simplified to $dR/dt=-K_{off}R$. The affinity constant can then be calculated as K_{on}/K_{off} [21, 22].

At equilibrium $R=R_{eq}$ and $dR/dt=0$. It follows that (after some algebra)

$$R_{eq} = R_{\max}\left(\frac{a_0 K_{eq}}{a_0 K_{eq} + 1}\right) \qquad (2.12)$$

Hence, the value of K_{eq} can be obtained from measurements of R_{eq} for a series of a_0 [20].

2.2.2. Limitation of Surface Plasmon Resonance Technique

2.2.2.1. Concentration Assays

The SPR technique is not appropriate for concentration measurements, because it requires the analysis of various participating factors samples in parallel, including the standard curve. A second problem is that, for optimal sensitivity, the concentration assays require long equilibration periods [17].

2.3 Resources by SPR Technique

Table 2.4 List of the SPR application

Mode of Studies	Application
Gas-sensing	chemical vapour interaction with fluouopolymer [27]
Gas-sensing	exposed a silicon-glycol copolymer by the anaesthetic gas halothane [32]
Gas-sensing	gas-adsorbing organic materials on a polyethylene glycohol thin film [28]
Gas-sensing	gas detection experiment involved two gases on the top of the Au:SiO2 films [29]
Gas-sensing	interaction of gas with polyaniline Langmuir-Blodgett films [25]

Filed of Studies	Application
Gas-sensing	remote sensing of tetrachloroethene with a micro-fiber optical gas sensor [24]
Biosensor	analyze sequential biomolecular recognition events [36-38]
Biosensor	characterized phospholipid bilayers [48]
Biosensor	degration and hydration properties of polymeric interfaces [49-52]
Biosensor	determination of kinetic rate constants of ligand-binding events [39]
Biosensor	determined isotype mesurements of 10 monoclonal antibodies comparing SPR with enzyme-linked immunoassays (ELISA) [45]
Biosensor	determine the conformational states of the viruses [42]
Biosensor	estrogen receptor-alpha interaction with DNA [33]
Biosensor	interaction between biotin and avidin or streptavidin [40, 41]
Biosensor	interaction of transforming growth factor-alpha with the epiaction growth factor extracellular domain [34]
Biosensor	a adsorption of albumin and IgG to SAM-modified silver and gold [46, 47]
Biosensor	kinetic of assembly and dissociation of human leucocyte antigen (HLA) class I hetertrmeric complex [35]
Biosensor	measurement the affinity kinetics of a monoclonal antibody binding to tobacco mosaic virus and related peptides [43]
Biosensor	measurement the antigen binding and domain interactions of recombinant anti-Z-DNA [44]
Biosensor	quantification of human IgE [31]
Biosensor	streptavidin arrays as supramolecular architectures [26]
Solid	determination of a function of doping and temperature of high temperature superconductors (HTSC) [30]

CHAPTER III
SURFACE PLASMON RESONANCE THEORY

3.1 Mathematical Treatment

The practical and commonly used method by which to excite surface plasmon was initially investigated by Kretschmann and Raether. In the Kretschmann configuration, the incident light falls on through a prism under total reflection condition and onto a metal film evaporated onto the base of the prism. The SPR system is composed of a prism, a gold film and a sample. The sequences of the optical media from prism to buffer are denoted by medium 1, 2, 3, 4 and 5. The symbols *x* and *z* are the directions of the coordinate system for the optical system as shown in Figure 3.1.

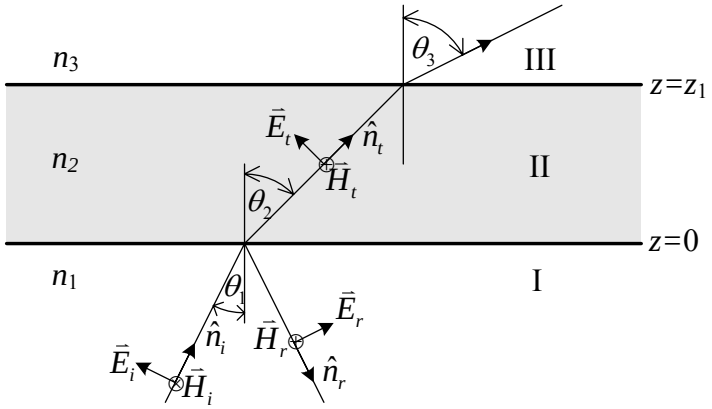

Figure 3.1 Propagation of an electromagnetic wave through a homogeneous film.

3.1.1 Maxwell's Equations

In general, electric and magnetic fields are vector quantities that have both magnitude and direction. The relations and variations of the electric and magnetic fields, charges, and current associated with electromagnetic waves are governed by physical laws, which are known as Maxwell's equations. These equations, as we have indicated, were arrived at mostly through various experiments carried out by different

investigations, but they were put in their final form by James Clerk Maxwell, a Scottish physicist and mathematician.

Maxwell's equations in differential and integral form are summarized and listed in Table 3.1 [53, 54].

Table 3.1 Maxwell's equations and the continuity equation in differential and integral forms for time-varying fields

Meaning	Integral form	Differential form
Faraday's induction law: time-varying magnetic fileds generate an electric field	$\oint_C \vec{E} \cdot d\vec{l} = -\iint_S \vec{M}_i \cdot d\vec{s} - \frac{\partial}{\partial t}\iint_S \vec{B} \cdot d\vec{s}$	$\nabla \times \vec{E} = -\vec{M}_i - \frac{\partial \vec{B}}{\partial t}$ (3.1a)
Ampere's law with Maxwell's supplement : time-varying electric fields generate a magnetic field	$\oint_C \vec{H} \cdot d\vec{l} = \iint_S \vec{J}_i \cdot d\vec{s} + \iint_S \vec{J}_c \cdot d\vec{s} + \frac{\partial}{\partial t}\iint_S \vec{D} \cdot d\vec{s}$	$\nabla \times \vec{H} = \vec{J}_i + \vec{J}_c + \frac{\partial D}{\partial t}$ (3.1b)
displacement flux through surface equals the enclosed electric charge	$\oiint_S \vec{D} \cdot d\vec{s} = q_e$	$\nabla \cdot \vec{D} = \rho_{ev}$ (3.1c)
solenoidality of magnetic field	$\oiint_S \vec{B} \cdot d\vec{s} = q_m$	$\nabla \cdot \vec{B} = \rho_{mv}$ (3.1d)

The definitions and units of the quantities are

$\vec{E}$ = electric field intensity (volts / meter)

$\vec{H}$ = magnetic field intensity (amperes / meter)

$\vec{D}$ = electric flux density (coulombs / square meter)

$\vec{B}$ = magnetic flux density (webers / square meter)

$\vec{J}_i$ = impressed (source) electric current density (amperes / square meter)

$\vec{J}_c$ = conduction electric current density (amperes / square meter)

$\vec{M}_i$ = impressed (source) magnetic current density (volts / square meter)

ρ_{ev} = electric charge density (coulombs / cubic meter)

ρ_{mv} = magnetic charge density (webers / cubic meter)

q_e = total electric charge (coulombs)

q_m = total magnetic charge (webers)

Materials contain charged particles. When these materials are subjected to electromagnetic fields, their charged particles interact with the electromagnetic field vectors, producing currents and modifying the electromagnetic wave propagation in these media (compared to that in free space). Maxwell's equations must be supplemented by relations, which describe the behavior of these charged particles under the influence of the field. These relations are known as constitutive relations (or material equations), which characterized by the conductivity σ (mhos / meter or siemens / meter), the permittivity of the material ε (farads / meter), the permeability of the material μ (henrys / meter)

$$\vec{D} = \varepsilon\vec{E} = \varepsilon_0\vec{E} + \vec{P} \tag{3.2}$$

where ε_0 is the permittivity of free space, $\varepsilon_0 = 8.854\times10^{-12} \approx 10^{-9}/36\pi$ F/m, ε_r is called the relative permittivity or dielectric constant, defined in $\varepsilon_r = \varepsilon/\varepsilon_0$, and $\vec{P}$ is polarization (coulombs / meter square)

$$\vec{B} = \mu\vec{H} = \mu_0(\vec{H} + \vec{M}) \tag{3.3}$$

where μ_0 is the permeability of free space, $\mu_0 = 4\pi\times10^{-7}$ H/m, μ_r is the relative permeability of the material, and $\vec{M}$ is the magnetization (amperes / meter)

$$\vec{J}_c = \sigma\vec{E} + \rho_{ev}\vec{u} \tag{3.4}$$

where $\vec{u}$ is a velocity of charge, of density ρ_{ev}.

3.1.2 Wave Vector of Surface Plasmons

The coupling surface plasmon with photon is concerned with the excitation of plasmon surface polaritons (PSPs) at the interface between a noble metal and a dielectric medium. A polariton is known as the quantum of the coupled phonon-photon transverse wave field. The free electron gas in the metal acts as a resonator driven by the incoming photon field, giving rise to substantial intensity enhancements compared to the mere dielectric configuration of Figure 3.1 [15].

To consider an interface in the xy-plane between two half-infinite spaces, 1 and 2, of materials the optical properties of which are described by their complex frequency-dependent dielectric functions $\tilde{\varepsilon}_{r1}(\omega)$ and $\tilde{\varepsilon}_{r2}(\omega)$, respectively, with non-magnetic materials [55, 56]. Surface polaritons can only be excited at such an interface by transversal magnetic (TM- or p-polarized) modes because the surface charge induce the discontinuity of the electric field in the surface normal *z*-direction. Transversal electric (TE- or s-polarized) waves propagating along the *x*-direction possess only electric field components, parallel to the surface (y-direction), i.e. TE waves have $\vec{E} = (0, \vec{E}_y, 0)$, and hence are unable to excite surface polaritons. Only p-polarized light with $\vec{E} = (\vec{E}_x, 0, \vec{E}_z)$, or, equivalently, $\vec{H} = (0, \vec{H}_y, 0)$, can couple to such modes [57]. The electric and magnetic field in medium 1 (air, $z > 0$) are given by

$$\vec{E}_1 = (E_{x1}\hat{a}_x + E_{z1}\hat{a}_z)e^{i(k_{x1}x + k_{z1}z - \omega t)} \tag{3.5a}$$

$$\vec{H}_1 = H_{y1}e^{i(k_{x1}x + k_{z1}z - \omega t)}\hat{a}_y \tag{3.5b}$$

and medium 2 (metal, $z < 0$)

$$\vec{E}_2 = (E_{x2}\hat{a}_x + E_{z2}\hat{a}_z)e^{i(k_{x2}x - k_{z2}z - \omega t)} \tag{3.6a}$$

$$\vec{H}_2 = H_{y2}e^{i(k_{x2}x - k_{z2}z - \omega t)}\hat{a}_y \tag{3.6b}$$

Since the tangential component of electric field must be continuous at the interface ($z = 0$). The only way this boundary condition will be satisfied by the waves in equations (3.5) and (3.6) for all x-direction is that

$$k_{x1} = k_{x2} = k_x \tag{3.7}$$

From this condition, we can get

$$E_{x1} = E_{x2} \tag{3.8}$$

$$E_{z1} = E_{z2} \tag{3.9}$$

$$H_{y1} = H_{y2} \tag{3.10}$$

From equation (3.1b) with no impressed electric current, $\vec{J}_c \approx 0$, and constitutive relations

$$\nabla \times \vec{H} = \frac{\partial \vec{D}}{\partial t}$$

$$\begin{vmatrix} \hat{a}_x & \hat{a}_y & \hat{a}_z \\ \dfrac{\partial}{\partial x} & \dfrac{\partial}{\partial y} & \dfrac{\partial}{\partial z} \\ 0 & H_y & 0 \end{vmatrix} = \varepsilon_0 \tilde{\varepsilon}_r \frac{\partial \vec{E}}{\partial t}$$

$$-\frac{\partial H_y}{\partial z}\hat{a}_x + \frac{\partial H_y}{\partial x}\hat{a}_z = -i\omega\varepsilon_0 \tilde{\varepsilon}_r \vec{E} \tag{3.11}$$

Consider the x-direction of the above equation

$$ik_{z1}H_{y1} = i\omega\varepsilon_0 \tilde{\varepsilon}_{r1} E_{x1} \tag{3.12}$$

$$ik_{z2}H_{y2} = -i\omega\varepsilon_0 \tilde{\varepsilon}_{r2} E_{x2} \tag{3.13}$$

From equation (3.8) give

$$\frac{k_{z1}H_{y1}}{\omega\varepsilon_0 \tilde{\varepsilon}_{r1}} = -\frac{k_{z2}H_{y2}}{\omega\varepsilon_0 \tilde{\varepsilon}_{r2}}$$

and equation (3.10) give

$$\frac{k_{z1}}{\tilde{\varepsilon}_{r1}} = -\frac{k_{z2}}{\tilde{\varepsilon}_{r2}} \tag{3.14}$$

From Equations $k = 2\pi/\lambda = \omega/v = n\omega/c$, and $\tilde{n} \approx \sqrt{\tilde{\varepsilon}_r}$, where $\tilde{n}$ is complex refractive index.

$$k^2 = k_x^2 + k_{zi}^2 = \tilde{\varepsilon}_{ri}\left(\frac{\omega}{c}\right)^2$$

$$k_{x1}^2 = \tilde{\varepsilon}_{r1}\left(\frac{\omega}{c}\right)^2 - k_{z1}^2 \tag{3.15}$$

$$k_{x2}^2 = \tilde{\varepsilon}_{r2}\left(\frac{\omega}{c}\right)^2 - k_{z2}^2 \tag{3.16}$$

From equation (3.7), (3.14), and (3.16) give

$$k_{x2}^2 = k_x^2 = \tilde{\varepsilon}_2\left(\frac{\omega}{c}\right)^2 - \left(-\frac{\tilde{\varepsilon}_2}{\tilde{\varepsilon}_1}k_{z1}\right)^2 \tag{3.17}$$

Substitute equation (3.17) into equation (3.15)

$$k_{x1}^2 = k_x^2 = \tilde{\varepsilon}_2\left(\frac{\omega}{c}\right)^2 - \left(\frac{\tilde{\varepsilon}_2}{\tilde{\varepsilon}_1}\right)^2\left(\tilde{\varepsilon}_1\left(\frac{\omega}{c}\right)^2 - k_x^2\right)$$

$$k_x^2(\tilde{\varepsilon}_1^2 - \tilde{\varepsilon}_2^2) = \left(\frac{\omega}{c}\right)^2 \tilde{\varepsilon}_1\tilde{\varepsilon}_2(\tilde{\varepsilon}_1 - \tilde{\varepsilon}_2)$$

$$k_x^2 = \left(\frac{\omega}{c}\right)^2\left(\frac{\tilde{\varepsilon}_1\tilde{\varepsilon}_2}{\tilde{\varepsilon}_1 + \tilde{\varepsilon}_2}\right) \tag{3.18}$$

$$k_{z1}^2 = \left(\frac{\omega}{c}\right)^2\left(\frac{\tilde{\varepsilon}_1^2}{\tilde{\varepsilon}_1 + \tilde{\varepsilon}_2}\right) \tag{3.19}$$

$$k_{z2}^2 = \left(\frac{\omega}{c}\right)^2\left(\frac{\tilde{\varepsilon}_2^2}{\tilde{\varepsilon}_1 + \tilde{\varepsilon}_2}\right) \tag{3.20}$$

If we remind that $\tilde{\varepsilon}_1 = \varepsilon_1' + i\varepsilon_1''$, $\tilde{\varepsilon}_2 = \varepsilon_2$

$$k_x^2 = \left(\frac{\omega}{c}\right)^2 \frac{(\varepsilon_1' + i\varepsilon_1'')\varepsilon_2}{(\varepsilon_1' + i\varepsilon_1'') + \varepsilon_2}$$

$$= \left(\frac{\omega}{c}\right)^2\left\{\left(\frac{(\varepsilon_1'(\varepsilon_1' + \varepsilon_2) + \varepsilon_1''^2)\varepsilon_2}{(\varepsilon_1' + \varepsilon_2)^2 + \varepsilon_1''^2}\right) + i\left(\frac{\varepsilon_1''\varepsilon_2^2}{(\varepsilon_1' + \varepsilon_2)^2 + \varepsilon_1''^2}\right)\right\} \tag{3.21}$$

If we assume besides a real ω and ε_2 that $\varepsilon_1'' < |\varepsilon_1'|$, we obtain a complex $k_x = k_x' + ik_x''$ with

$$k_x' = \frac{\omega}{c}\left(\frac{\varepsilon_1'\varepsilon_2}{\varepsilon_1' + \varepsilon_2}\right)^{1/2} \tag{3.22}$$

$$k_x'' = \frac{\omega}{c}\left(\frac{\varepsilon_1'\varepsilon_2}{\varepsilon_1' + \varepsilon_2}\right)^{3/2}\frac{\varepsilon_1''}{2\varepsilon_1'^2} \tag{3.23}$$

The surface plasmon decay in x-direction can be evaluated from k_x'' because the intensity decreased as $e^{-2k_x''x}$. The decay length l may be obtained as

$$l = \frac{1}{2k_x''} = \frac{c}{\omega}\left(\frac{\varepsilon_1'\varepsilon_2}{\varepsilon_1' + \varepsilon_2}\right)^{-3/2} \frac{\varepsilon_1'^2}{\varepsilon_1''} \tag{3.24}$$

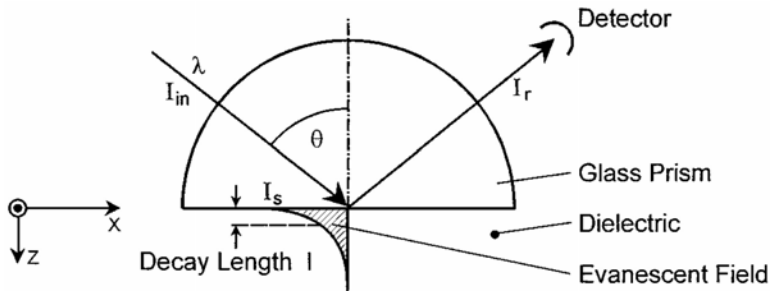

Figure 3.2 Total internal reflection of a plane wave of wavelength λ and intensity I_{in}. [15]

The decay length l is the key parameter to carry out a SPR imaging measurements [58].

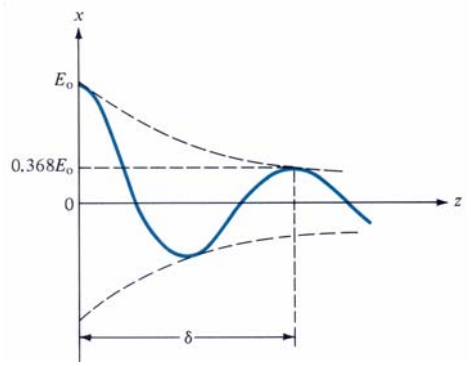

Figure 3.3 The wave penetrates into the medium [57].

In the z-direction the dielectric filed of the surface plasmon decays exponentially as $e^{-|k_{zi}||z|}$, normal to the surface. The value of the (skin) depth at which the field falls to 1/e, become

$$\hat{z} = \frac{1}{|k_{zi}|}. \tag{3.25}$$

If we assume $\varepsilon_1'' < |\varepsilon_1'|$, the depth become

in the metal with ε_1: $$\hat{z}_1 \approx \frac{c}{\omega}\left(\frac{\varepsilon_1' + \varepsilon_2}{\varepsilon_1^2}\right)^{1/2} \tag{3.26}$$

in the medium with ε_2: $$\hat{z}_2 \approx \frac{c}{\omega}\left(\frac{\varepsilon_1' + \varepsilon_2}{\varepsilon_2^2}\right)^{1/2} \tag{3.27}$$

$\varepsilon_1' + \varepsilon_2 < 0$ then k_{zi} is purely imaginary. For He-Ne laser light (632.8 nm) on the gold surface obtains $\hat{z}_1$=32 nm, $\hat{z}_2$=285 nm.

Form the $\vec{k}$ component of equation (2.11) in z-direction

$$ik_{x1}H_{y1} = -i\omega\varepsilon_0\tilde{\varepsilon}_{r1}E_{z1} \tag{3.28}$$

$$ik_{x2}H_{y2} = -i\omega\varepsilon_0\tilde{\varepsilon}_{r2}E_{z2}\,. \tag{3.29}$$

Form x-direction of equation (2.11-2.12) and equation (2.31-2.32)

$$H_{y1} = -\frac{\omega\varepsilon_0\tilde{\varepsilon}_{r1}E_{x1}}{k_{z1}} = -\frac{\omega\varepsilon_0\tilde{\varepsilon}_{r1}E_{z1}}{k_x}$$

$$\frac{E_{z1}}{E_{x1}} = \frac{k_x}{k_{z1}} \tag{3.30}$$

$$H_{y2} = -\frac{\omega\varepsilon_0\tilde{\varepsilon}_{r2}E_{x2}}{k_{z2}} = -\frac{\omega\varepsilon_0\tilde{\varepsilon}_{r2}E_{z2}}{k_x}$$

$$\frac{E_{z2}}{E_{x2}} = -\frac{k_x}{k_{z2}}\,. \tag{3.31}$$

At large k_x, $\tilde{z}_i$ is given by about $1/k_x$ leading to a strong concentration of the field near the surface in both media.

At low k_x or large $|\varepsilon_1'|$ values, the field in air has a strong (transverse) component E_z compared to the (longitudinal) component E_x, namely $E_z/E_x = -i|\varepsilon_1'|^{1/2}$ and extends far into the air space; it resembles thus a guided photon field (Zenneck-Sommerfeld wave). In the metal, E_z is small against E_x since $E_z/E_x = i|\varepsilon_1'|^{-1/2}$. These relations are derived from $\nabla \cdot E = 0$, valid outside the surface air/metal. At large k_x both components E_x and E_z become equal: $E_z = \pm iE_x$ (air: +*i*, metal: -*i*).

3.2 **Surface Plasmon Resonance Curve by Fresnel Formulae**

The relation of reflectivity (R) and angle of incidence (θ_0)can be evaluated via Fresnel Formulae as follows [59]:

Fresnel formulae:
$$R_{\parallel} = \frac{n_2 \cos\theta_1 - n_1 \cos\theta_2}{n_2 \cos\theta_1 + n_1 \cos\theta_2} A_{\parallel} \tag{3.32}$$

$$n = \sqrt{\varepsilon} \tag{3.33}$$

and condition that the tangential components of the propagation vectors be continuous (called the phase matching conditions), as Figure 3.1,

$$k_1 \sin\theta_1 = k_2 \sin\theta_2 \tag{3.34}$$

we get

$$\frac{\sin\theta_2}{\sin\theta_1} = \frac{k_1}{k_2} = \frac{n_1}{n_2} = \sqrt{\frac{\varepsilon_1}{\varepsilon_2}} \tag{3.35}$$

get

$$\frac{R_{\parallel}}{A_{\parallel}} = \frac{\sqrt{\varepsilon_{m+1}}\cos\theta_m - \sqrt{\varepsilon_m}\cos\theta_{m+1}}{\sqrt{\varepsilon_{m+1}}\cos\theta_m + \sqrt{\varepsilon_m}\cos\theta_{m+1}} \tag{3.36}$$

but

$$\cos\theta_m = \sqrt{1-\sin^2\theta_m} = \sqrt{1-\frac{\varepsilon_1}{\varepsilon_m}\sin^2\theta_1} = \frac{1}{\sqrt{\varepsilon_m}}\sqrt{\varepsilon_m - \varepsilon_1 \sin^2\theta_1} \tag{3.37}$$

$$\cos\theta_{m+1} = \sqrt{1-\sin^2\theta_{m+1}} = \sqrt{1-\frac{\varepsilon_1}{\varepsilon_{m+1}}\sin^2\theta_1} = \frac{1}{\sqrt{\varepsilon_{m+1}}}\sqrt{\varepsilon_{m+1} - \varepsilon_1 \sin^2\theta_1} \tag{3.38}$$

where m=1,2,3,…, M-1, and M is the total number of layers, we get

$$r_{m,m+1} = \frac{R_{\parallel}}{A_{\parallel}} = \frac{\frac{\sqrt{\varepsilon_{m+1}}}{\sqrt{\varepsilon_m}}\sqrt{\varepsilon_m - \varepsilon_1 \sin^2\theta_1} - \frac{\sqrt{\varepsilon_m}}{\sqrt{\varepsilon_{m+1}}}\sqrt{\varepsilon_{m+1} - \varepsilon_1 \sin^2\theta_1}}{\frac{\sqrt{\varepsilon_{m+1}}}{\sqrt{\varepsilon_m}}\sqrt{\varepsilon_m - \varepsilon_1 \sin^2\theta_1} + \frac{\sqrt{\varepsilon_m}}{\sqrt{\varepsilon_{m+1}}}\sqrt{\varepsilon_{m+1} - \varepsilon_1 \sin^2\theta_1}}$$

$$= \frac{\varepsilon_{m+1}\sqrt{\varepsilon_m - \varepsilon_1 \sin^2\theta_1} - \varepsilon_m\sqrt{\varepsilon_{m+1} - \varepsilon_1 \sin^2\theta_1}}{\varepsilon_{m+1}\sqrt{\varepsilon_m - \varepsilon_1 \sin^2\theta_1} + \varepsilon_m\sqrt{\varepsilon_{m+1} - \varepsilon_1 \sin^2\theta_1}} \tag{3.39}$$

reflectivity coefficient

$$r_{M-(m+1),M} = \frac{r_{M-(m+1),M-m} + r_{M-m,M}e^{2i\beta_{M-m}}}{1 + r_{M-(m+1),M-m}r_{M-m,M}e^{2i\beta_{M-m}}} \tag{3.40}$$

where
$$\beta_{M-m} = \frac{2\pi}{\lambda}\sqrt{\varepsilon_{M-m}}d_{M-m}\cos\theta_{M-m}$$

$$= \frac{2\pi}{\lambda} d_{M-m} \sqrt{\varepsilon_{M-m} - \varepsilon_1 \sin^2 \theta_1} \tag{3.41}$$

where m=1,2,3,…, M-2.

The reflectivity is given by

$$R = \left| r_{1,M} \right|^2 \tag{3.42}$$

3.3 Dispersion Relations for Surface Plasmons

In Figure 3.4, the dispersion relations of surface plasmons at the metal/vacuum and metal/dielectric interfaces are plotted. Within the area between light (vacuum) line (dash-dot-dot) and light (prism) line (short dash-dot), the surface plasmons can be excited by the attenuated total reflectance (ATR) method at both interfaces [60]. An excitation is possible via irradiation with electrons since the momentum transfer is varied inside the solid by variation of the scattering angle. In order to couple light to surface plasmons an increase in the wave vector by Δk_x is necessary for given photon energy (corresponding to a rotation of the light line to the right in Fight 3.4). This may be achieved by modification of the surface with a lattice structure or more generally by invoking surface roughness, which adds additional reciprocal lattice vectors to the initial wave vector of the light [61].

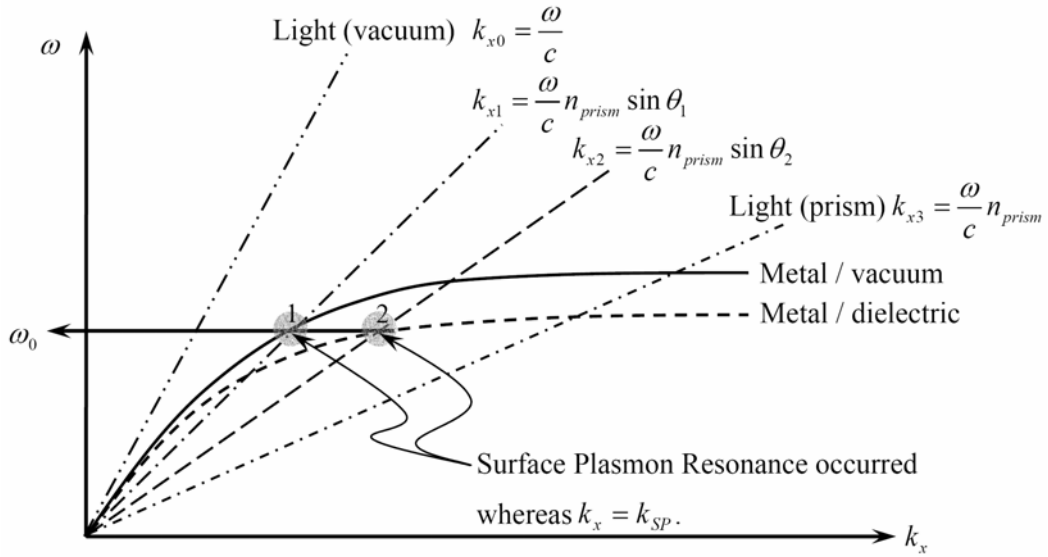

Figure 3.4 Schematic dispersion diagrams

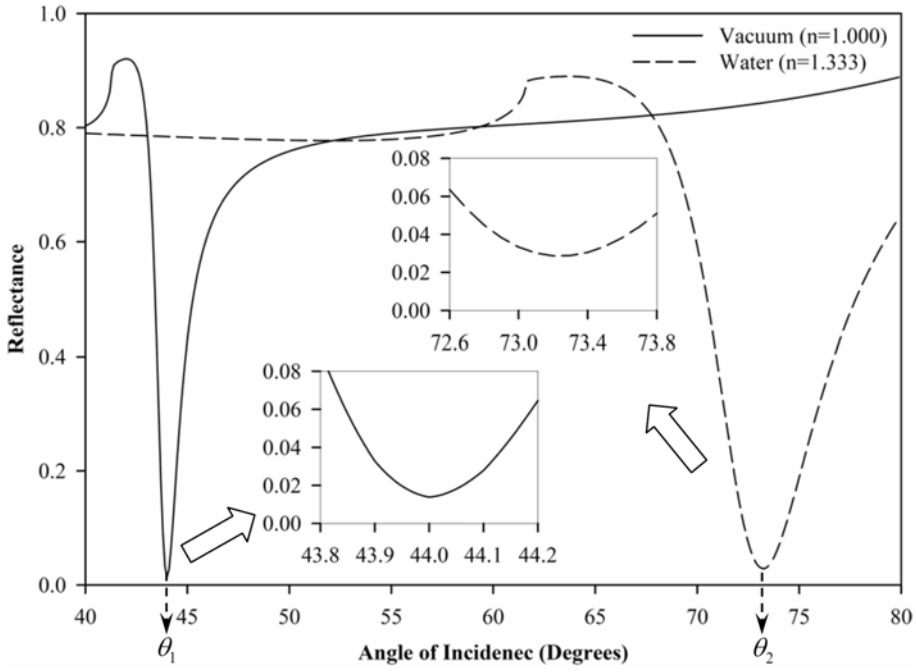

Figure 3.5 SPR curves of the vacuum and water.

The dispersion curves for metal/vacuum and metal/dielectric interface are exemplified. The shaded circles show the position, whereas the SPR take places. Due to the frequency of the light source (ω_0) is fixed, k_x is changed by variation of incidence angle. The first and second shaded circles relate to the angle of incidence θ_1 and θ_2 respectively, as shown in Figure 3.5. In this case, the dielectric is water.

Considering the reflectance of the SPR curves of the vacuum and water, we found the difference of the minima reflectance, where SPR occurred (θ_1 and θ_2), as called SPR angle.

CHAPTER IV
SURFACE TREATMENT AND APPARATUS

4.1 Preparation of Sensor Chip

Surface plasmon resonance (SPR) technique is highly sensitive for detecting any material on surface by measurement the optical property or mass changes. However, this technique is non specific to identify the exact kind of chemicals or biomolecular molecules. Therefore, we had to develop a more specific detection method of biosensor chip by using leptospiral bacteria as a model.

4.1.1 Materials

4.1.1.1 Buffers and Chemical

Deionized and free organic water, H_2O

Deionized water obtained from the Central Instrument Facility (CIF), Faculty of science, Mahidol University was used as purified water (maximum resistivity of 18.2 MΩ/cm at 25 °c).

Organic contaminants include pesticides, herbicides, decayed plant and animal tissues, gasoline (centuries old decayed plant and animal tissue), and plasticizers (made from petroleum products). Plasticizers leach out of plumbing lines, fittings and storage tanks, so ironically, the purification system itself can contaminate the water if it is not properly constructed. The absence of organic substances is especially important in research that involves tissue cultures, and also in HPLC (high performance liquid chromatography), gas chromatography, electrophoresis, and fluoroscopy [62].

Ethyl alcohol or Ethanol (EtOH) <!>, 99.9% of CH_3CH_2OH, has 46.07 of molecular weight. This chemical was purchased from Mallinckrodt.

CAUTION: Please see Appendix B for appropriate handling of materials marked with <!>.

Diethyl ether (Ether) <!>, Et_2O or $(C_2H_5)_2O$, has 84.18 of molecular weight. This chemical was purchased from Lab-Scan Analytical Sciences.

11-Mercaptoundecanoic acid (MUA) <!>, $C_{11}H_{22}O_2S$, has 218.36 of molecular weight. This chemical was purchased from Aldrich. It was diluted in ethanol to 1 mM.

0.01 M Phosphate-buffered saline (PBS)

pH 7.2

0.514 g $NaH_2PO_4 \cdot 2H_2O$

0.951 g Na_2HPO_4 (anhydrous)

8.5 g NaCl

Add H_2O to 1 liter

By varying the amount of each salt, a range of buffers can be prepared that buffer well between pH 5.8 and pH 8.0.

Poly-L-lysine hydrobromide (PLL) <!>, with the molecular weight of 1,000 - 4,000 g/mol.

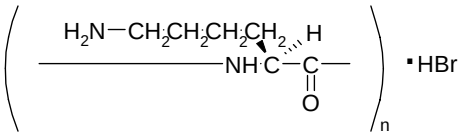

Figure 4.1 Chemical Formula of PLL

It is diluted in PBS, and adjusted 100 μg/mL PLL with 50 mM Na_2CO_3 in H_2O to pH 9.5. It is available commercially from Sigma as a 0.5% solution in H_2O.

***N*-(3-Dimethylaminopropyl)-*N′*-ethylcarbodiimide hydrochloride (EDC) <!>, $C_8H_{17}N_3 \cdot HCl$,** [FW 191.70 g/mol]. This chemical was purchased from Fluka. It was diluted in water to 75 mM.

***N*-Hydroxysuccinimide (NHS) <!>, $C_4H_5NO_3$,** [FW 115.09 g/mol]. This chemical was purchased from Fluka. It was diluted in water to 15 mM.

CAUTION: Please see Appendix B for appropriate handling of materials marked with <!>.

Bovine serum albumin (BSA)

This serum, obtained from Pathobiology Department, is used as the blocking agent.

Ethanolamine (Ethanolamine) <!>, [MWt 61.08 g/mol]. This chemical was purchased from Fluka. It was diluted in water to 1 M.

Lens washing solution <!>

This is mixture of ethanol and ether (1:2). Wipe the half circular prism, which is stained with the index matching gel.

Index matching gel

Cargille's BK 7 glass Matching Liquid (Cargilles Labs, USA) with refractive index 1.5167 was used in this study. The solution was applied between the half circular prism and sensordisk-gold, which were made from BK7 glass. This was done in order to avoid an interference at the interfaces.

4.1.1.2 Basis of Immunology

The protective factors produced following immune responses were found in serum and called antibodies by Emil von Behring in 1890. In 1930, Heidelberger showed that antibodies are proteins, for example when pneumococcal polysaccharide antigens were added to antiserum, will formed a precipitate.

Immunity is brought about in the host through a variety of leukocytes (white blood cells), including immune cell, such as macrophages and lymphocytes, which derived from undifferentiated stem cells in the bone marrow. Leukocytes can leave the bloodstream and patrol the tissues to combat invading agents [64].

For determination of antibodies, electrophoresis can be used to characterize by their different electrophoretic mobility. A serum will be separated under an electrical power. The positively charged protein molecules are attracted toward the cathode, the neutral molecules remain stationary, and the negatively charged molecules are attracted toward the anode, which each protein moves at a rate dependent on its net charge.

CAUTION: Please see Appendix B for appropriate handling of materials marked with <!>.

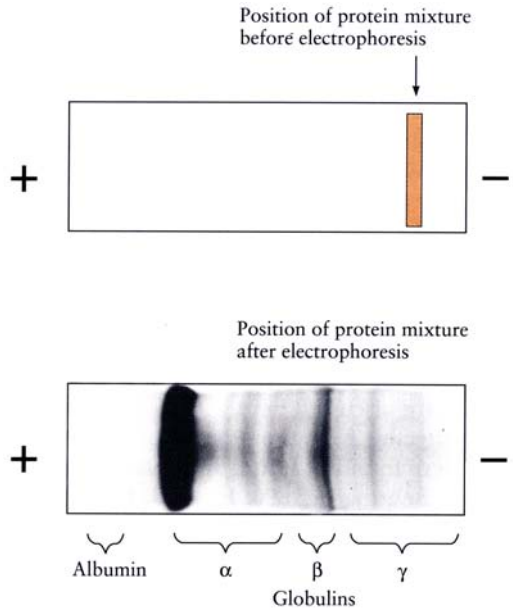

Figure 4.2 Electrophoresis of a serum sample on strip of cellulose acetate. It can be resolved into about ten distinct bands in this way [65].

When serum is electrophoresed, it consistently separates into four major fractions. The most negatively charged fraction consists of a single protein called serum albumin. The other three major fractions are classified into α, β, and γ globulins according to their electrophoretic mobility as shown in Figure 4.2. Antibody activity is mainly found nearest to the cathode, the γ globulins, although some type of antibodies are found among β globulins region. Because antibody proteins belong to a class of glycoproteins called immunoglobulins (Ig) [65].

The fundamental structure of immunoglobulins was first established by Gerald Edelman and Rodney Porter. Each chain is made up of identifiable domains; some are constant in sequence and others are variable. The constant domains have a characteristic structure known as the immunoglobulin fold. There are three constant domains in each heavy chain and one in each light chain. The heavy and light chains also have one variable domain, in which most of the variability in amino acid residue sequence is found. The variable domains associate antigen-binding site [64].

Antibody molecules called isotypes or class are named IgA, IgD, IgE, IgG, and IgM (Figure 4.3). In humans, IgA and IgG isotypes can be subdivided into subclasses or subtypes, called IgA1 and IgA2, and IgG1, IgG2, IgG3, and IgG4,

respectively. The heavy chain C regions of all antibody molecules of one isotype or subtype have essentially the same amino acid sequence. This sequence is different in antibodies of other isotypes or subtypes. Heavy chains are designated by the letter of the Greek alphabet corresponding to the overall isotype of the antibody: IgA1 contains α1 heavy chains; IgA2, α2; IgD, δ; IgE, ε; IgG1, γ1; IgG2, γ2; IgG3, γ3; IgG4, γ4; and IgM, μ.

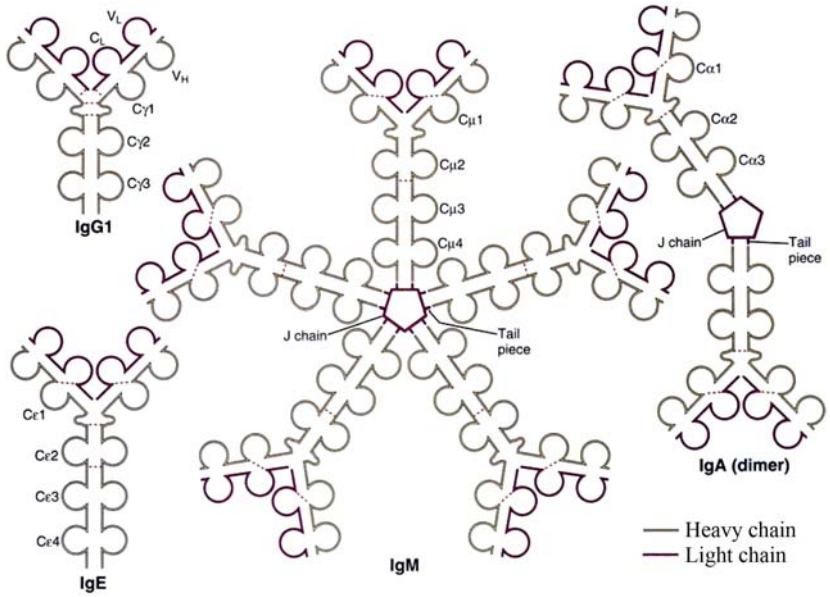

Figure 4.3 Schematic diagrams of various Ig isotypes are shown with depictions of Ig domain structure. IgG and IgE circulate as monomers, whereas secreted forms of IgA and IgM are dimmers and pentamers, respectively, stabilized by the joining (J) chain. (Some IgA molecules are trimers, not shown.) Ig, immunoglobulin [66].

IgG plays a major role in antibody-mediated defense mechanism, because of their highest concentration in blood (Figure 4.4). It will weight about 160 kilodalton and γ heavy chains. Because of its relatively small size, IgG can escape from blood vessels more easily than other immunoglobulins. Therefore, it participates in specific defense mechanism of tissue spaces and body surface, by opsonization, agglutination or precipitation of antigens but it can activate classical complement pathways whit multiple IgG molecules that accumulated in a correct configuration to the antigen surface.

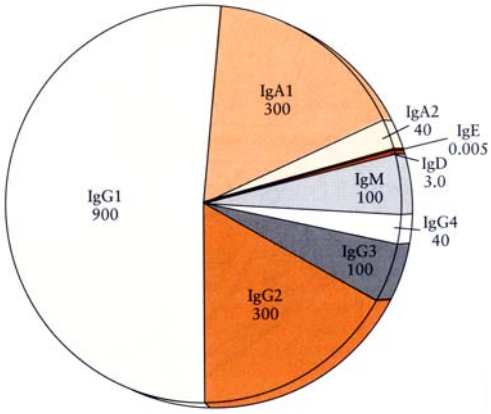

Figure 4.4 Various immunoglobulins classes found in human. The underneath numbers are the average serum concentrations in mg/dl [65].

Primary immune responses result from activation of previously unstimulated naive B cells, whereas secondary responses are due to stimulation of expanded clones of memory B cells. Thus, secondary immune response, a larger amount of antibodies is produced (see Figure 4.5). Heavy chain isotype switching and affinity maturation also increase with repeated exposures to antigens.

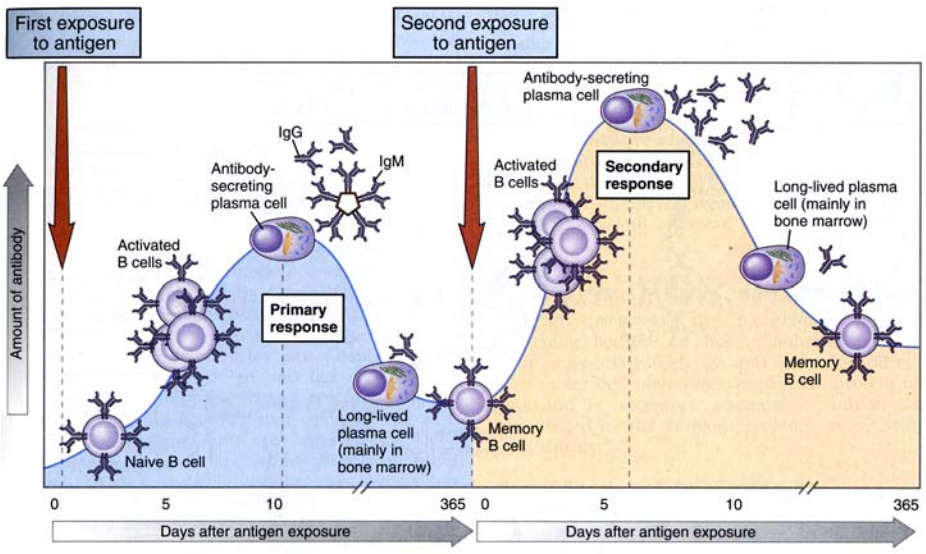

Figure 4.5 Kinetics of primary and secondary humoral immune responses.

Antibodies may be expressed in secreted or membrane-associated forms, which differ in the amino acid sequence of the carboxyl terminal end of the last constant heavy chain (C_H) domain. In the secretory form, found in blood and other extracellular fluids, the C_H sequence terminates with charged and hydrophilic amino acid residues. The membrane form of antibody, found only on the plasma membrane

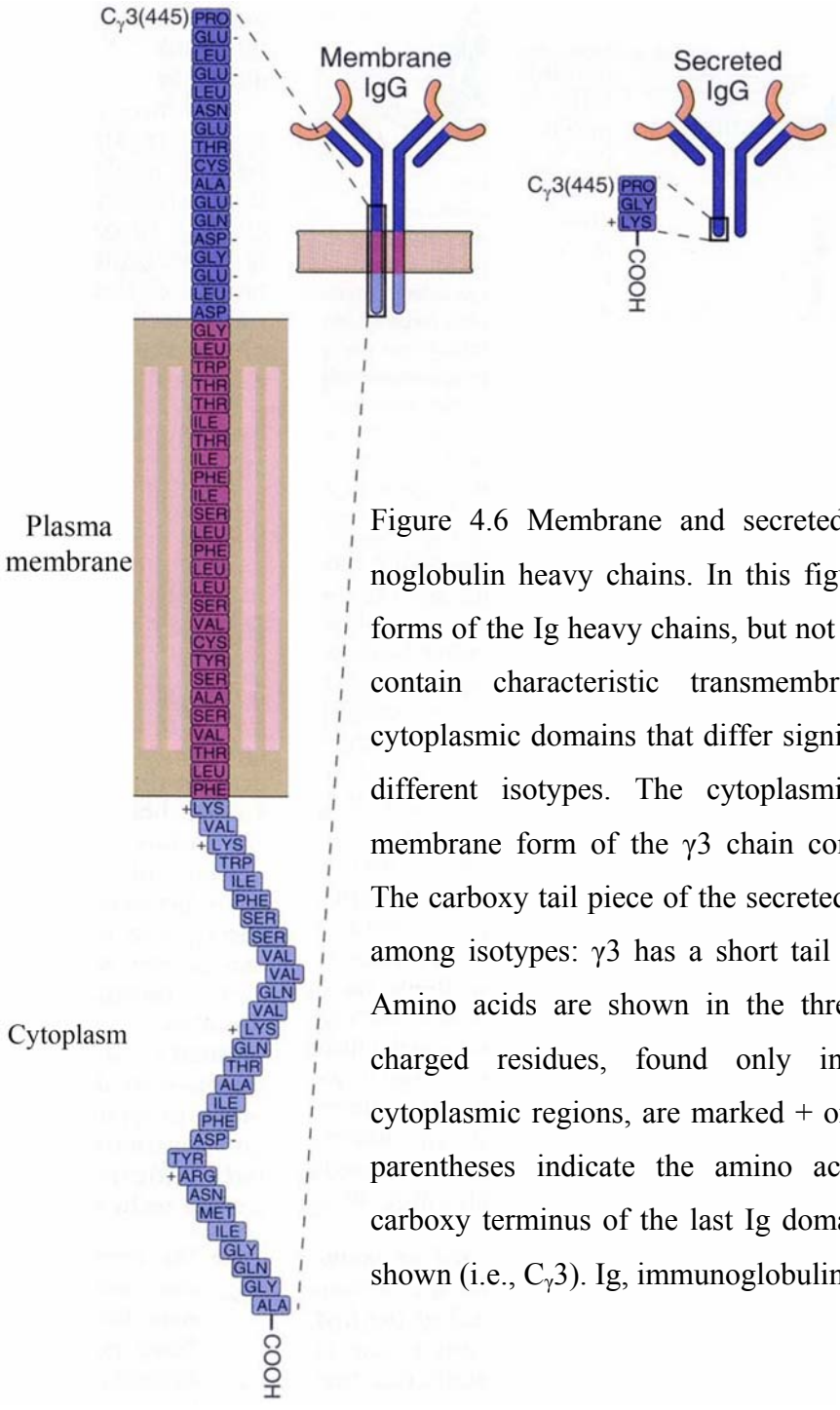

Figure 4.6 Membrane and secreted forms of immunoglobulin heavy chains. In this figure, the membrane forms of the Ig heavy chains, but not the secreted forms, contain characteristic transmembrane regions and cytoplasmic domains that differ significantly among the different isotypes. The cytoplasmic portion of the membrane form of the γ3 chain contains 28 residues. The carboxy tail piece of the secreted forms also differs among isotypes: γ3 has a short tail piece (3 residues). Amino acids are shown in the three-letter code, and charged residues, found only in extracellular or cytoplasmic regions, are marked + or -; the numbers in parentheses indicate the amino acid residue of the carboxy terminus of the last Ig domain in each isotype shown (i.e., $C_\gamma 3$). Ig, immunoglobulin [66].

of the B lymphocytes that synthesize the antibody, has C_H domains with carboxyl terminal sequences that include 26 amino acids with hydrophobic side chains followed by variable numbers of basic amino acid residues (see Figure 4.6). IgG has a relatively globular Y shaped structure of height 12 nm [67].

In this research, we use rabbit anti-*Leptospira* antibodies (Ab) that were mainly IgG class and vary the concentration of the antibodies with PBS. The serovar specific antibodies were prepared by Assoc. Prof. Galayanee Doungchawee, Pathobiology department, Mahidol University.

4.1.1.3 Leptospiral Antigens

Leptospira bacteria with microaerophilic are the thinnest (<0.1 μm) and tightly coiled (12 to 24 turns) as shown in Figure 4.7. They have hooked ends and progressive motion. *Leptospira* are blood and tissue parasites that can be cultivated in media with serum.

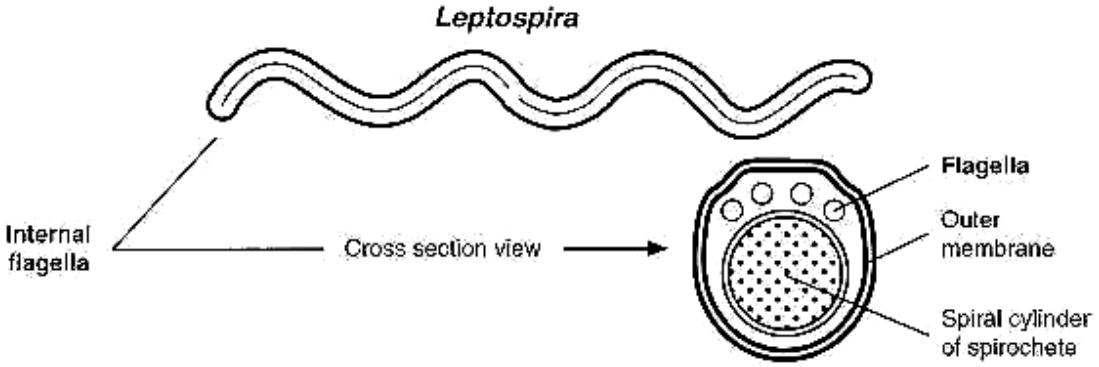

Figure 4.7 Morphological comparison of Leptospira [68]

Leptospirosis is a zoonotic disease caused by *Leptospira interrogans* comprised of more than 260 serotypes [69]. The leptospires or leptospira used in this study is serovar Canicola, Canicola serogroup, *interrogans* species, and the most common found in domestic animal, dog [70]. The leptospiral antigens were prepared after optimal growth by washing centrifugation and collecting as whole dead cell as antigens in determinations step (see Section 4.4.4).

4.1.2 Metal Surface

The glass slide evaporated by gold was purchased from IBIS (the Netherlands) [71]. The surface area of SensorDisk is approximately 9.62 cm^2, as shown in Figure 4.8.

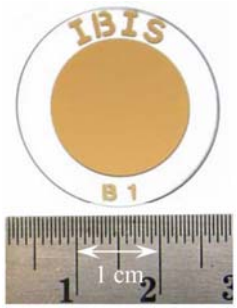

Figure 4.8 The normal coating of IBIS-gold SensorDisk.

In general, the sensor surface is prepared by evaporating the glass slide with 5 nm of chromium followed by 50 nm of gold [72]. The refractive index of the gold (n_{Au}) is given by [73]

$$n_{Au} = \sqrt{(30.3723 - 0.065272\lambda) + i(17.1691 - 0.0468757\lambda + 3.48485 \times 10^{-5}\lambda^2)} \; . \quad (4.1)$$

In these experiments, the IBIS-gold SensorDisks consist of at least three layers. In Figure 4.9 show the evaporation of overlapping metal layer. Denoted "Layer 1", "Layer 2", and "Layer 3" represent the top, middle, and bottom layer of

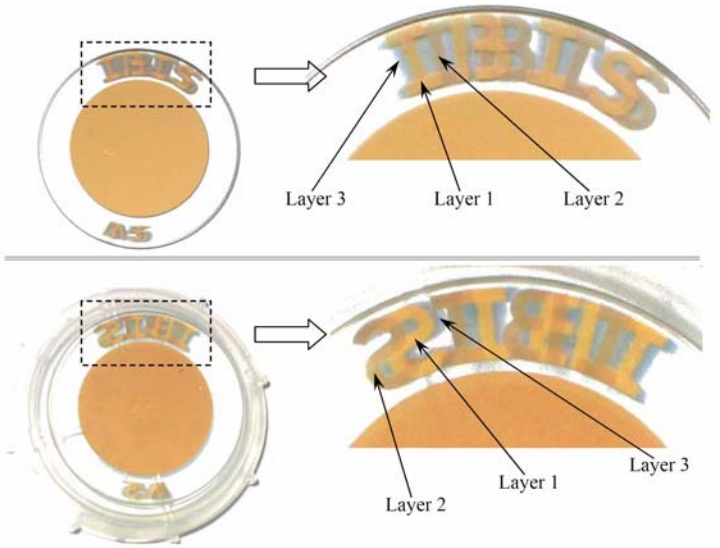

Figure 4.9 IBIS-gold SensorDisks was in evaporating error. Top panel: the front sensor surface. Bottom panel: turn over the sensor that is contained in box.

the disk respectively by looking at a back of the sensor, as shown in bottom panel in Figure 4.9. On the other side, denoted “Layer 1”, “Layer 2”, and “Layer 3” represent the bottom, middle, and top layer respectively when look at a front of sensor, as shown in top panel in Figure 4.9. The properties of each layer can be evaluated by ellipsometer. These are important to calculate in numerical analysis. The sensors have smudge on back of glass slide, so they are cleaned by lens washing solution.

4.2 Surface Plasmon Resonance Spectroscope

The SPR setup is built by electro-optics section, National Electronics and Computer Technology Center (NECTEC).

4.2.1 Hardware

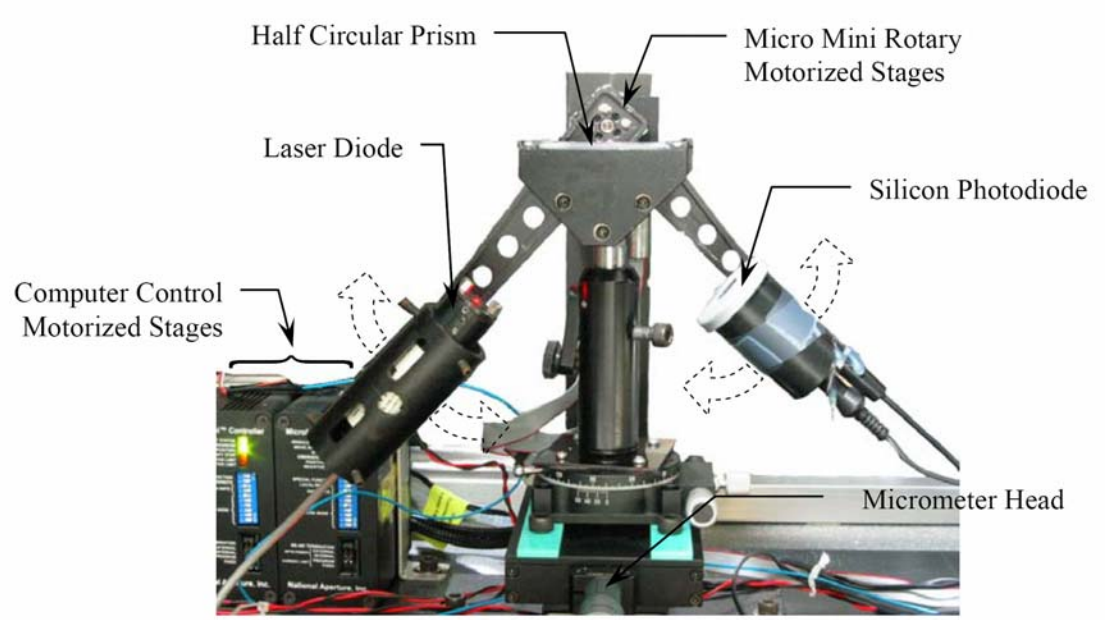

Figure 4.10 Surface plasmon resonance spectroscope setup

Laser diode (Semiconductor laser [74]) was purchased from Edmund Optics Inc. The specifications of instrument as shown below;

Laser Material	GaAsP
Wavelength	670 ±10 nm
Beam Diameter	5mm x 2mm with mask
Beam Divergence	<0.5 mrad

Focusing Range	20 mm to Infinity
Beam Size at Nearest Focus	<100 microns

Micro Mini Rotary Motorized Stages was purchased from Edmund Optics Inc. The specifications of instrument as shown below [75, 76];

Rotation	360°	Counts	204,800 per 360°
Repeatability	±40 arc sec.	Rotor backlash	0
Accuracy	±80 arc sec.	Top Load Capacity	2 kg

Computer Control Single Axis Standard Motorized Stages was purchased from Edmund Optics Inc. Use RS-485 Communication Port (RS-232 to RS-485 Adapter Included)

Half Circular Prism is glass type BK7. The index of refraction data were obtained by using the dispersion formula.

$$n = \sqrt{\frac{B_1\lambda^2}{\lambda^2 - C_1} + \frac{B_2\lambda^2}{\lambda^2 - C_2} + \frac{B_3\lambda^2}{\lambda^2 - C_3} + 1} \qquad (4.2)$$

Here λ, the wavelength, must be in micrometers, and the dispersion constants B_1 through C_3 were obtained by using the constants listed below.

$B_1 = 1.03961212$ $C_1 = 6.00069867\times10^{-3}$

$B_2 = 2.31792344\times10^{-1}$ $C_2 = 2.00179144\times10^{-2}$

$B_3 = 1.01046945$ $C_3 = 1.03560653\times10^{2}$

Note that the dispersion formula is valid only within 350 – 2350 nm of the wavelength. It can be used to interpolate refractive index at other wavelengths within

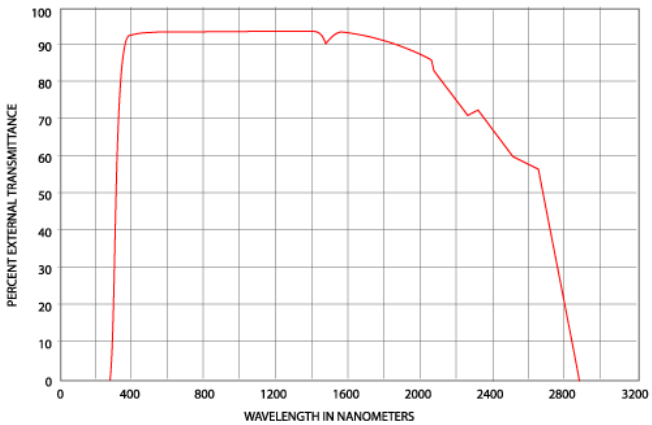

Figure 4.11 Percent external transmittance versus wavelength for glass type BK7.

this range (to a precision of 1×10^{-5} or better), but it should not be used to extrapolate to wavelengths beyond this range. Furthermore, the actual melt-to-melt tolerance on the index of refraction typically is about ±0.001 [77].

4.2.2 Data Processing

Software is run on the Labview 6.0i program [78]. There are two interface programs for applying to SPR spectroscope. The program was developed by Ratthasart Amarit, atElectro-Optics Laboratory, National Electronics and Computer Technology Center (NECTEC). The front end and the flowchart are shown in the Figure 4.12, 4.13, 4.14, and 4.15 respectively. Second program is modified, from SPR curve program, by Jarupat Disrattakit. This program is used for kinetic study, or monitor SPR angle and minimum reflection intensity. The front end and flowchart of second program is shown in Figure 4.16 and 4.17 respectively.

4.2.2.1 Screening and Programming of SPR Curve Program

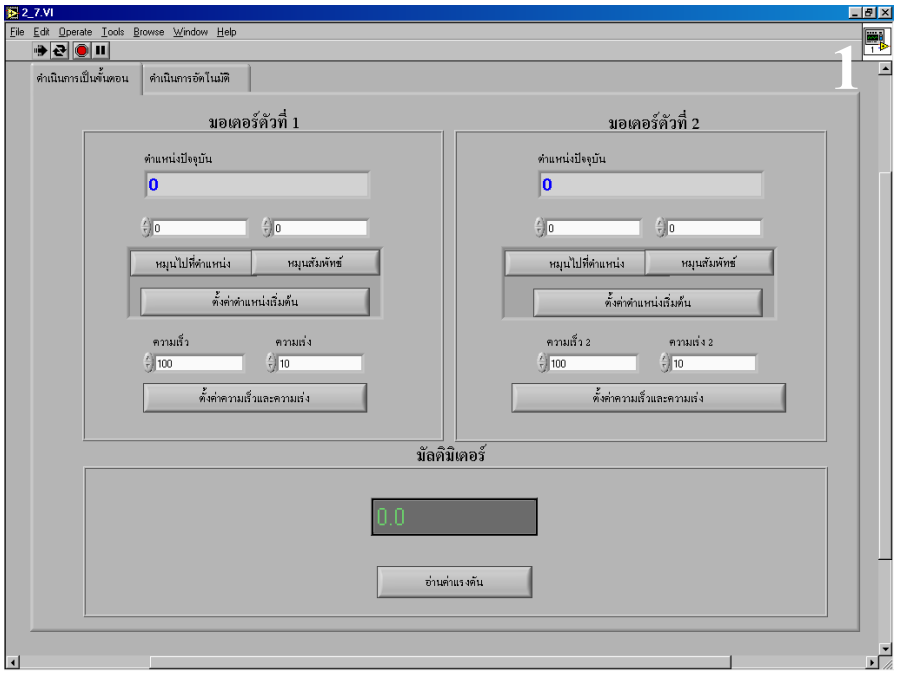

Figure 4.12 The initialized screen is denoted by “1”. This number is related to the flowchart in zone 1 as Figure 4.15 and 4.17.

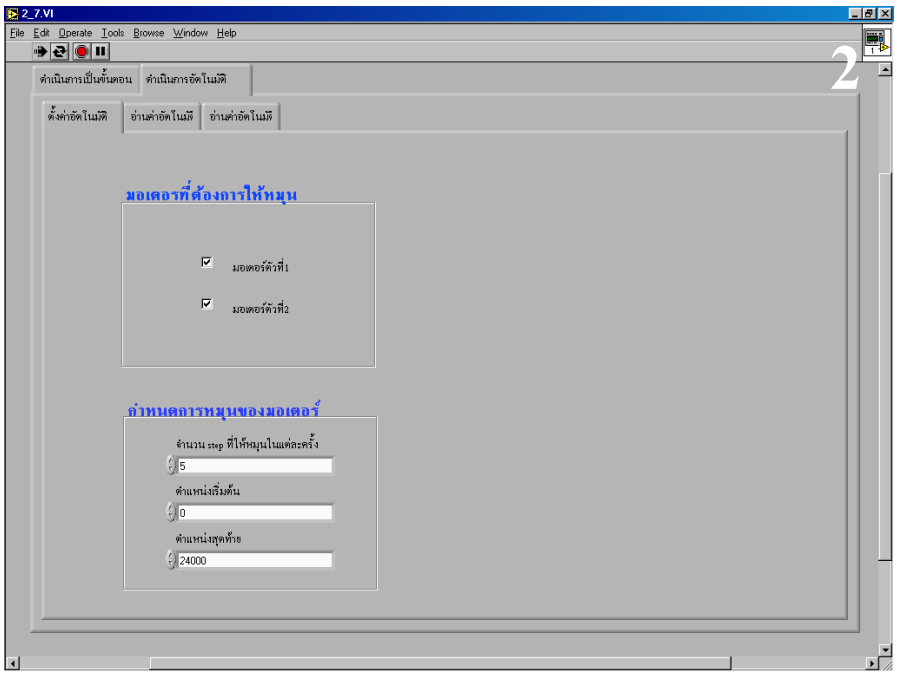

Figure 4.13 The definition of boundary variable screen is denoted by “2”. This number is related to the flowchart of SPR curve program in zone 2.

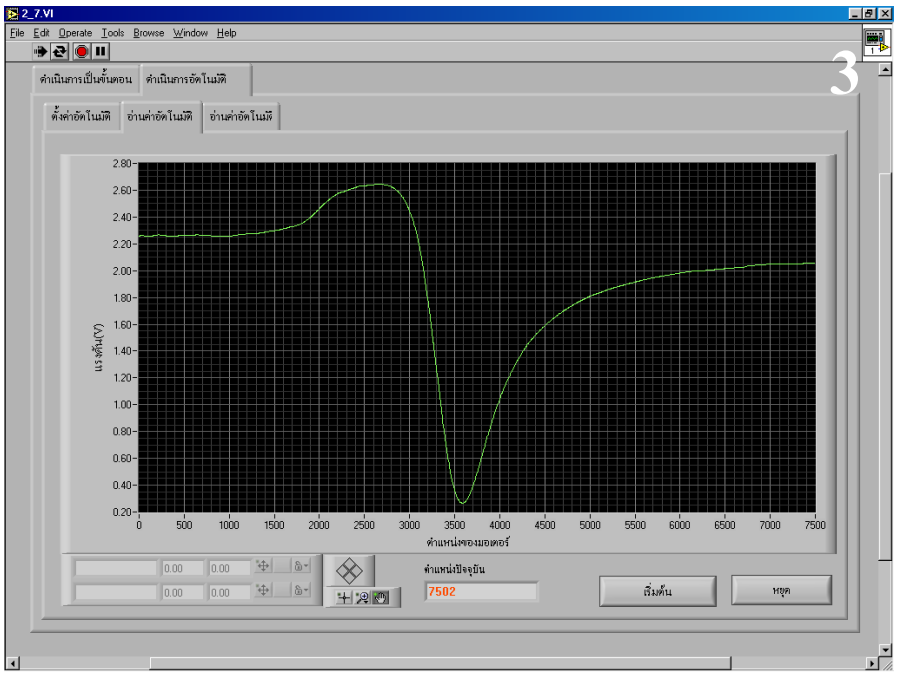

Figure 4.14 The SPR curve preview screen is denoted by “3”. This number is related to the flowchart of SPR curve program in zone 3.

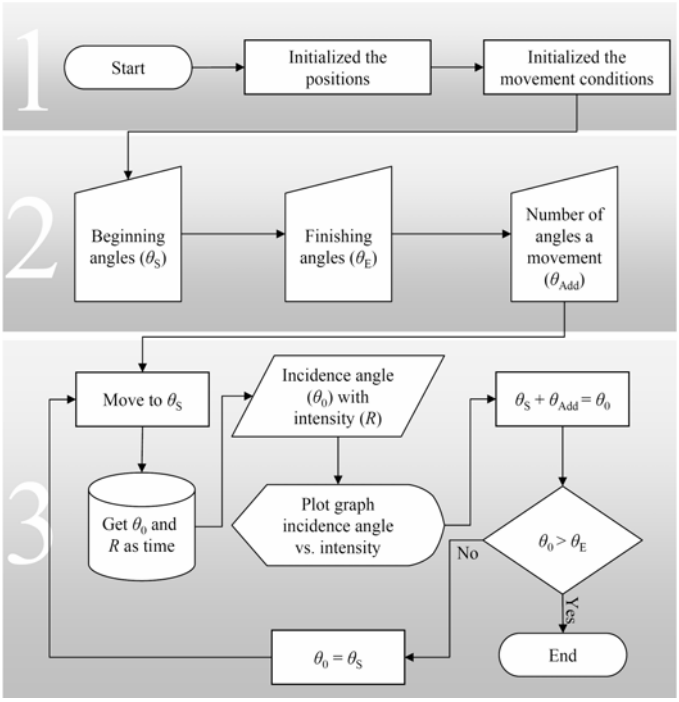

Figure 4.15 The procedure for SPR curve programming.

4.2.2.1 Screening and Programming of Kinetic Study Program

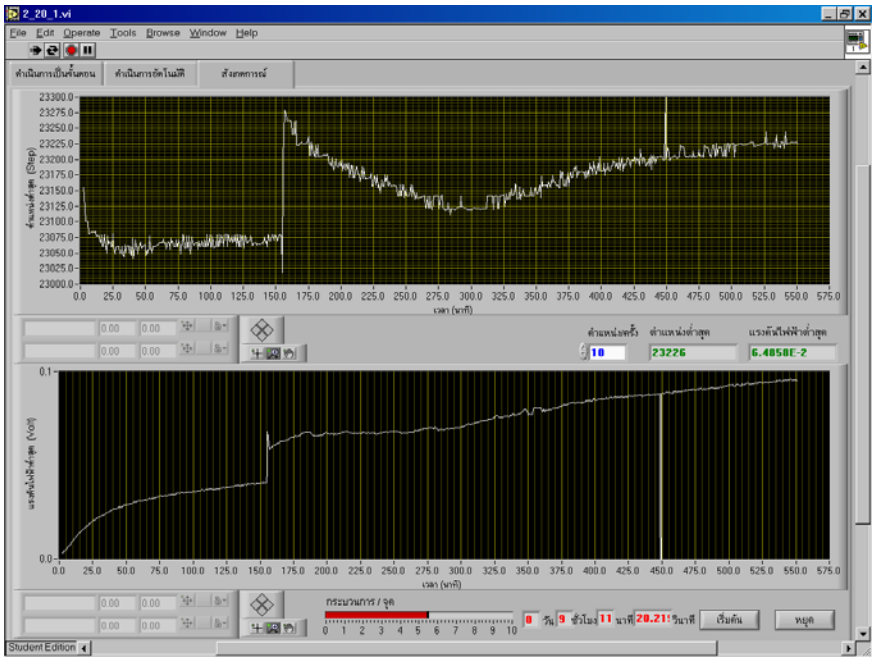

Figure 4.16 Top panel: the monitoring of SPR angle change as time. Bottom panel: the monitoring of minimum reflection intensity. The procedure of this program is shown in automation part in Figure 4.17 and subroutines part in Figure 4.18.

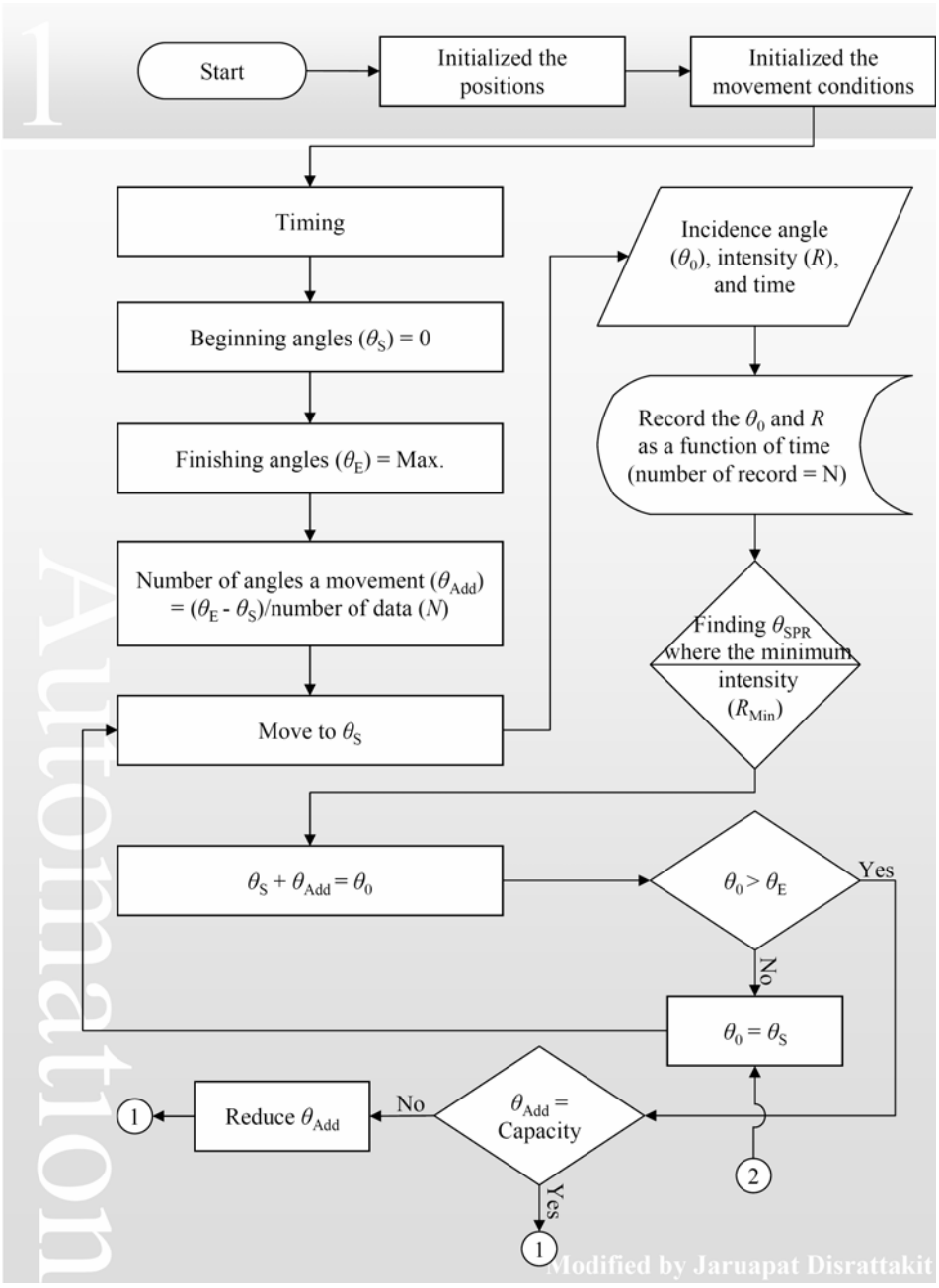

Figure 4.17 The procedure for kinetic study programming. The variables in program, are constant, are evaluated before running. The valuations of variables depend on the capacity of machine and the setup putting.

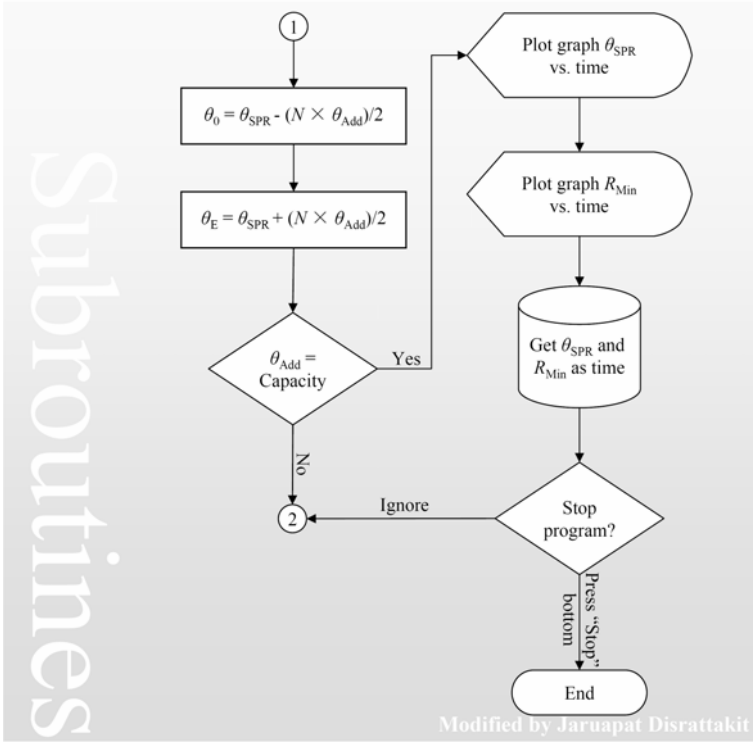

Figure 4.18 The procedure for kinetic study programming in subroutines part.

4.3 Flow System

The flow system consists of the tubing pump system and the flow cell (see Figure 4.19). The variable-speed drive can vary adjust motor rate from 7 to 200 round per minute on scale number 1 to 10. The head pump, is model 77200-50, is supported the pump tubing [79]. The pump tubing has inside diameter 3.1 mm, and is made of

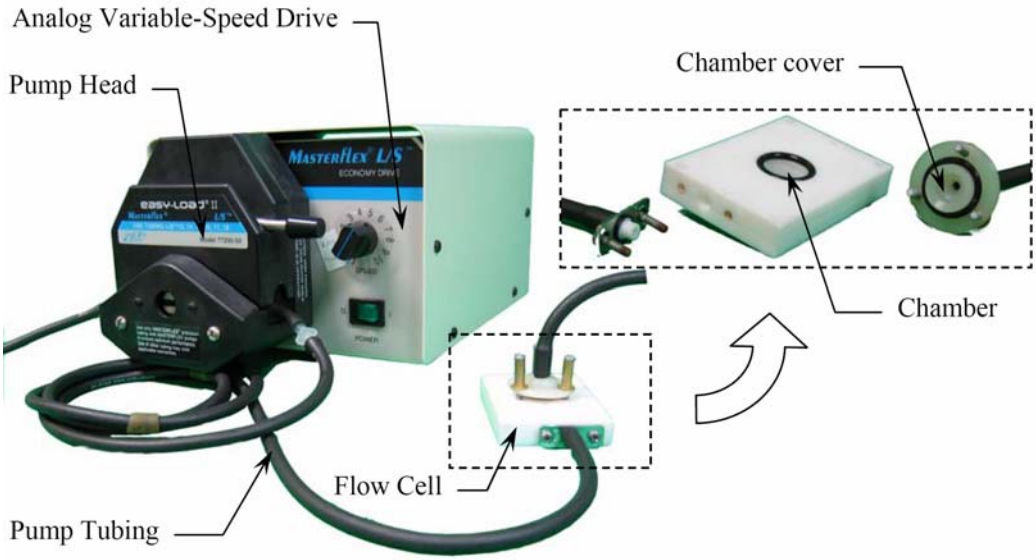

Figure 4.19 Tubing pump system and the flow cell.

viton. All instruments were purchased from Masterflex, USA. The flow cell was made by Electro-Optics Laboratory, National Electronics and Computer Technology Center (NECTEC). The volume of the chamber with cover is approximately 2.5 ml.

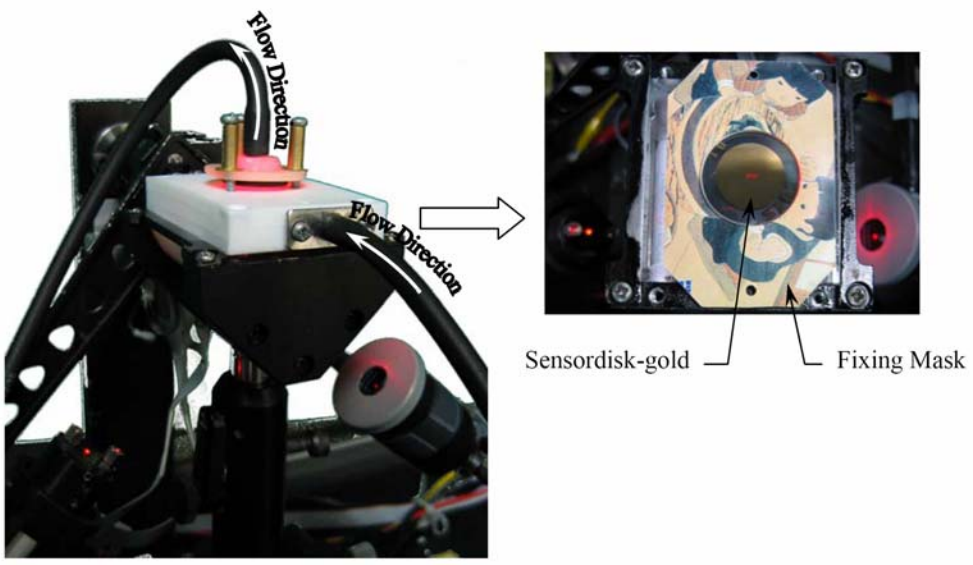

Figure 4.20 Flow cell installation. The sensordisk-gold was mounted on top of the prism.

The sensordisk-gold is fixed by mask as shown in Figure 4.20. Before place sensordisk-gold on prism, the index matching gel is dropped on the prism surface for ridding the gab. The flow rate is about 1.6 ml/min, and the direction of flow as shown in Figure 4.20.

4.4 Immobilization of the antibody onto the sensor chip surface

4.4.1 MUA attachment

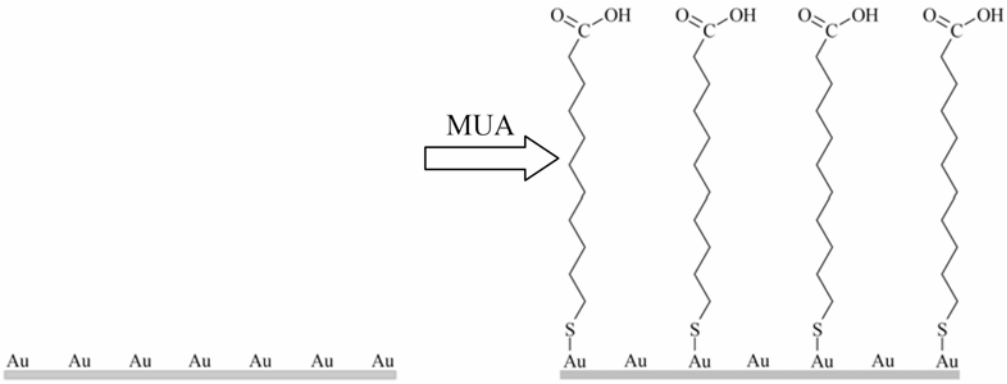

Figure 4.21 MUA is dropped on the gold surface for at least 18 hours to ensure a complete formation of the monolayer [80].

4.4.2 Non-covalent Binding Surface

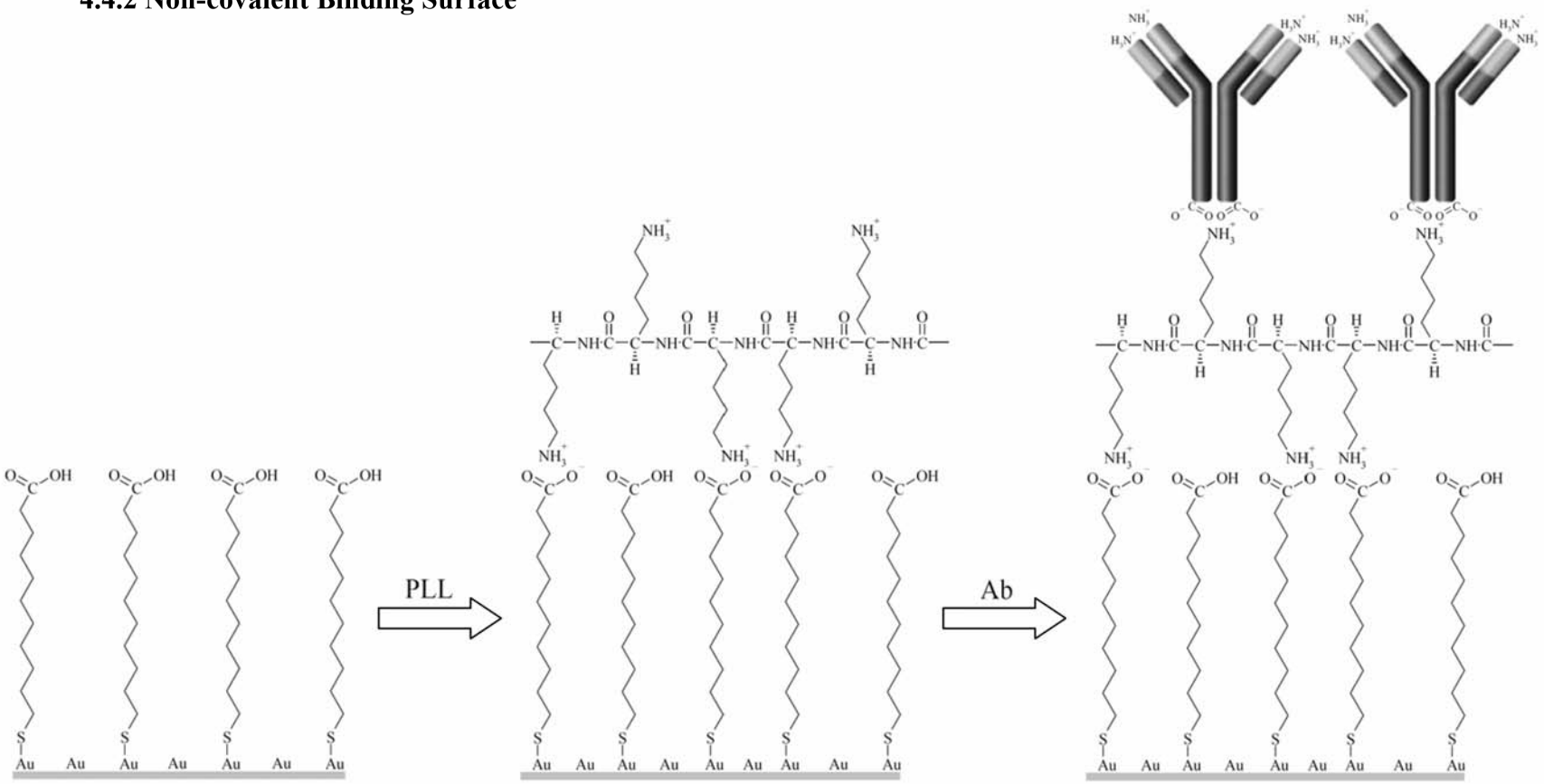

Figure 4.22 An amine group of the PLL reacts with a carboxylic acid group of the MUA to form an electrostatic bond. PLL is attached to the MUA surface for 30 minutes. Subsequent reaction with Ab occurs for 30 minuets; during this time the remaining amine groups of the PLL react with the carboxylic acid groups of the Ab to form an ionic bond [72].

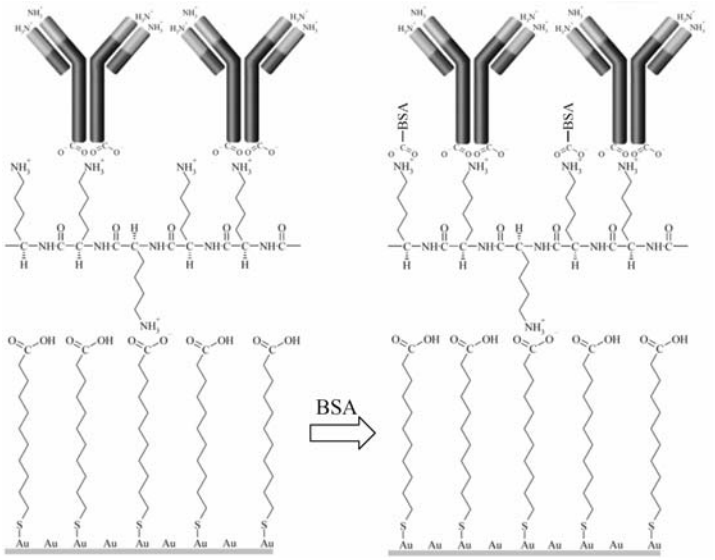

Figure 4.23 Blocking the unreacted amine groups with BSA.

4.4.3 Covalent Binding Surface

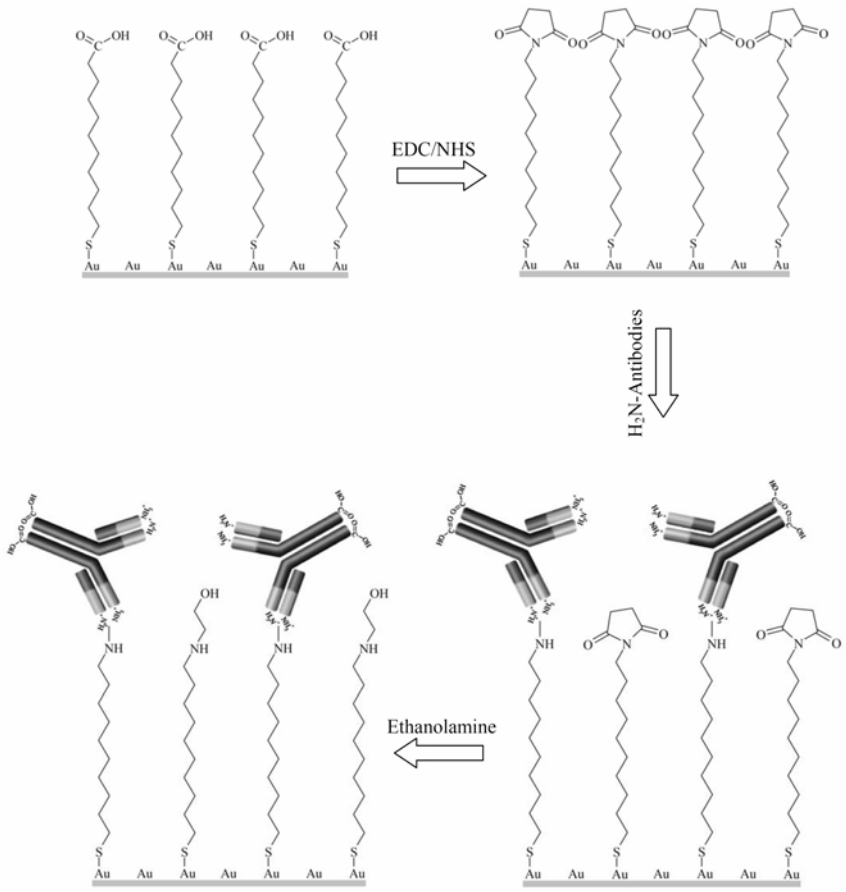

Figure 4.24 Schematic illustration of the Ab immobilization on the MUA surface [81].

Amine coupling introduces NHS esters on the surface of MUA with a mixture of NHS and EDC. The activated NHS esters can react spontaneously with amine on the Ab protein to form covalent bond for 30 minuets. After coupling reaction of Ab to activated surface, ethanolamine was used to deactivate the unreacted esters. The schematic illustration of the immobilization procedures is described in Figure 4.24 [82].

4.4.4 Antigen Adsorption

After the antibody was adsorbed onto the ligands, is amine or carboxylic groups. Then, the antibody surface was blocked the uureacted site. The antigen was dropped onto this specific surface.

CHAPTER V
RESULTS AND DISCUSSIONS

5.1 Surface Functionalization Creating the Charged Surface

11-Mercaptoundecanoic acid (MUA) was adsorbed onto the gold surface. This was done in order to convert the gold surface into a carboxylate surface. The adsorption was monitored by SPR. The results of MUA absorption are shown in Figure 5.1 and Table 5.1.

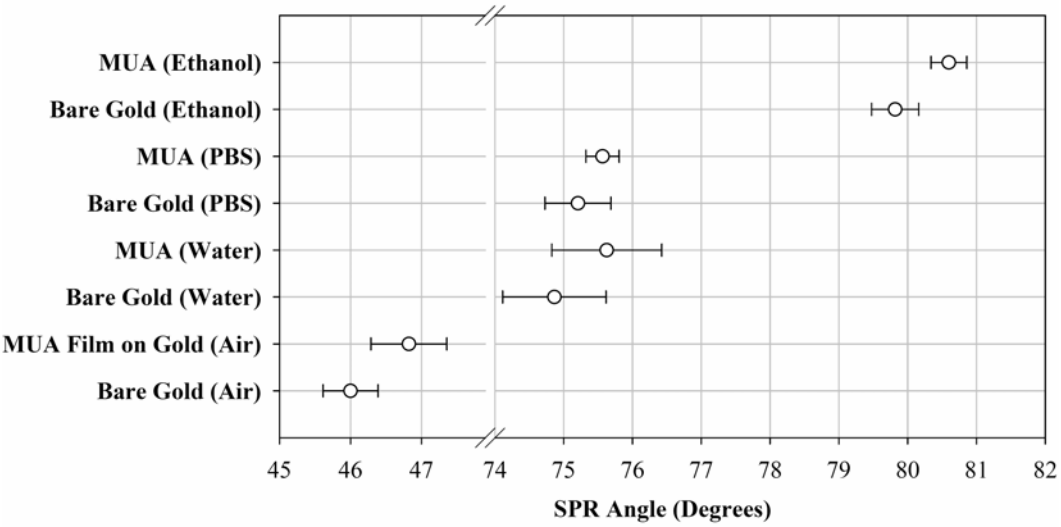

Figure 5.1 SPR angle of bare gold surface and MUA treated surface in PBS and ethanol solution

Table 5.1 Mean of SPR angles with standard deviations of bare gold surface and MUA treated film.

	SPR Angle		P value
	Bare Gold	MUA Film	
Air	45.999 ± 0.388°	46.822 ± 0.535°	0
Water	74.863 ± 0.752°	75.625 ± 0.798°	7.4601×10^{-5}
PBS	75.207 ± 0.479°	75.565 ± 0.241°	1.4157×10^{-1}
Ethanol	79.818 ± 0.342°	80.599 ± 0.260°	0

The probability value (P value) is compared with the significance level and, if it is smaller (P value < 0.05), the result is significant [92].

5.2 Non-Covalent Binding Surface

Poly-L-lysine (PLL) was used as the adsorbed cationic layer which is used for fixing an antibody onto the sensor surface.

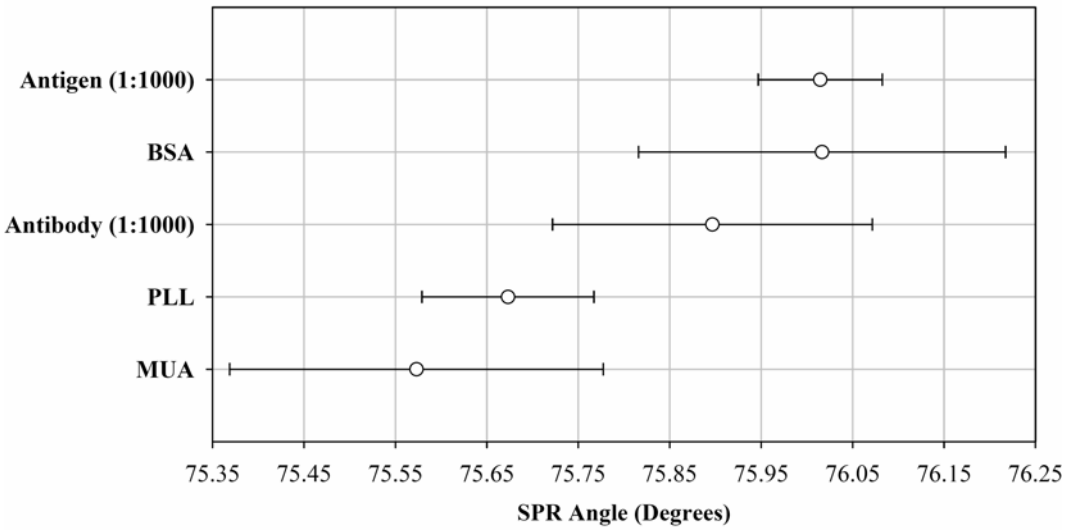

Figure 5.2 SPR angle of preparation of non-covalent (or positively charged) binding surface in PBS.

The chemical structure of PLL is shown below

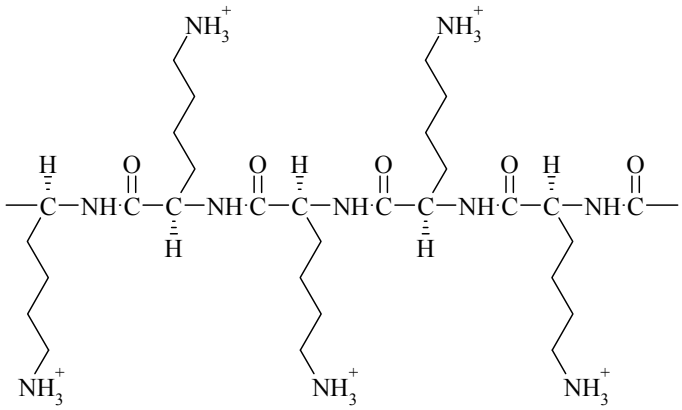

Figure 5.3 Structure of PLL

The NH_3^+ group of PLL is interacting with the carboxylic acid groups of the MUA and leaving the non interacting NH_3^+ for the next layer. PLL is known to bind to

tumor cells with high affinity both in vivo and vitro and can serve as a primary component in the construction of the binding layer for antibody and protein [80]. Bovine Serum Albumin (BSA) will be used as the blocking layer to prevent a non-specific binding which may arise from the free NH_3^+ group on the surface.

Table 5.2 The average SPR angle of non-covalent binding surface preparation in PBS.

	MUA	PLL	Antibody	BSA	Antigen
	75.573 ± 0.204°	75.673 ± 0.094°	75.897 ± 0.175°	76.017 ± 0.201°	76.015 ± 0.068°
P value		0.4269543530	0.0967782521	0.5894570820	0.9907186572	

5.2.1 Characterization of Non-Covalent Binding Surface with BSA Blocking by SPR Spectroscopy

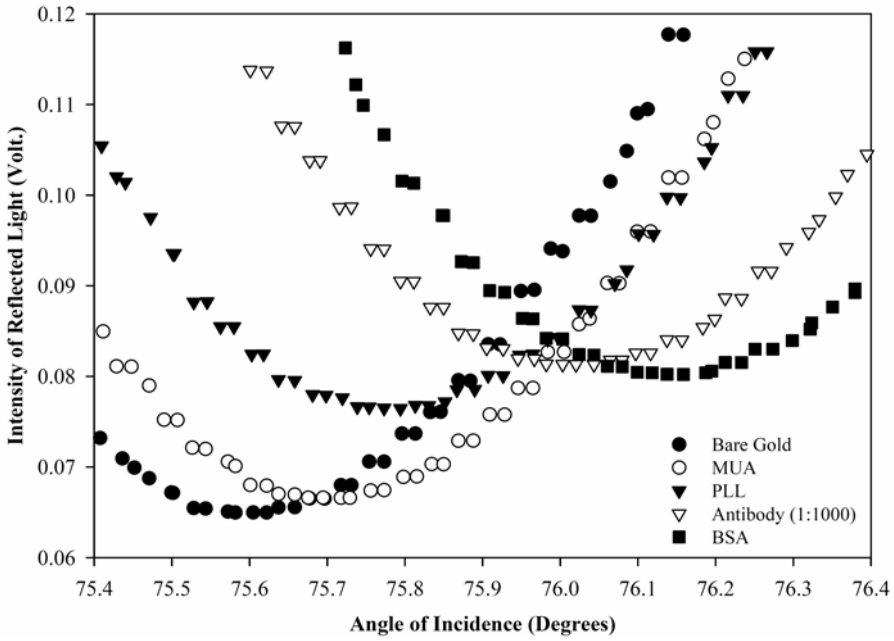

Figure 5.4 Expanded viewed of the experimental SPR curves for positively charged surface with BSA.

In Figure 5.4, the MUA was adsorbed onto the gold substrate from 1mM ethanolic solutions. The adsorption was done until no change in the SPR angle was observed, around 6 hours 35 minutes. The film was rinsed with deionized water (DI water) and phosphate-buffered saline (PBS) in order to wash physisorbed. PLL,

antibody, and BSA were sequentially adsorbed onto the MUA monolayer with equilibrated time of 35, 39, and 33 minutes, respectively. The sample was washed with PBS. 1 μL of rabbit anti-*Leptospira* antibodies were diluted in 1000 μL of PBS solution and will be used in this study. Various dilutions of Leptospiral samples were incubated onto the surface for 1 hour. All of the results are shown in Figure 5.5.

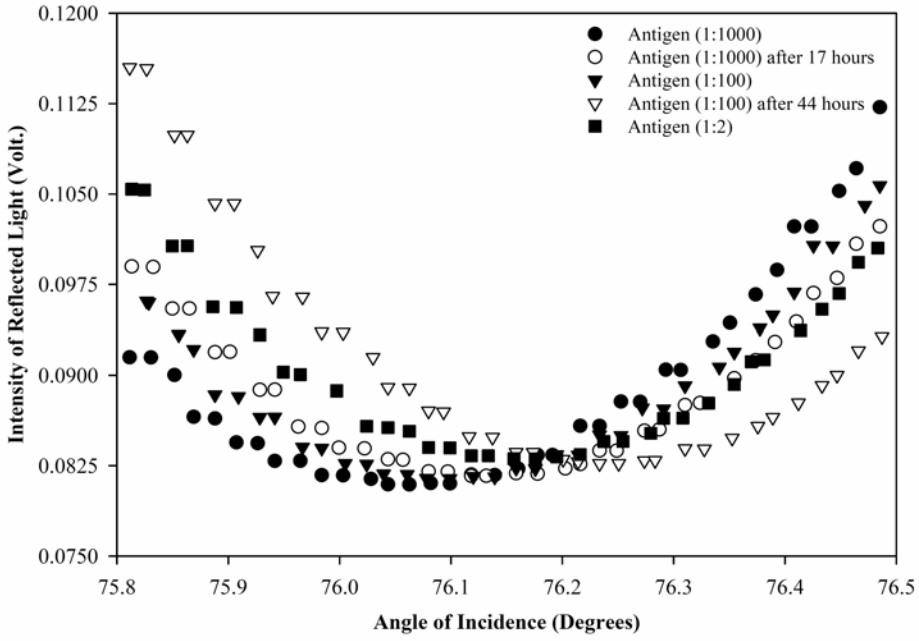

Figure 5.5 The SPR curves for antigen adsorption at different dilution. The film was washed with PBS and left for a measurement.

Antigen solution consists of canicola serovar at various dilution in PBS which are 1000, 100, and 2 μL, Figure 5.5. The change of the SPR angle is increased as the equilibration time is increased. These phenomena were caused by aggregation of the antigen on the sensor surface. In Figure 5.5 an increase of the antigen concentration also leads to the further shift of the SPR angle. For example, in the dilution of 1:1000 (black circle), 1:100 (black triangle down), and 1:2 (black square) of antigen sample give the SPR angles of 76.063°, 76.099°, and 76.176°, respectively. This is due to a greater number of the antigen is adsorbed on the surface.

5.2.2 Uniformity of Sensor Surface

The shifted of SPR angle depends on the changed of the optical property, the refractive index or thickness, of the film. On the other side, it depends on the concentration or mass of substance, which is attached onto the gold surface. The uniformity of the film can be observed by varying of the detecting position.

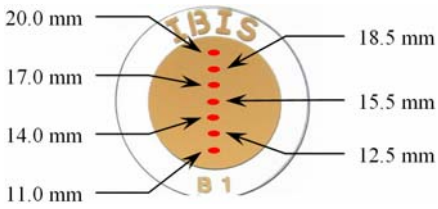

Figure 5.6 Position of detecting.

The reference position is at 15.5 mm which is located at the middle of the surface. The measurements were done along the line perpendicular to the set up. Those are labeled as 11.0, 12.5, 14.0, 15.5, 17.0, 18.5, and 20.0 mm. The results are shown in Table 5.3.

Table 5.3 The value of SPR angles.

		BSA	**Antigen (1:1000)**
11.0 mm	SPR Angle	75.949 ± 0.023°	75.935 ± 0.016°
	P Value	0.1001916027	
12.5 mm	SPR Angle	75.937 ± 0.039°	75.925 ± 0.007°
	P Value	0.2902346333	
14.0 mm	SPR Angle	76.078 ± 0.013°	76.058 ± 0.022°
	P Value	0.0205050068	
15.5 mm	SPR Angle	76.099 ± 0.017°	76.084 ± 0.009°
	P Value	0.0209122020	
17.0 mm	SPR Angle	76.116 ± 0.005°	76.081 ± 0.014°
	P Value	1.592×10^{-7}	
18.5 mm	SPR Angle	76.058 ± 0.009°	75.973 ± 0.015°
	P Value	0	

Table 5.3 (cont.)

		BSA	Antigen (1:1000)
20.0 mm	SPR Angle	76.040 ± 0.006°	75.925 ± 0.006°
	P Value	0	

Table 5.3 shows the changed of the SPR angles. It is shown that the BSA shows a higher affinity toward the adsorption on the surface than antigen.

5.2.3 Characterization of Non-Covalent Binding Surface without Blocking Layer

A similar experiment was carried out without the blocking layer. The results are presented in Section 5.2.1 and 5.2.2. No adsorption was observed in this experiment after the antigen was flowed on the sensor surface, Figure 5.7.

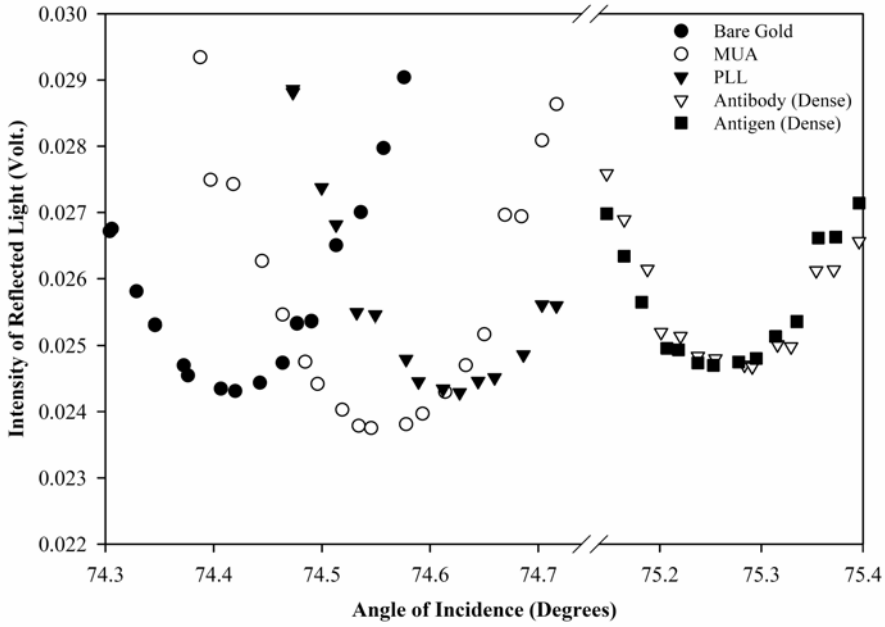

Figure 5.7 The experimental SPR curve for a antigen absorption with no BSA blocking in PBS.

The SPR angle of the gold surface is 74.420°. The MUA, PLL, antibody, and antigen were subsequently adsorbed onto the surface with an observed angle at 74.545°, 74.627°, 75.291°, and 75.253°, respectively. The lack of the binding of antigen onto antibody may cause by an improper orientation of the antibody on the sensor surface.

5.3 Covalent Binding Surface

The covalent binding was investigated in this experiment.

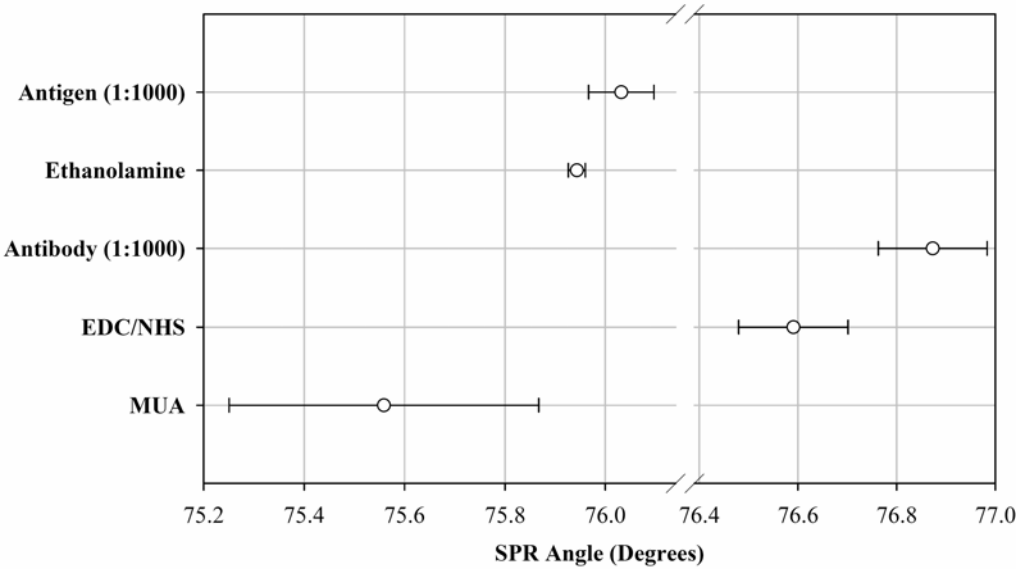

Figure 5.8 SPR angle of preparation of covalent (or negatively charged) binding surface in PBS.

The covalently coupled antibody is stable and not subject to a solvent-mediated desorption. It also offers a possibility of reusing the sensors. In this study, an amine coupling is selected for antibody immobilization. The N-hydroxysuccinimide esters was introduced on the surface of self-assembled monolayer by the modification of carboxylic acid group with a mixture of *N*-(3-Dimethylaminopropyl)-*N*′-ethylcarbodiimide hydrochloride (EDC) and *N*-Hydroxysuccinimide (NHS). The activated NHS esters can react spontaneously with amines of the antibody to form an amide linkage. After coupling reaction of antibody to activated surface, ethanolamine was used to deactivate the unreacted esters. An illustration of the immobilization procedures is shown in Figure 4.24 [82].

Table 5.4 The average SPR angle of covalent binding surface preparation in PBS.

	MUA	EDC/NHS	Antibody	Ethanolamine	Antigen (1:1000)
SPR Angle	75.559 ± 0.308°	76.591 ± 0.111°	76.873 ± 0.110°	75.943 ± 0.017°	76.032 ± 0.065°
P value		0	0.0010855234	0	61×10^{-10}

5.3.1 Characterization of Covalent Binding Surface by SPR Spectroscopy

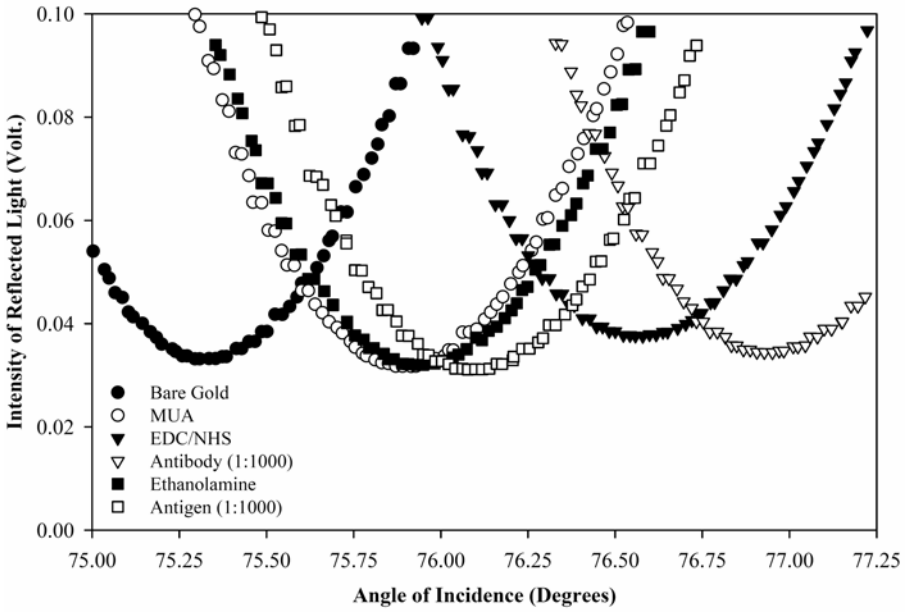

Figure 5.9 Expanded views of the experimental SPR curves for negatively charged surface with BSA blocking in PBS.

The MUA monolayers were self-assembled onto the gold film from 1mM ethanolic solutions for 8 hours. The film was rinsed with deionized water (DI water) and phosphate-buffered saline (PBS). The mixture of EDC and NHS, antibody, ethanolamine, and antigen were adsorbed onto the MUA monolayer by equilibrate the solution on the substrate for 22 hours, 6 hours, 56 minutes, and 19 hours 36 minutes, respectively. The substrated was rinsed with PBS every time when the solution was changed. Antibody and antigen used these experiments were diluted by 1000 μL of PBS with 1 μL of rabbit anti-*Leptospira* antibodies, and canicola serovar, *L. interrogans* species, respectively, Figure 5.9. The solution of antibody and antigen were prepared by pathology laboratory. After ethanolamine absorption, the SPR angle was decreased. This result is discussed in Section 5.3.3.

5.3.2 Surface Blocking Test

5.3.2.1 Antibody Adsorption onto Ethanolamine Film

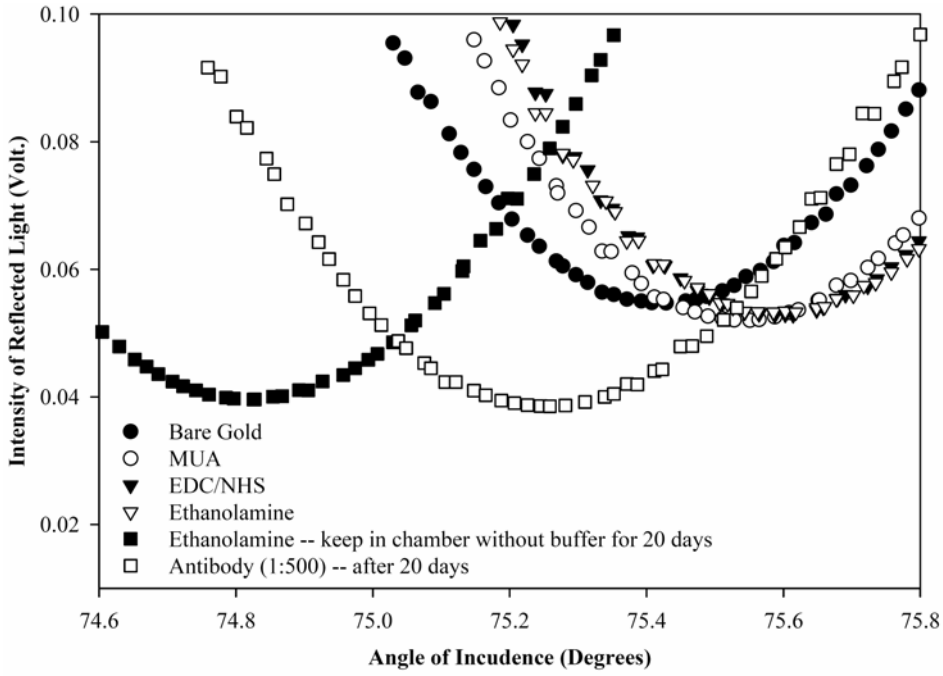

Figure 5.10 SPR curves of surface blocking preparation in DI water

The reactive NHS ester sites were blocked with ethanolamine to prevent a nonspecific adsorption. All SPR curves are reported in Figure 5.10 where the adsorptions were measured against DI water background. The sample was dry and left in the air for 20 days in order to test the stability of the film. After that, the film was rinsed with PBS where the SPR angles changed from 75.618° (blank triangle down) to 73.358° (black square) was observed. It is possible that the ethanolamine layer still present on the NHS ester surface. The antibody was absorbed onto the ethanolamine layers that give rise to a shift in SPR angle. A shift of SPR angle of about 0.422° when compare with the SPR angle of the ethanolamine layers in PBS (blank triangle down), antibody layers in PBS (blank square). This result interprets as the antibody is adsorbed onto the ethanolamine layers.

5.3.2.2 Antigen Absorption onto Ethanolamine Film

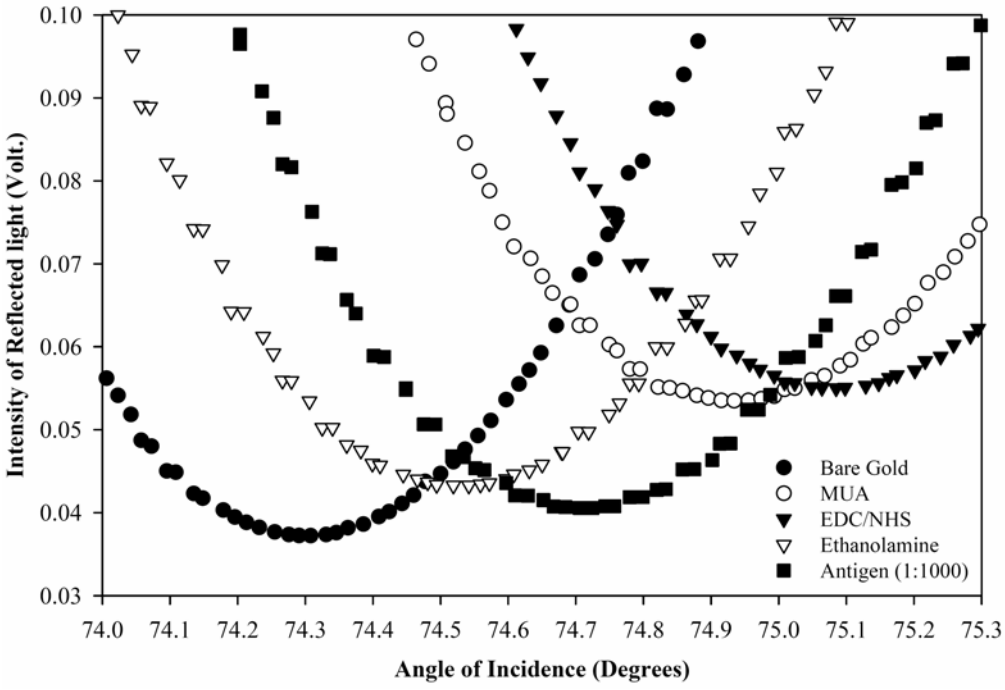

Figure 5.11 SPR curves of surface blocking preparation and testing of antigen absorption in PBS.

The activate surfaces are blocked with ethanolamine prior to immersing in the antigen. It was done in order to test for the resistant of the ethanolamine layer to a nonspecific binding. The SPR angle is shifted from 74.519° (blank triangle down) to 75.986° (black square). This indicates that the antigen can be adsorbed onto the ethanolamine layers. This may be due to an incomplete coverage of ethanoamine on the surface.

5.3.3. Process of Associations

Figure 5.12 depicts the changed of SPR angle as a function of time. It was found that the adsorption of 1 μL of antibody which are diluted in 1000 μL of PBS reaches saturation after 3.5 hours at room temperature. One intriguing observation is the stepwise nature of the adsorption curve where several plateaus were observed. This may originate from a layer-by-layer adsorption of the antibody which gives rises to the multilayer.

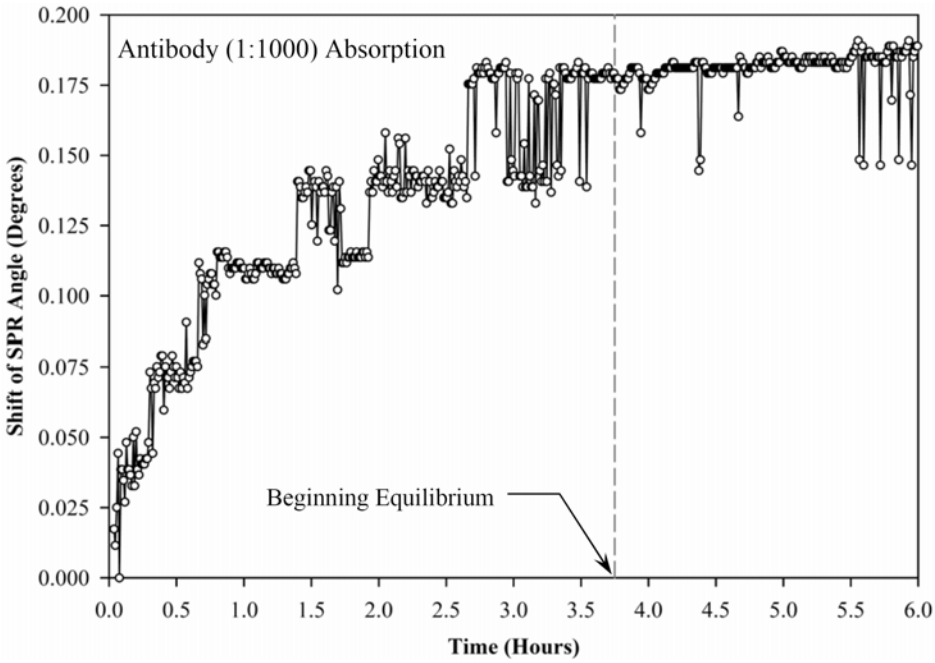

Figure 5.12 The absorption kinetic of the antibody onto the reactive NHS ester layers.

After antibody was adsorbed onto the reactive NHS ester layers, the surface was rinsed with PBS. The remaining reactive NHS ester sites were blocked with ethanolamine. The process of the ethanolamine association is shown in Figure 5.13.

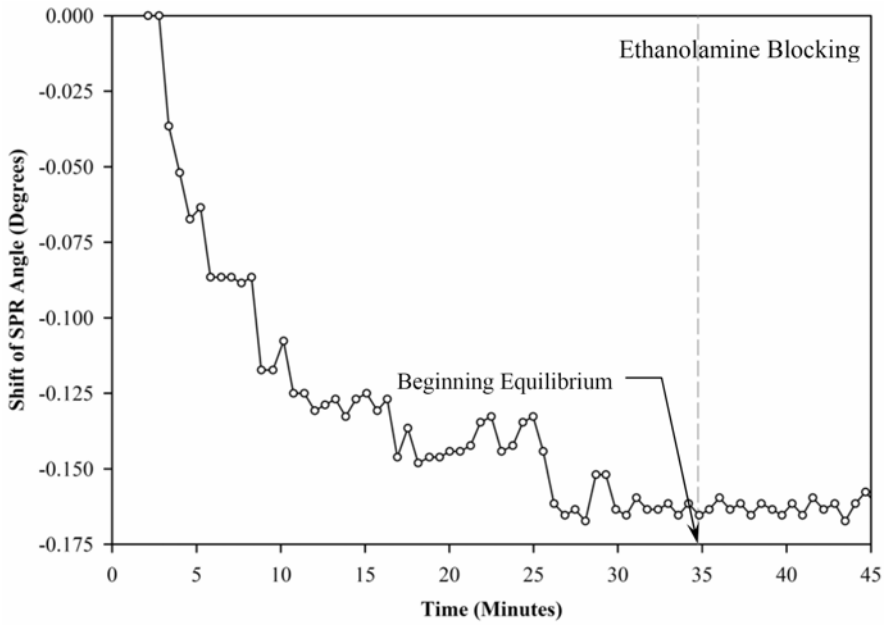

Figure 5.13 The adsorption kinetic of ethanolamine to passivate an unreacted carboxyl groups.

The shift of SPR angle decreases as the ethanolamine was adsorbed onto the NHS ester sties. This is not expected; however, the result is consistent with the literatures [81, 83, 84], Figure 5.14. This is possible that there is a changed in the refractive index of the film to counteract the changed in the film thickness.

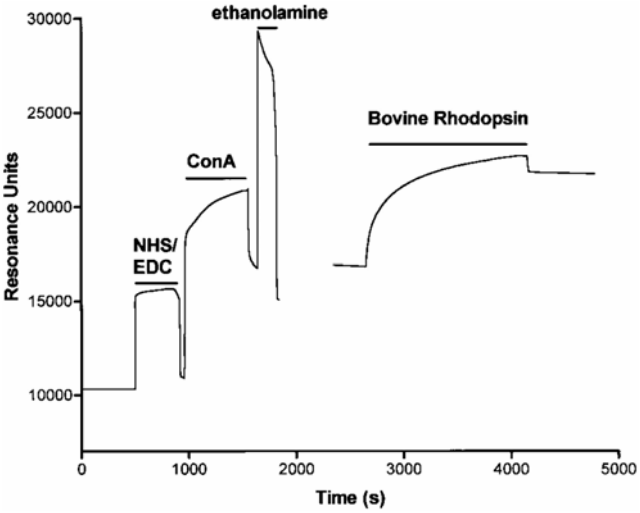

Figure 5.14 Immobilization of rhodopsin by binding to concanavalin A (ConA) [84].

The antigen was tested against the antibody surface. The association process of antigen is shown in Figure 5.15.

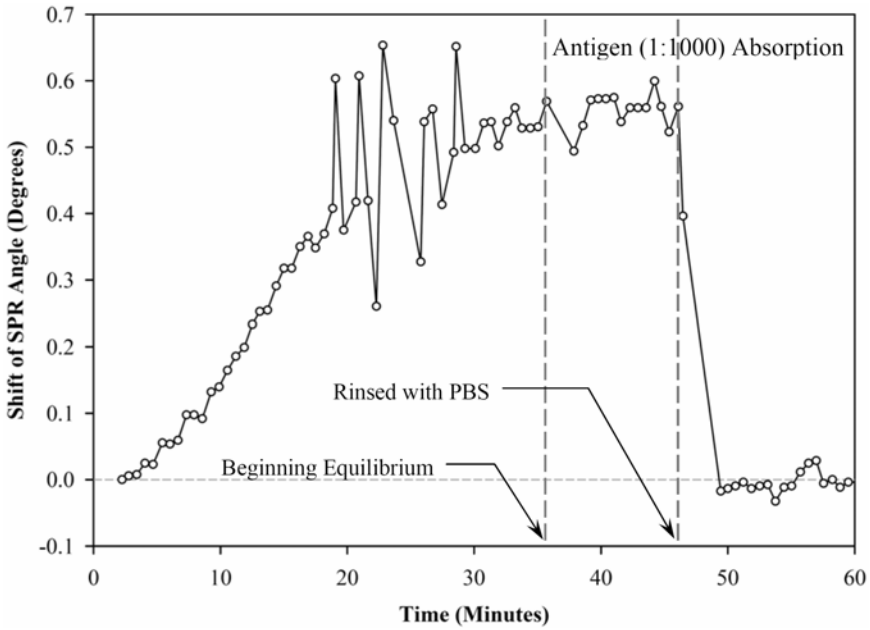

Figure 5.15 The adsorption kinetic of the antigen onto the specific surface.

5.5 Characterization of Non-Covalent Binding Surface by Contact Angle Measurement and Scanning Probe Microscope

5.5.1 Hydrophobicities Analysis

Contact angle is used for the surface characterization. The contact angle of films were measured, with a homemade instrument, and listed in Table 5.5.

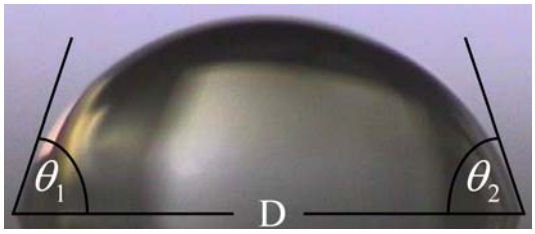

Figure 5.16 The photography of the water drop on the surface specimens. The contact angles, are left and right hand side of the base of the water drop, are represented by θ_1 and θ_2, respectively. The width of the water drop is represented by "D".

The contact angle measurement was carried out for the non-covalent binding [72]. A bare gold surface exposed to a solution of 10 mM MUA for 39 hours, rinsed with water, and followed by PBS. The film was then immersed into a solution of 100 μg/mL of PLL for 97 minutes in 0.05 M Na_2CO_3 buffered to a pH 9.5. The surface was exposed to 1 μL of antibody for 73 minutes in 200 μL of PBS for the last treatment.

Table 5.5 The value of the contact angles of the water drop on the several surface specimens.

	Bare Gold	**MUA layer**	**PLL layer**
θ_1	77.5 ± 2.4°	64.0 ± 2.2°	53.7 ± 2.9°
P value	4.22×10^{-8}	1.2656×10^{-6}	
θ_2	77.8 ± 1.6°	63.7 ± 2.2°	55.1 ± 3.3°
P value	3.3×10^{-9}	2.66877×10^{-5}	
D (mm)	2.82 ± 0.09	3.23 ± 0.05	3.43 ± 0.09
P value	6.59×10^{-8}	1.045283×10^{-4}	

5.5.2 Atomic Force Microscopy Analysis

The microscope "SPI3800 Probe Station" with "SPA-400 Multi-Function Unit" from "SII NanoTechnology Inc." with a non-contact (tapping) mode was used for this study [85]. The atomic force microscopy (AFM) measures the topography by detecting the forces between the tip and the sample. It can be applied to any surface but has proved to be a great tool on insulating surface and is a surface-sensitive instrument capable of imaging biological samples at nanometer resolution in all environments including liquids. The sensitivity of the AFM cantilever, to forces in the pico Newton range, has been exploited to measure breakaway forces between biomolecules and to measure folding-unfolding forces within single proteins [86, 87].

Previously, the bare gold surface was tested by non-contact mode as in Figure 5.17. A left panel shows the bare gold surface imaged. A top-right panel shows the cross section of the surface from the line-plots traces as in the left panel (Figure 5.17). A table in bottom-right panel shows the information of the surface sample from line-plots traces.

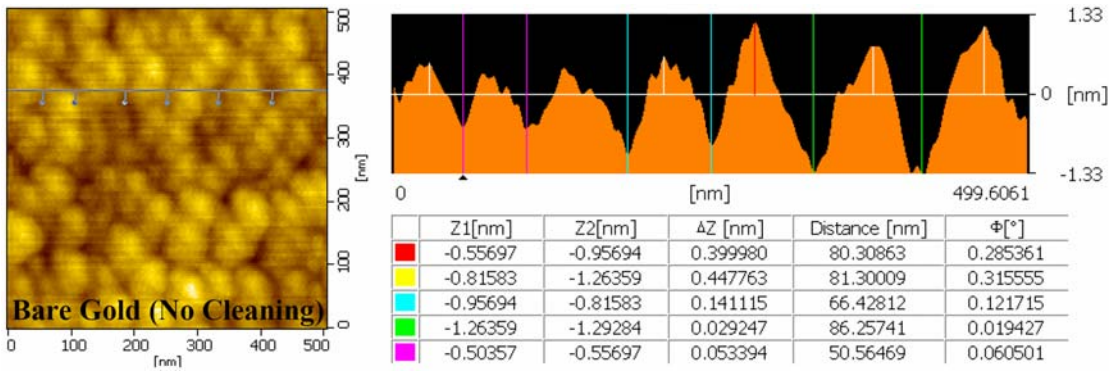

	Z1[nm]	Z2[nm]	ΔZ [nm]	Distance [nm]	Φ[°]
	-0.55697	-0.95694	0.399980	80.30863	0.285361
	-0.81583	-1.26359	0.447763	81.30009	0.315555
	-0.95694	-0.81583	0.141115	66.42812	0.121715
	-1.26359	-1.29284	0.029247	86.25741	0.019427
	-0.50357	-0.55697	0.053394	50.56469	0.060501

Figure 5.17 The surface analyze panel of the bare gold surface.

The gold surface was rinsed with absolute ethanol and DI water and dried with nitrogen prior to the scanning. Figure 5.18 shows the clean gold surface imaged obtained from a non-contact mode. The gold surface shows a roughness which is originated from the evaporation process. The grain size is around 7.738 nm^2.

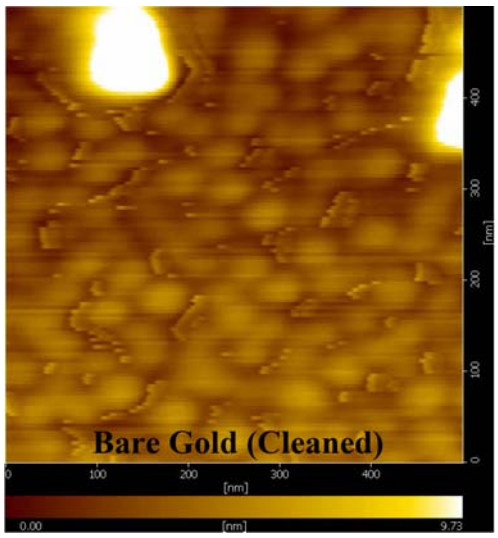

Figure 5.18 AFM images recorded in air under non-contact mode of the clean gold surface.

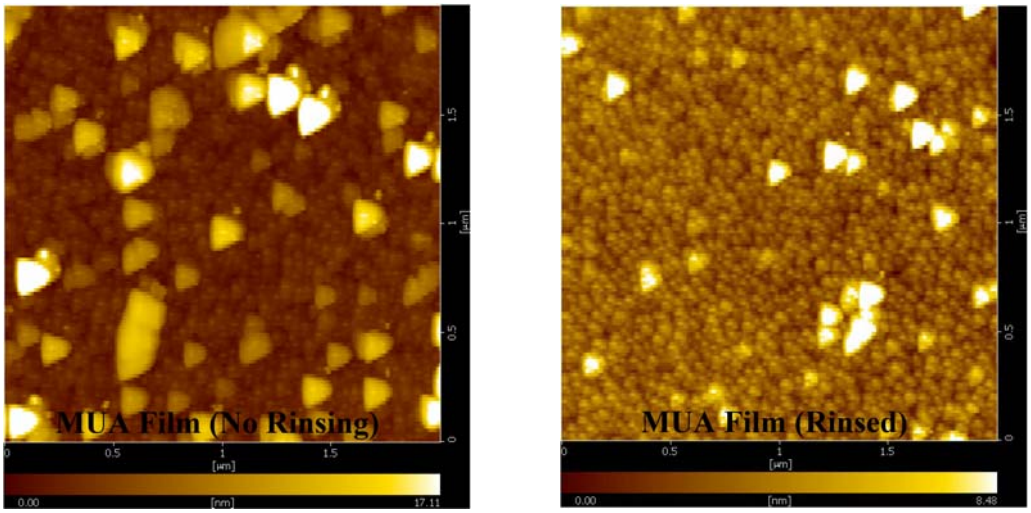

Figure 5.19 MUA absorbed to gold, imaged in air with non-contact mode.

The MUA monolayers were self-assembled onto the gold films. After the MUA solutions were removed from the surface, the MUA films were probed by AFM under a non-contact mode as in the left panel (Figure 5.19). The films were rinsed with DI water and PBS. The maximum height as in Figure 5.19 changed from 17.11 nm (before rinsing) to 8.48 nm (after rinsing). The film after rinsed with the PBS shows clearer image of the surface. The grain of the gold is still preserved. This is not

surprised because the MUA is about 20 Å in length while the grain size of MUA is around 80 $Å^2$.

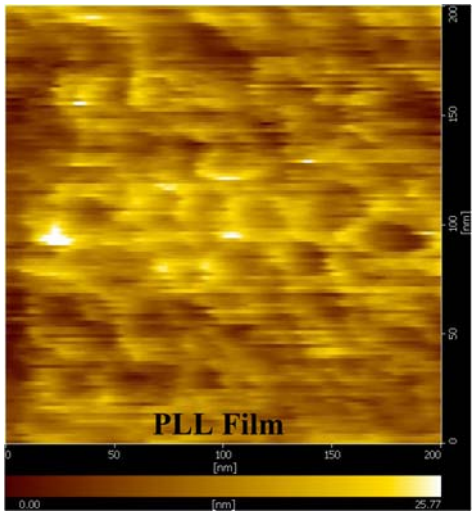

Figure 5.20 AFM images of PLL films

The PLL was adsorbed onto the MUA monolayers. Figure 5.20 shows the PLL layers on MUA layers after rinsing with DI water. The adsorption of the PLL was analyzed by contact angle measurement and AFM. A clear changed in the surface morphology was observed after PLL treatment. The grain size of the gold is no longer observed. The image represents the PLL chain lying on the MUA layer. It is clear that it is not uniform throughout the surface. This may be due to the nature of the polymer where the conformation change is needed to be taken into a consideration.

5.6 Conclusion

Two methods of antibody immobilization were used in this study. The first method is based on an ionic interaction, or non-covalent binding. The surface modification was made by a sequential adsorption of the MUA, PLL, and antibody on the gold coating glass slide. The non specific site was blocked using BSA. No change in SPR signal was detected after adding the antigen onto the sensor surface. This indicates that the antibody and antigen molecules did not have interaction or an appropriate coating of the interactive molecules.

The second method is based on the covalent binding where the antibody was covalent attached to the sensor surface. A changed in the SPR signal was detected when the antigen was flowed through the sensor surface. The role of the surface blocking still needs a further investigation to maximize the reaction condition and its coverage.

REFERENCES

1 John M. Walker, and Ralph Rapley. Molecular biology and biotechnology. 4th ed. Country: Cambridge; 2000.

2 Kim R. Rogers. Principles of affinity-based biosensors. Molecular biotechnology. 2000; 14: 109-29.

3 Ti.com [homepage on the Internet]. United States: Texas Instruments Inc.; [cited 2004 Dec 20]. Available from: http://www.ti.com/.

4 Xantec.com [homepage on the Internet]. Hong Kong: XanTec bioanalytics; [cited 2004 Dec 20]. Available from: http://www.xantec.com/.

5 Biotul.de [homepage on the Internet]. Germany: Measurement Laboratory; [cited 2003 Nov 4]. Available from: http://www.biotul.de/.

6 Affinity-sensor.com [homepage on the Internet]. [cited 2004 Jun 22]. Available from: http://www.affinity-sensor.com/iasys.htm/.

7 Joseph Sambrook, and David W. Russell. Molecular cloning: a laboratory manual, 3rd ed., New York: Cold Spring Harbor; 2001.

8 Kit.nl [homepage on the Internet]. The Netherlands: Royal Tropical Institute; [cited 2004 Nov 22]. Available from: http://www.kit.nl/biomedical _research /html/ leptospirosis_reference.a/.

9 Saranya Narayan. Diagnosis of early Leptospirosis [monograph on the Internet]. 2000 [cited 2003 Sep 17]. Available from: http://www.caving.org.uk /wdic/-madras2000.

10 Chem.ch.huji.ac.il [homepage on the Internet]. Israel: Hebrew University of Jerusalem; [cited 2004 Jun 22]. Available from: http://chem.ch.huji.ac.il /~eugeniik/spr.htm.

11 I.Pockrand. Surface plasma oscillations at silver surfaces with thin transparent and absorbing coatings. Surface science. 1978; 72: 577-88.

12 Rebecca J. Green, Richard A. Frazier, Kevin M. Shakesheff, Martyn C. Davies, Clive J. Roberts, and Saul J.B. Tendler. Surface plasmon resonance

analysis of dynamic biological interactions with biomaterials. Biomaterials. 2000; 21: 1823-35.

13 Charles Kittel. Introduction to solid state physics, 8th ed. New Jersey: John Wiley & Sons; 1996.

14 Home.hccnet.nl [homepage on the Internet]. [cited 2004 Nov 14]. Available from: http://home.hccnet.nl/ja.marquart/SPRpages.htm.

15 Wolfgang Knoll. Interfaces and thin films as seen by bound electromagnetic waves. Annu. Rev. Phys. Chem. 1998; 49: 569-638.

16 Xiao Caide, and Sen-Fang Sui. Characterization of surface plasmon resonance biosensor. Sensors and actuators B. 2000; 66: 174-7.

17 P. Anton van der Merwe. Surface plasmon resonance. Medical research council. In press 2000.

18 Kenneth W. Whitten, Raymond E. Davis, M. Larry Peck, and George G. Stanle. General chemistry. 7th ed. London: Brooks/Cole--Thomson Learning; 2004.

19 Product information; Biacore® 3000. [database on the Internet]. Switzerland: Biacore [cited 2004 Jan 29]. Available from: http://www.biacore.com.

20 Steve Russo, and Mike Silver. Introductory chemistry. 2nd ed. London: Banjamin Cummings; 2002.

21 Kretchmann E. The determination of the optical constants of metals by excitation of surface plasmons. Z Phys 1971; 241: 313-24.

22 Cheng YL, Darst SA, and Robertson CR. Bovine serum albumin and desorption rates on solid surfaces with varying surface properties. J Colloid Interface Sci 1987; 118: 212-23.

23 Peter Atkins, and Julio de Paula. Atkins' physical chemistry, 7th ed. New York: Oxford University Press; 2002.

24 Matthias Niggemann, Andreas Katerkamp, Maria Pellmann, Peter Bolsmann, Jörg Reinbold, and Karl Cammann. Remote sensing of tetrachloroethene with a micro-fiber optical gas sensor based on surface plasmon resonance spectroscopy. Sensors and Actuators B. 1996; 34: 328-33.

25 N.E. Agbor, J.P. Cresswell, M.C. Petty, and A.P. Monkman. An optical gas sensor based on polyaniline Langmuir-Blodgett films. Sensors and Actuators B. 1997; 41: 137-41.

26 Wolfgang Knoll, Manfred Zizlsperger, Thorsten Liebermann, Stefan Arnold, Antonella Badia, Martha Liley, Darko Piscevic, Franz-Josef Schmitt, and Jürgen Spinke. Streptavidin arrays as supramolecular architectures in surface plasmon optical sensor formats. Colloids and Surfaces A: Physicochemical and Engineering Aspects. 2000; 161: 115-137.

27 A. Abdelghani, J.M. Chovelon, N. Jaffrezic-Renault, C. Veilla, and H. Gagnaire. Chemical vapor sensing by surface plasmon resonance optical fiber sensor coated with fluoropolymer. Analytica Chimica Acta. 1997; 337: 225-32.

28 Shozo Miwa, and Tsuyoshi Arakawa. Selective gas detection by means of surface plasmon resonance sensors. Thin Solid Films. 1996; 281-82: 466-68.

29 W.P. Hu, S-J Chen, K.-T. Huang, J.H. Hsu, W.Y. Chen, G. L. Chang, and K.-A. Lai. A novel ultrahigh-resolution surface plasmon resonance biosensor with an Au nanocluster-embedded dielectric film. Biosensors and Bioelectronics. 2004; 19: 1465-71.

30 G. A. Farnan, G. F. Cairns, P. Dawson, S. M. O'Orey, M. P. McCurry, and D. C. Walmsley. Mid-infrared *a-b* plane response of $YBa_2Cu_3O_{7-\delta}$ as a function of doping and temperature determined by attenuated total reflection. Physica C. 2004; 403: 67-85.

31 Xiaodi Su, and Jian Zhang. Comparison of surface plasmon resonance spectroscopy and quartz crystal microbalance for human IgE quantification. Sensors and Actuators B. 2004; 100: 309-14.

32 Bo Liedberg, Claes Nylander, and Ingemar Lundstrom. Surface plasmon resonance for gas detection and biosensing. Sensors and Actuators. 1983; 4: 299-304.

33 Cheskis BJ, Karathanasis S, and Lyttle CR. Estrogen receptor ligands modulate its interaction with DNA. J Biol Chem. 1997; 272: 11384–91.

34 De Crescenzo G, Grothe S, Lortie R, Debanne MT, and O'Connor-McCourt M. Real-time kinetic studies on the interaction of transforming growth

factor α with the epidermal growth factor receptor extracellular domain reveal a conformational change model. Biochem. 2000; 39: 9466–76.

35 Morgan CL, Newman DJ, Cohen SBA, Lowe P, and Price CP. Real-time analysis of cell surface HLA class I interactions. Biosens Bioelectron. 1998; 13: 1099–105.

36 Nelson RW, Krone JR, and Jansson O. Surface plasmon resonance biomolecular interaction analysis mass spectrometry: 1. Chip-based analysis. Anal Chem. 1997; 69: 4363–8.

37 Nelson RW, Krone JR, and Jansson O. Surface plasmon resonance biomolecular interaction analysis mass spectrometry: 2. Fiber optic-based analysis. Anal Chem. 1997; 69: 4369–74.

38 Nelson RW, Nedelkov D, and Tubbs KA. Biomolecular interaction analysis mass spectrometry. BIA/MS can detect and characterize proteins in complex biological fluids at the low-to subfemptomole level. Anal Chem. 2000; 72: 404A–11A.

39 Polzius R, Dießel E, Bier FF, and Bilitewski U. Real-time observation of affinity reactions using grating couplers: determination of the detection limit and calculation of kinetic rate constants. Anal Biochem. 1997; 248: 269–76.

40 Daniels PB, Deacon JK, Eddowes MJ, and Pedley DG. Surface plasmon resonance applied to immunosensing. Sensors Actuators. 1988; 15: 11-8.

41 Morgan H, Taylor DM, and D'Silva C. Surface plasmon resonance studies of chemisorbed biotin streptavidin multilayers. Thin Solid Films. 1992; 209: 122-6.

42 Dubs M-C, Altschuh D, Van Regenmortel MHV. Interaction between viruses and monoclonal antibodies studied by surface plasmon resonance. Immunol Lett. 1991; 31: 59-64.

43 Altschuh D, Dubs M-C, Weiss E, Zeder-Lutz G, and Van Regenmortel MHV. Determination of kinetic constants for the interaction between a monoclonal antibody and peptides using surface plasmon resonance. Biochemistry 1992; 31: 6298-304.

44 Polymenis M, and Stollar BD. Domain interactions and antigen binding of recombinant anti-Z-DNA antibody variable domains. The role of heavy

and light chains measured by surface plasmon resonance. J Immunol. 1995; 154: 2198-208.

45 Johne B, Gadnell M, and Hansen K. Epitope mapping and binding kinetics of monoclonal antibodies by real-time biospecific interaction analysis using surface plasmon resonance. J Immunol Meth. 1993; 160: 191-8.

46 Silin VI, Balcytis GA, Zhizhin GN, and Yakovlev VA. Application of surface electromagnetic wave and surface plasmon techniques in a protein adsorption study and sensor construction. Vib Spectrosc. 1993; 5: 133-42.

47 Silin V, Weetall H, and Vanderah DJ. SPR studies of the nonspecific adsorption kinetics of human IgG and BSA on gold surfaces modified by self-assembled monolayers (SAMs). J Colloid Interface Sci. 1997; 185: 94-103.

48 Striebel Ch, Brecht A, and Ganglitz G. Characterization of biomembranes by spectral ellipsometry, surface plasmon resonance and interferometry with regard to biosensor application. Biosens Bioelectron. 1994; 9: 139-46.

49 Chen X, Shakesheff KM, and Davies MC, et al. Degradation of a thin polymer film studied by simultaneous in situ atomic force microscopy and surface plasmon resonance analysis. J Phys Chem. 1995; 99: 11537-42.

50 Chen X, Davies MC, Roberts CJ, Shakesheff KM, Tendler SJB, and Williams PM. Dynamic surface events measured by simultaneous probe microscopy and suface plasmon detection. Anal Chem. 1996; 68: 1451-5.

51 Frazier RA, Davies MC, and Matthijs G, et al. In situ surface plasmon resonance analysis of dextran monolayer degradation by dextranase. Langmuir. 1997; 13: 7115-20.

52 Green RJ, Corneillie S, and Davies MC, et al. The investigation of the hydration kinetics of novel PEO containing polyurethanes. Langmuir. 2000; 16: 2744-50.

53 Constantine A. Balanis. Advanced engineering electromagnetics. New York: John Wiley & Sons; 1989.

54 Walter Benenson, John W. Harris, Horst Stocker, and Holger Lutz. Handbook of physics. New York: Springer; 2002.

55 David J. Griffiths. Introduction to electrodynamics. 3rd ed. New Jersey: Prentice-Hall International; 1999.

56 Eugene Hecht. Optics. 4th ed. San Francisco: Addison Wesley; 2002.

57 Matthew N. O. Sadiku. Elements of electromagnetics. 2nd ed. New York: Oxford University Press; 1995.

58 Masahiro Yamamoto. Surface plasmon resonance (SPR) theory: tutorial. Kyoto: Kyoto University; [cited 2004 Jul 20]. Available from: http://fm.ehcc.kyotou.ac.jp.

59 Max Born, and Emil Wolf. Principles of Optics: electromagnetic theory of propagation, interference and diffraction of light. 7th ed. London: Cambridge University Press; 2003.

60 Heinz Raether. Surface plasmon on smooth and rough surfaces and on gratings. Berlin: Springer-Verlag; 1988.

61 Fys.ou.dk [homepage on the Internet]. [cited 2003 May 5]. Available from: http://www.fys.ou.dk/Fys72/html/F72proj6.html.

62 Apswater.com [homepage on the Internet]. United States: APS Water Services Inc.; [cited 2005 Jan 5]. Available from: http://www.apswater.com.

63 Sigmaaldrich.com [homepage on the Internet]. United States: Sigma-Aldrich Co.; [cited 2004 Dec 30]. Available from: http://www.sigma aldrich.com/Help_Pages/Help_Welcome/Product_Search/Risk___Safety _Statements.html.

64 David L. Nelson, and Michael M. Cox. Lehninger: Principles of biochemistry. 4th ed. New York: W. H. Freeman and Company; 2005.

65 Ian R. Tizard. Immunology: An introduction. 4th ed. New York: Saunders College Publishing; 1995.

66 Abul K. Abbas, Andrew H. Lichtman, and Jordan S. Pober. Cellular and molecular immunology. 4th ed. W.B. London: Saunders company; 2000.

67 R.J. Green, J. Davies, MC Davies, C. J. Roberts, and S. J.B. Tendler. Surface plasmon resonance for real time in situ analysis of protein adsorption to polymer surfaces, Biomaterials. 1997; 18: 405-13.

68 Gsba.utmb.edu [homepage on the Internet]. United States: University of Texas Medical Branch; [cited 2005 Feb 10]. Available from: http://gsbs.utmb.edu/ microbook/ch035.htm.

69 Edward D. Frohlich. Ryoins' basic sciences review. 18th ed. Philadelphia: Lippincott Williams & Wilkins; 2001.

70 Solly Faine, and Ben Adler, Carole Bolin. Philippe Perolat. Leptospira and Leptospirosis. 2nd ed. Melbourne: MediSci; 1999.

71 Ibis-spr.nl [homepage on the Internet]. The Netherlands: IBIS Technologies bv; [cited 2003 Aug 16]. Available from: http://www.ibis-spr.nl/products/ spr/index.htm.

72 S. D. Gillmor, A. J. Thiel, T. C. Strother, L. M. Smith, and M. G. Lagally. Hydrophilic/Hydrophobic patterned surfaces as templates for DNA arrays. Langmuir. 2000; 16: 7223-8.

73 Xiao Caide, and Sen-Fang Sui. Numerical simulations of surface plasmon resonance system for monitoring DNA hybridization and protein-lipid film interactions. Eur Biophys J. 1999; 28: 151-7.

74 Marvin J. Weber. Handbook of laser. London: CRC Press; 2000.

75 Edmundoptics.com [homepage on the Internet]. United States: Edmund Optics Inc.; [cited 2005 Feb 9]. Available from: http://www.edmund optics.com/.

76 Naimotion.com [homepage on the Internet]. United States: National Aperture, Inc; [cited 2005 Mar 25]. Available from: http://www.naimotion.com/ index.htm.

77 Mellesgriot.com [homepage on the Internet]. United States: Melles Griot Inc.; [cited 2003 Dec 17]. Available from: http://www.mellesgriot.com/ products/ optics/mp_3_1.htm.

78 Robert H. Bishop. Learning with LabVIEW 6i. 2nd ed. New Jersey: Prentice Hall; 2001.

79 Encyclopedia masterflex vol.2. Illinois: Cole-Parmer instrument company; 2003.

80 Claire E. Jordan, Brian L. Frey, Steven Kornguth, and Robert M. Corn. Characterization of poly-L-lysine adsorption onto alkanethiol-

modulation Fourier transform infrared spectroscopy and surface plasmon resonance measurements. Langmuir. 1994; 10: 3642-8.

81 Paula Gomes, and David Andreu. Direct kinetic assay of interactions between small peptides and immobilized antibodies using a surface plasmon resonance biosensor. Journal of immunological Methods. 2000; 259: 217-30.

82 Renjun Pei, Zhiliang Cheng, Erkang Wang, and Xiurong Yang. Amplification of antigen-antibody interactions based on biotin labeled protein-Streptavidin network complex using impedance spectroscopy. Biosensors & Bioelectronics. 2001; 16: 355-61.

83 Xiaoqiang Cui, Fan Yang, Yufang Sha, and Xiurong Yang. Real-time immunoassay of ferritin using surface plasmon resonance biosensor. Talanta. 2003; 60: 53-61.

84 William A. CLARK, Xiaoying JIAN, Loren CHEN, and John K. NORTHUP. Independent and synergistic interaction of retinal G-protein subunits with bovine rhodopsin measured by surface plasmon resonance. Biochem. J. 2001; 358: 389-97.

85 Siint.com [homepage on the Internet]. Japan: SII NanoTechnology Inc.; [cited 2005 Mar 28]. Available from: http://www.siint.com/en/index.shtml.

86 Monet.physik.unibas.ch [homepage on the Internet]. Germany: University of Basel; [cited 2004 Jun 22]. Available from: http://monet.physik. unibas.ch/ ~hegner/.

87 A. Raab, W. Han, D. Badt, S. J. Smith-Gill, S. M. Lindsay, H. Schindler, and P. Hinterdorfer. Antibody recognition imaging by force microscopy. Nature biotechnology. 1999; 17: 902-5.

88 Shengfu Chen, Lingyun Liu, Jian Zhou, and Shaoyi Jiang. Controlling Antibody Orientation on Charged Self-Assembled Monolayers. Langmuir 2003; 19: 2859-64.

89 O. Ouerghi, A. Touhami, A. Othmane, H. Ben Ouada, C. Martelet, C. Frtigny, N. Jaffrezic-Renault. Investigating antibody-antigen binding with atomic force microscopy. Sensors and Actuators B 2002; 84: 167-75.

90 Beth Dawson, and Robert G. Trapp. Basic & clinical biostatistics. 3rd ed. Boston: McGraw-Hill; 2001.

91 Judith Green-McKenzie. Leptospirosis [monograph on the Internet]. United States: University of Pennsylvania School of Medicine; [cited 2005 Jun 16]. Available from: http://www.emedicine.com/EMERG/topic856.htm.

92 Valerie J. Easton, and John H. McColl. [monograph on the Internet]. United Kingdom: The Higher Education Funding Council for England; [cited 2005 May 3]. Available from: http://www.cas.lancs.ac.uk/glossary_v1.1/hyptest.html#pvalue

APPENDIX

APPENDIX A
NUMERICAL ANALYSIS OF SURFACE PLASMON RESONANCE

A.1 Three layer modeling

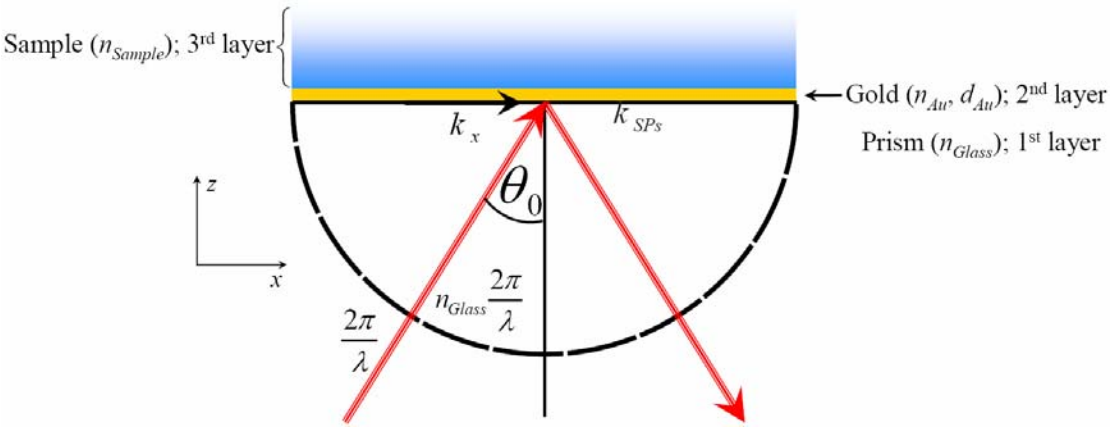

Figure A.1 A schematic view of the Kretschmann configuration.

A.1.1 SPR and minimal reflectance of three layer model

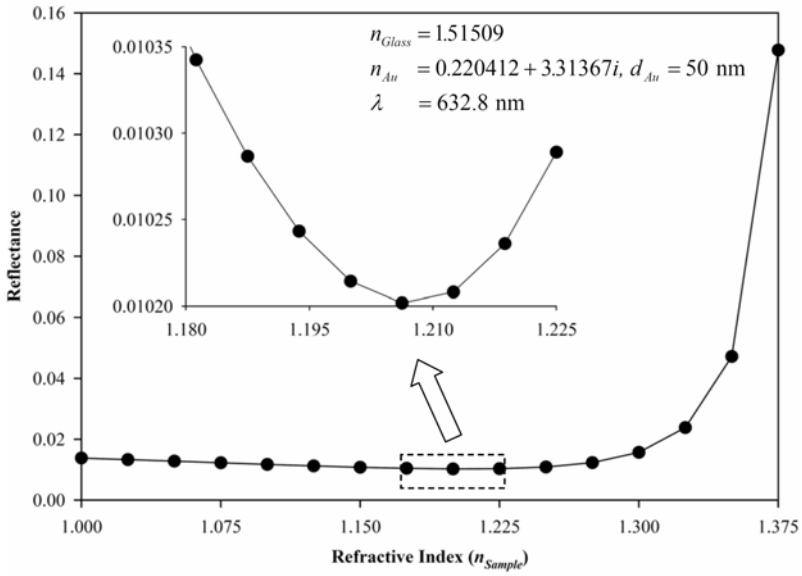

Figure A.2 Numerical analysis results of the effects of refractive index of the bulk medium (n_{Sample}) on minimal reflectance (R_{min}).

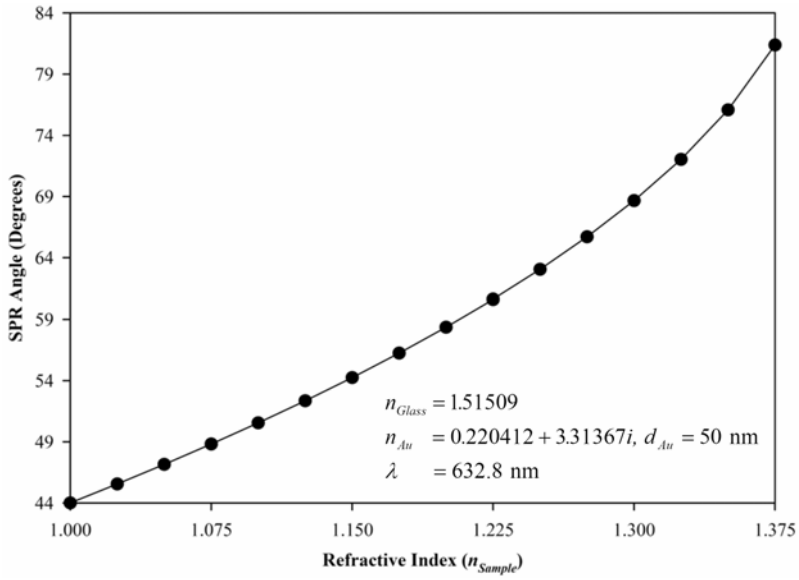

Figure A.3 Numerical analysis results of effects of the refractive index of the bulk medium (n_{Sample}) on SPR angle (θ_{SPR}).

Table A.1 Values of R_{min} and θ_{SPR} with n_{Sample} analyzed by calculation.

n_{Sample}	θ_{SPR} (°)	R_{min}
1.00000	44.0029	0.0138051
1.02500	45.5500	0.0132906
1.05000	47.1515	0.0127635
1.07500	48.8136	0.0122321
1.10000	50.5437	0.0117082
1.12500	52.3509	0.0112098
1.15000	54.2461	0.0107632
1.17500	56.2432	0.0104096
1.18125	56.7603	0.0103425
1.18750	57.2853	0.0102866
1.19375	57.8183	0.0102432

n_{Sample}	θ_{SPR} (°)	R_{min}
1.20000	58.3599	0.0102142
1.20625	58.9103	0.0102017
1.21250	59.4701	0.0102080
1.21875	60.0397	0.0102360
1.22500	60.6197	0.0102890
1.25000	63.0548	0.0108408
1.27500	65.7121	0.0122964
1.30000	68.6644	0.0156652
1.32500	72.0373	0.0238017
1.35000	76.0840	0.0471789
1.37500	81.3839	0.1477570

A.1.2 SPR experimental three layer modeling

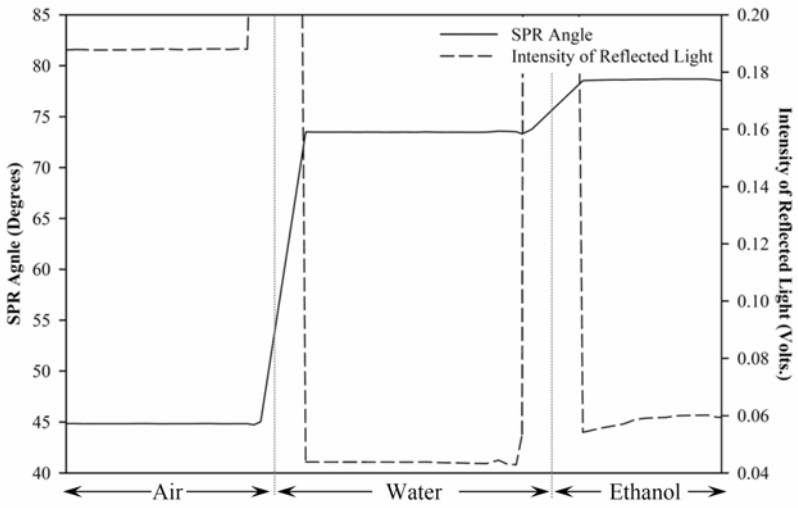

Figure A.4 The effects of n_{Sample} on R_{min} and θ_{SPR} according to experimental results.

A.2 Four layer modeling

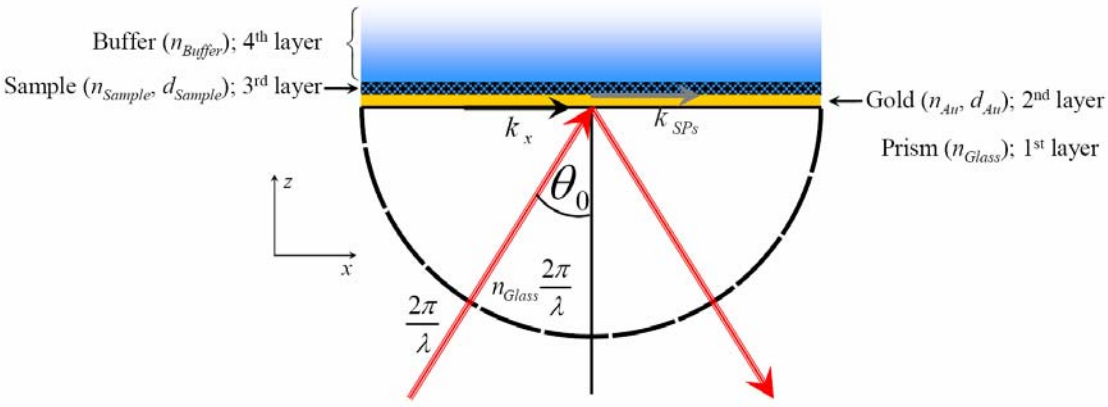

Figure A.5 A schematic view of the SPR system consisting of sample layer with thickness d_{Sample} and refractive index n_{Sample} under the bulk layer (buffer) with refractive index n_{Buffer}.

A.2.1 Thickness variation of lower refractive indices

A.2.1.1 Modeling results

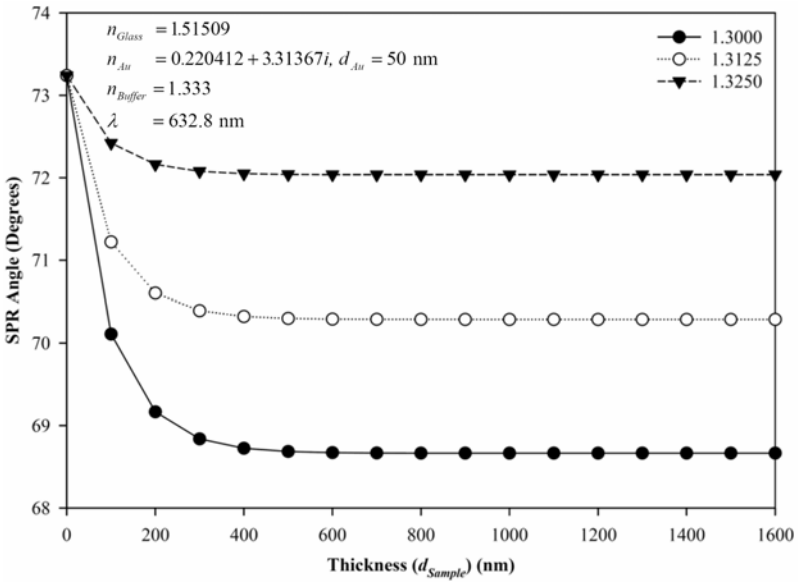

Figure A.6 The effect of d_{Sample} under variable values of refractive index n_{Sample}, are less than n_{Buffer}, on θ_{SPR} according to numerical analysis.

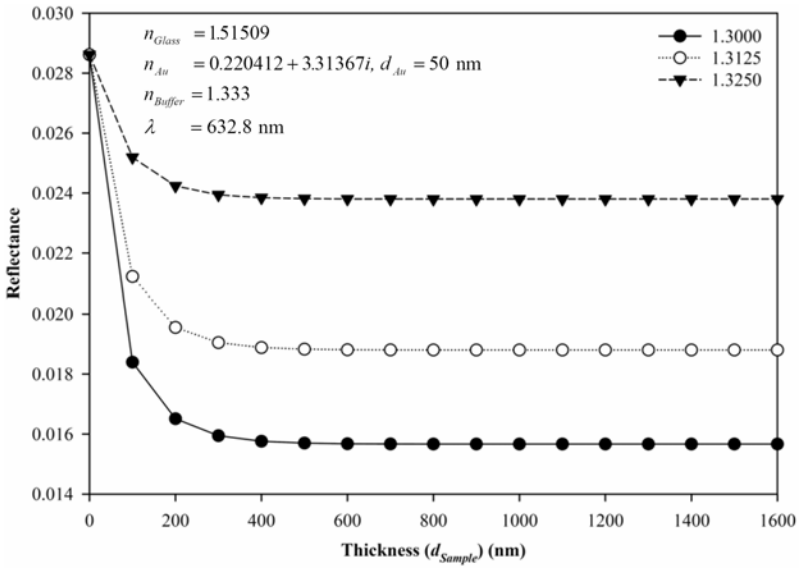

Figure A.7 The effect of d_{Sample} under variable values of refractive index n_{Sample}, are less than n_{Buffer}, on R_{min} according to numerical analysis.

A.2.1.2 Experimental results

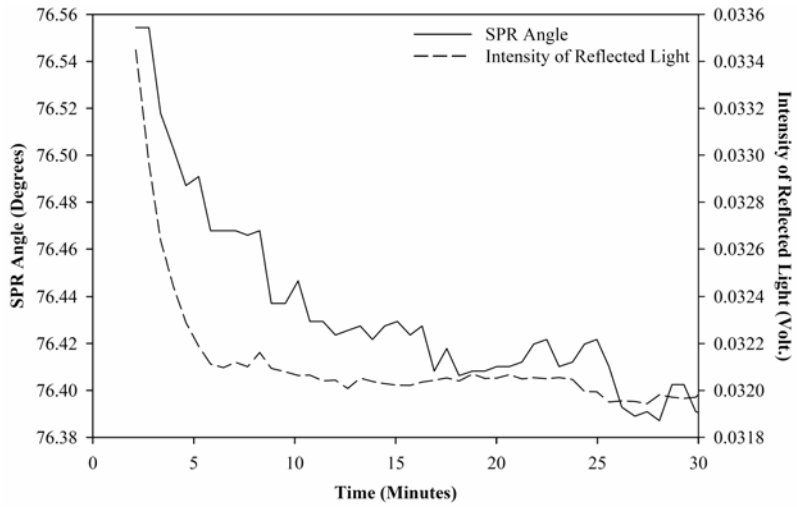

Figure A.8 The process of ethanolamine adsorption.

An increase of the sample layer thickness (d_{Sample}) was shown as Figure A.6 and A.7. This is possible that the refractive index of ethanolamine is less then the buffer that is the 75 mM aqueous solutions.

A.2.2 Thickness variation of upper refractive indices

A.2.2.1 Modeling results

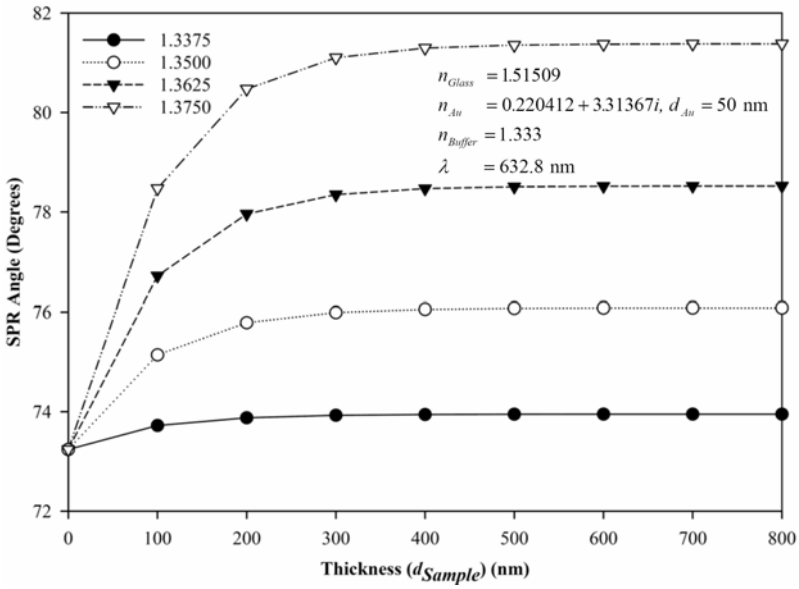

Figure A.9 The effect of d_{Sample} under variable values of refractive index n_{Sample}, are more than n_{Buffer}, on θ_{SPR} according to numerical analysis.

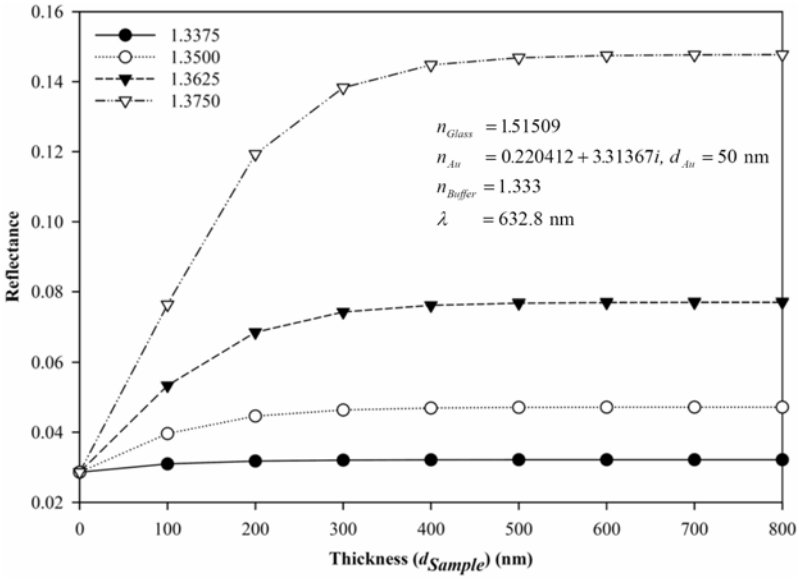

Figure A.10 The effect of d_{Sample} under variable values of refractive index n_{Sample}, are more than n_{Buffer}, on R_{min} according to numerical analysis.

A.2.2.2 Experimental result

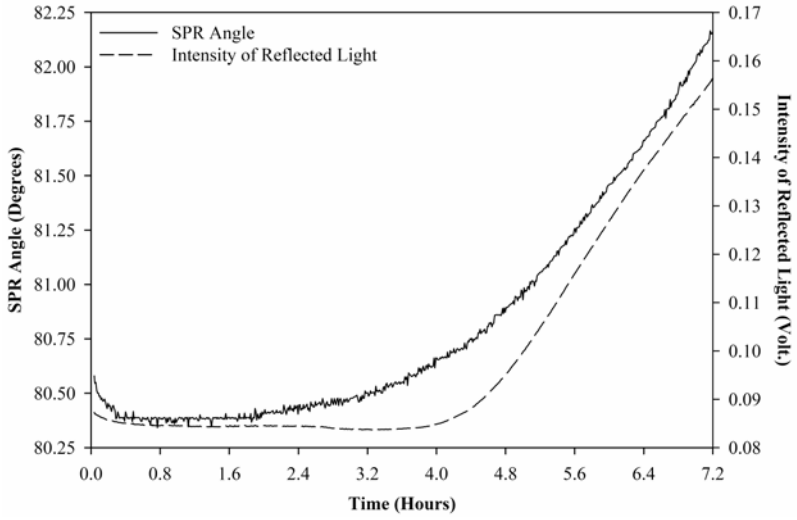

Figure A.11 The process of MUA adsorption.

Figure A.11 depicts the increase of the sample layer thickness (d_{Sample}) as Figure A.9 and A.10. This is possible that the refractive index of MUA is more then the buffer. In the experimental results, the buffer is not the water, but it is the ethanolic solution of 1 mM.

A.2.3 Variation of refractive indices

A.2.3.1 Modeling results

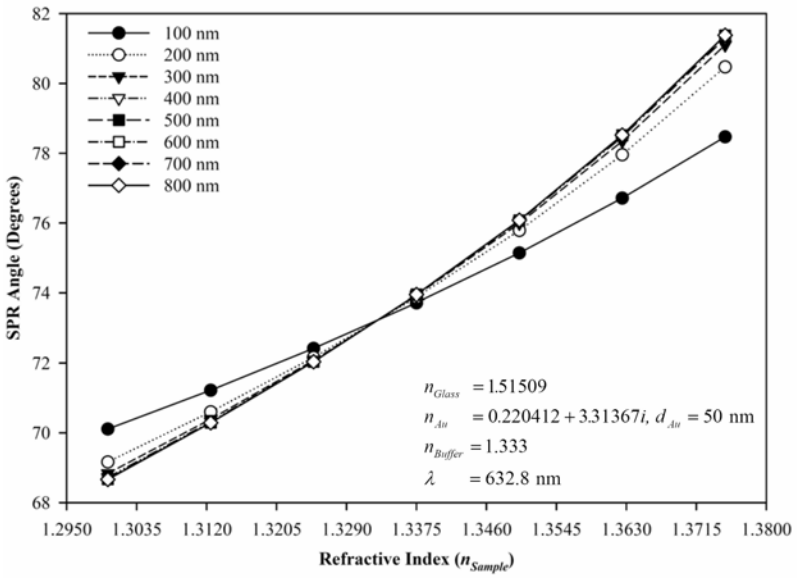

Figure A.12 The effect of n_{Sample} under variable values of the sample thickness d_{Sample} on θ_{SPR} according to numerical analysis.

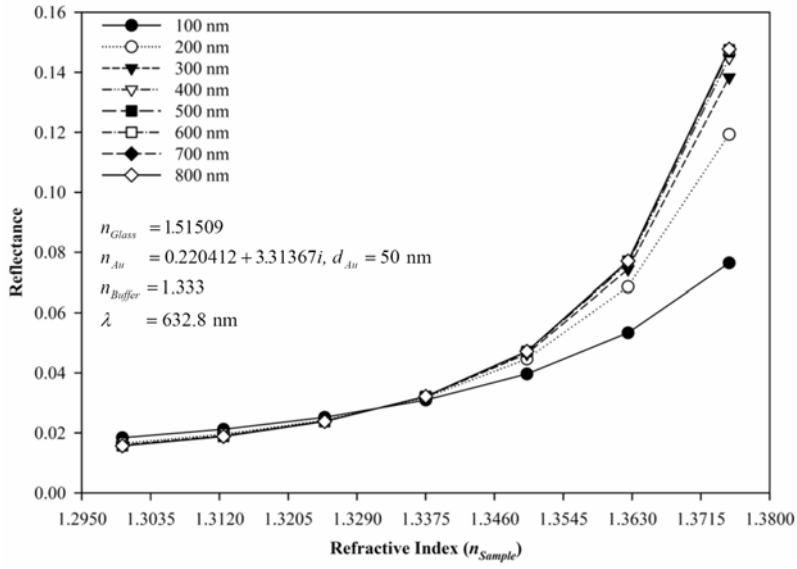

Figure A.13 The effect of n_{Sample} under variable values of the sample thickness d_{Sample} on θ_{SPR} according to numerical analysis.

Table A.2 Values of R_{min} and θ_{SPR} with n_{Sample} under different values of d_{Sample} analyzed by calculation.

d_{Simple} (nm) \ n_{Sample}		1.3000	1.3125	1.3250	1.3375	1.3500	1.3625	1.3750
0	θ_{SPR} (°)	73.2405	73.2405	73.2405	73.2405	73.2405	73.2405	73.2405
	R_{min}	0.0286183	0.0286183	0.0286183	0.0286183	0.0286183	0.0286183	0.0286183
100	θ_{SPR} (°)	70.1092	71.2213	72.4207	73.7217	75.1439	76.7148	78.4707
	R_{min}	0.0183968	0.0212179	0.0251921	0.0309558	0.0396330	0.0533469	0.0764761
200	θ_{SPR} (°)	69.1654	70.6005	72.1624	73.8781	75.7890	77.9588	80.4736
	R_{min}	0.0165104	0.0195550	0.0242414	0.0317732	0.0446325	0.0685722	0.1193050
300	θ_{SPR} (°)	68.8377	70.3920	72.0781	73.9280	75.9918	78.3490	81.1043
	R_{min}	0.0159464	0.0190483	0.0239437	0.0320398	0.0463656	0.0743735	0.1383050
400	θ_{SPR} (°)	68.7236	70.3219	72.0506	73.9439	76.0551	78.4693	81.2977
	R_{min}	0.0157600	0.0188833	0.0238478	0.0321253	0.0469227	0.0762701	0.1447920
500	θ_{SPR} (°)	68.6844	70.2985	72.0416	73.9489	76.0749	78.5065	81.3572
	R_{min}	0.0156972	0.0188288	0.0238167	0.0321525	0.0470984	0.0768653	0.1468410
600	θ_{SPR} (°)	68.6711	70.2907	72.0387	73.9506	76.0811	78.5181	81.3756
	R_{min}	0.0156760	0.0188108	0.0238066	0.0321612	0.0471536	0.0770502	0.1474750
700	θ_{SPR} (°)	68.6666	70.2882	72.0378	73.9511	76.0831	78.5216	81.3813
	R_{min}	0.0156688	0.0188049	0.0238033	0.0321640	0.0471710	0.0771075	0.1476700
800	θ_{SPR} (°)	68.6651	70.2873	72.0375	73.9512	76.0837	78.5228	81.3831
	R_{min}	0.0156664	0.0188029	0.0238022	0.0321649	0.0471764	0.0771252	0.1477300

A.3 Useful of Analysis of Reflectance

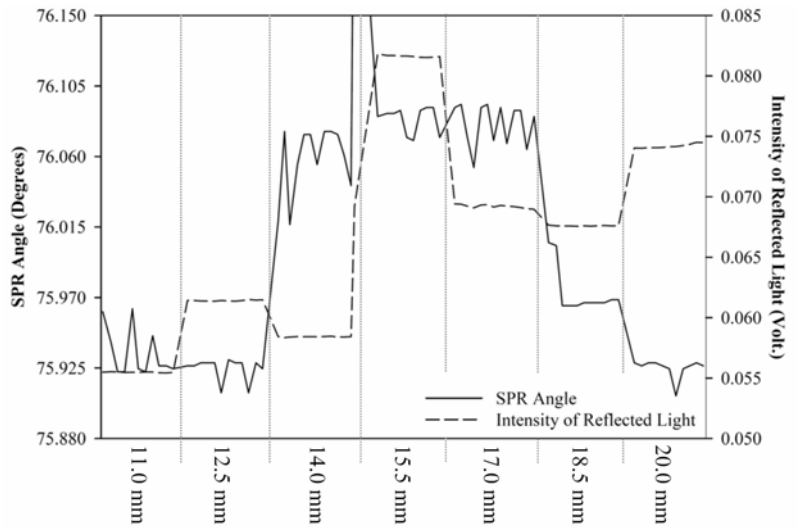

Figure A.14 The variation of detecting area of antigen layer. The intensity of reflected light can present the different in positions of detection, where the SPR angles are not different.

APPENDIX B
SAFTY AND RISK

Ethyl alcohol or Ethanol (EtOH), 99.9% of CH_3CH_2OH, is highly flammable, may be harmful by inhalation and in contact with skin. Keep away from sources of ignition - no smoking, and wear suitable protective clothing and gloves. In case of accident or if you feel unwell, seek medical advice immediately [63].

Diethyl ether (Ether), Et_2O or $(C_2H_5)_2O$, is extremely volatile and flammable, and may form explosive peroxides. It is irritating to the eyes, mucous membranes, and skin. It is also a central nervous system (CNS) depressant with anesthetic effects. It may be harmful by inhalation, ingestion, or skin absorption. Avoid breathing the vapors. Wear appropriate gloves and safely glasses. Always use in a chemical fume hood. Explosive peroxides can form during storage or on exposure to air or direct sunlight. Keep away from heat, sparks, and open flame [7].

11-Mercaptoundecanoic acid (MUA), $C_{11}H_{22}O_2S$, is irritating to eyes, respiratory system and skin. In case of contact with eyes, rinse immediately with plenty of water and seek medical advice. Wear suitable protective clothing [63].

Poly-L-lysine hydrobromide (PLL), do not breathe the dust, and avoids contact with skin and eyes [63].

N-(3-Dimethylaminopropyl)-N′-ethylcarbodiimide hydrochloride (EDC), $C_8H_{17}N_3 \cdot HCl$, is irritating to the mucus membranes and upper respiratory tract. It may be harmful by inhalation, ingestion, or skin absorption [7]. It is risk of serious damage to eyes. In case of contact with eyes, rinse immediately with plenty of water and seek medical advice. Wear suitable protective clothing, gloves and eye/face protection. Handle with care [63].

N-Hydroxysuccinimide (NHS), $C_4H_5NO_3$, is an irritant and may be harmful by inhalation, or skin absorption. Do not breathe the dust, and avoid contact with skin and eyes. Wear appropriate gloves and safety glasses [7].

Ethanolamine (Ethanolamine), C_2H_7NO, is toxic and harmful by inhalation, ingestion, or skin absorption. Handle with care and avoid any contact with the skin. Wear appropriate gloves and goggles. Use in a chemical fume hood. Ethanolamine is highly corrosive and reacts violently with acids [7].

Lens washing solution, is extremely flammable, may be harmful if swallowed. Keep container in a well-ventilated place, and away from sources of ignition - No smoking. Do not empty into drains. Take precautionary measures against static discharges.

APPENDIX C
Fourier Transform Infrared and Nuclear Magnetic Resonance Spectra

C.1 Fourier Transform Infrared (FTIR) Spectra (Condensed Phase)

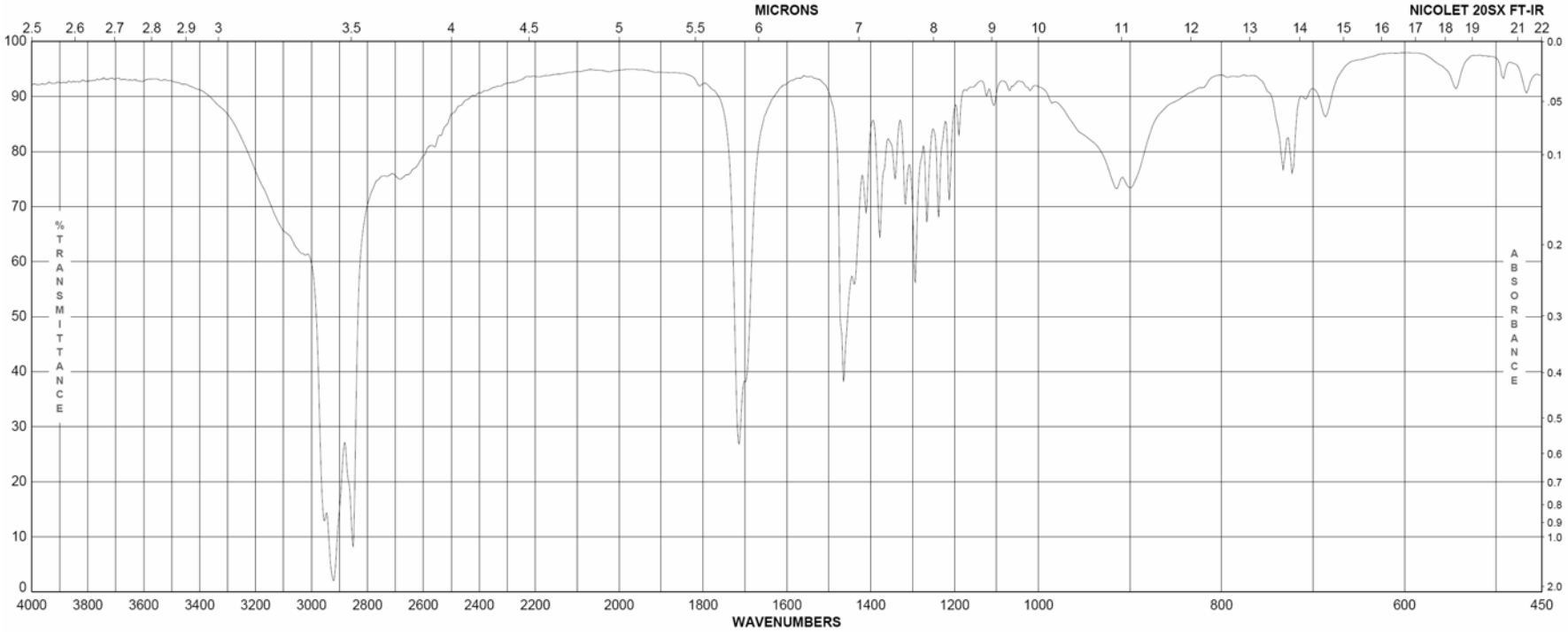

Figure C.1 FTIR spectrum for 11-Mercaptoundecanoic acid (MUA) [63].

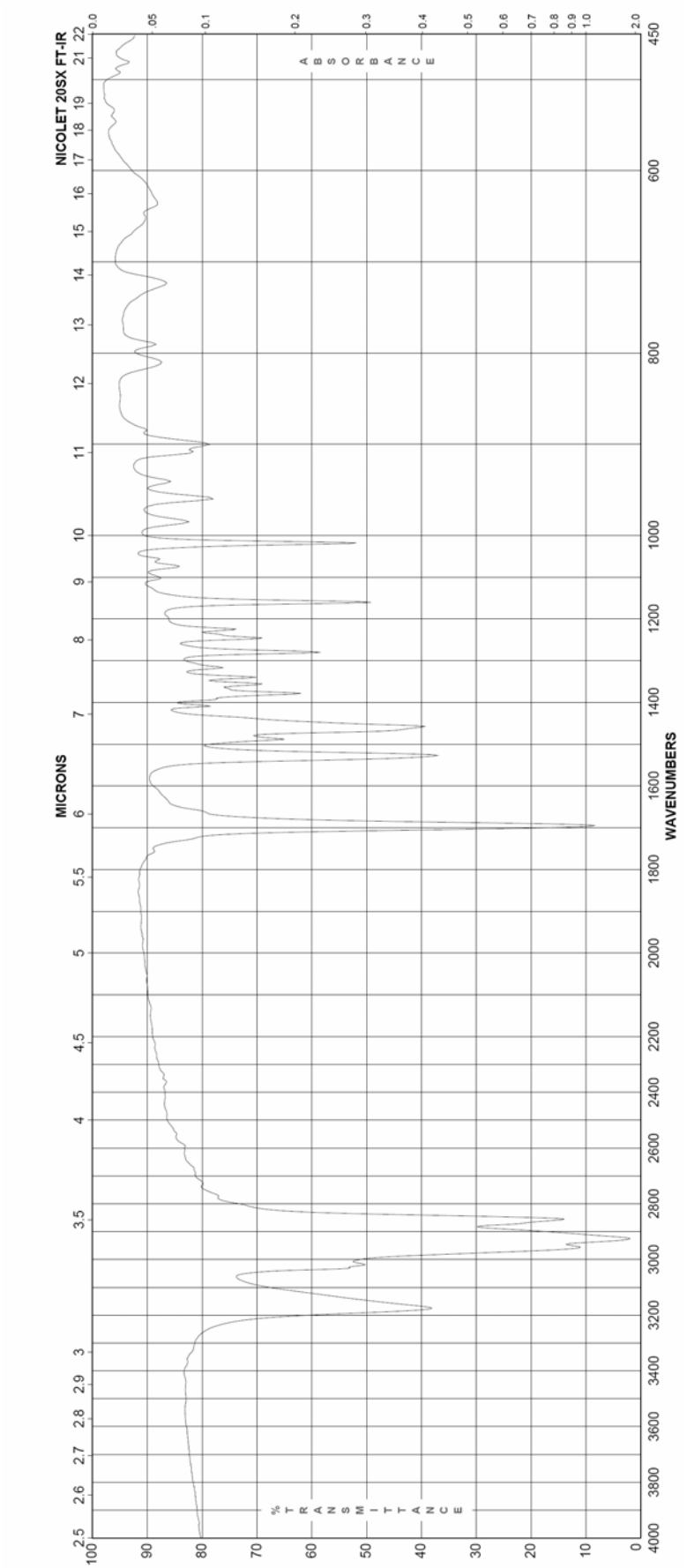

Figure C.2 FTIR spectrum for *N*-(3-Dimethylaminopropyl)-*N'*-ethylcarbodiimide hydrochloride (EDC) [63].

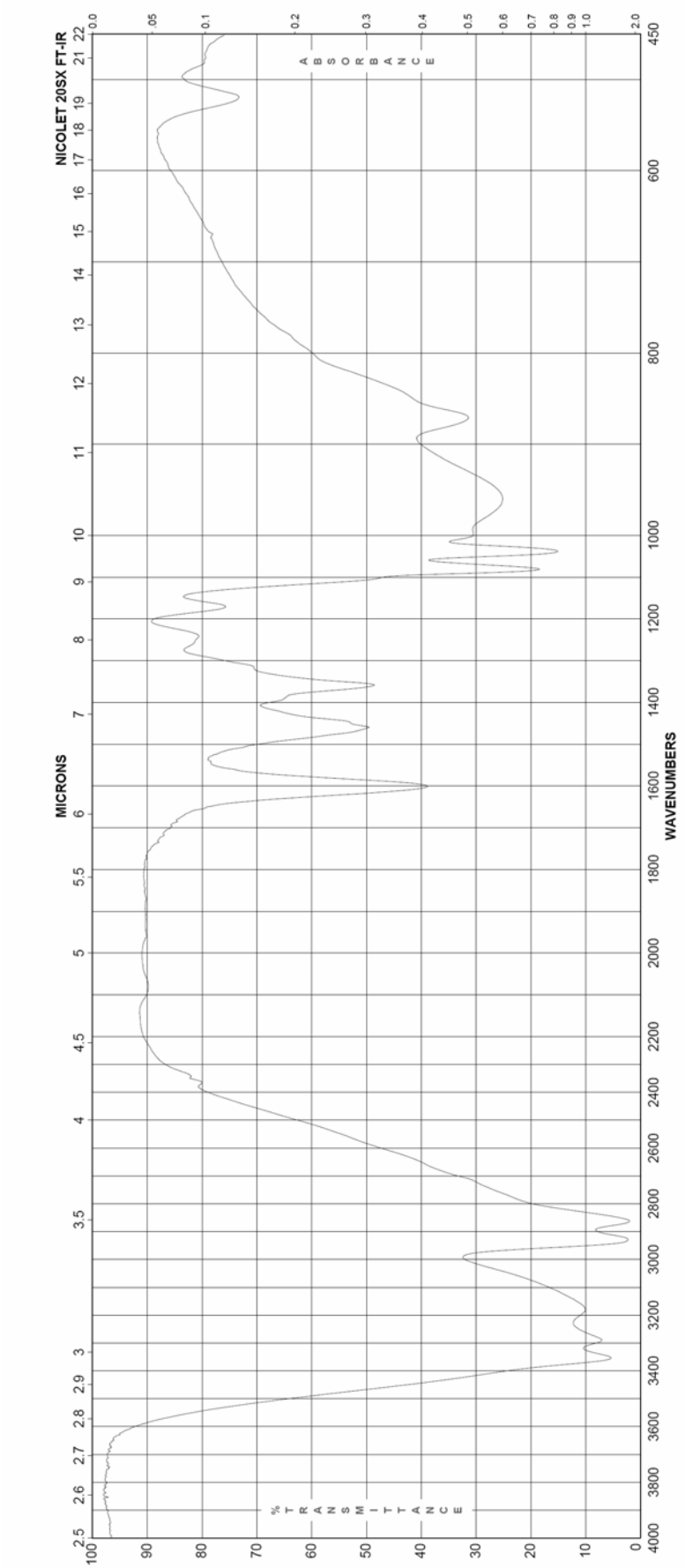

Figure C.3 FTIR spectrum for Ethanolamine [63].

C.2 Fourier Transform Infrared -Raman Spectra

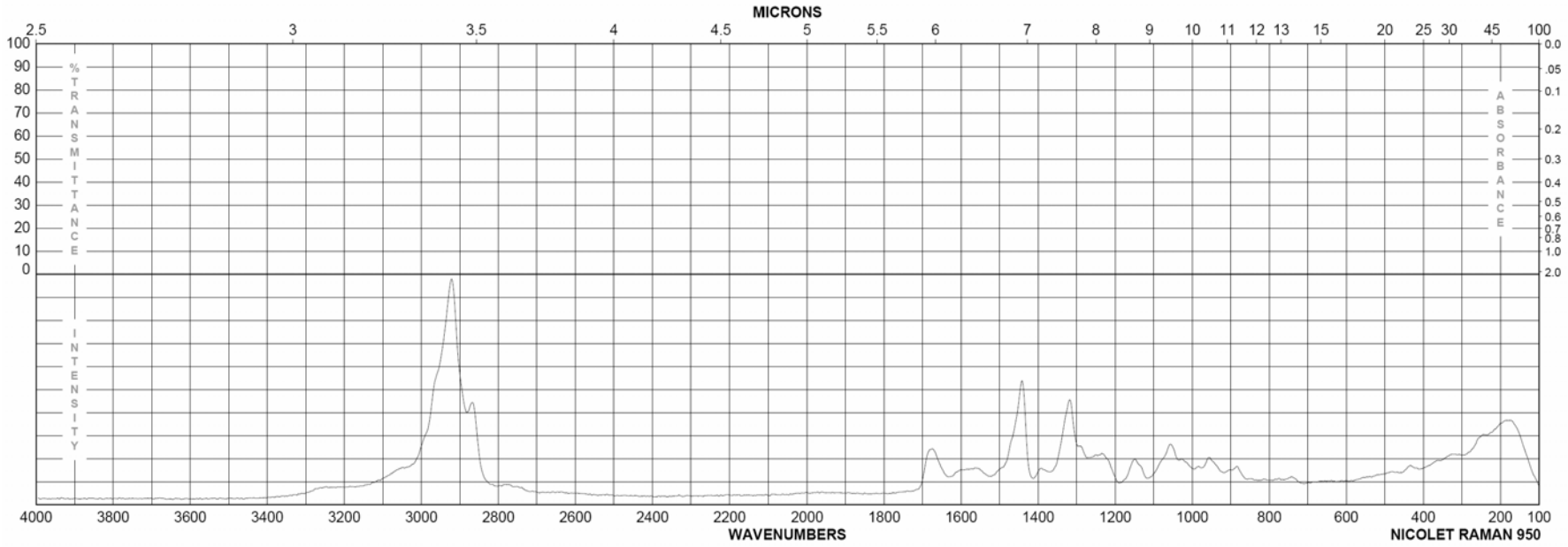

Figure C.4 FTIR-Raman spectrum for Poly-L-lysine hydrobromide (PLL) [63].

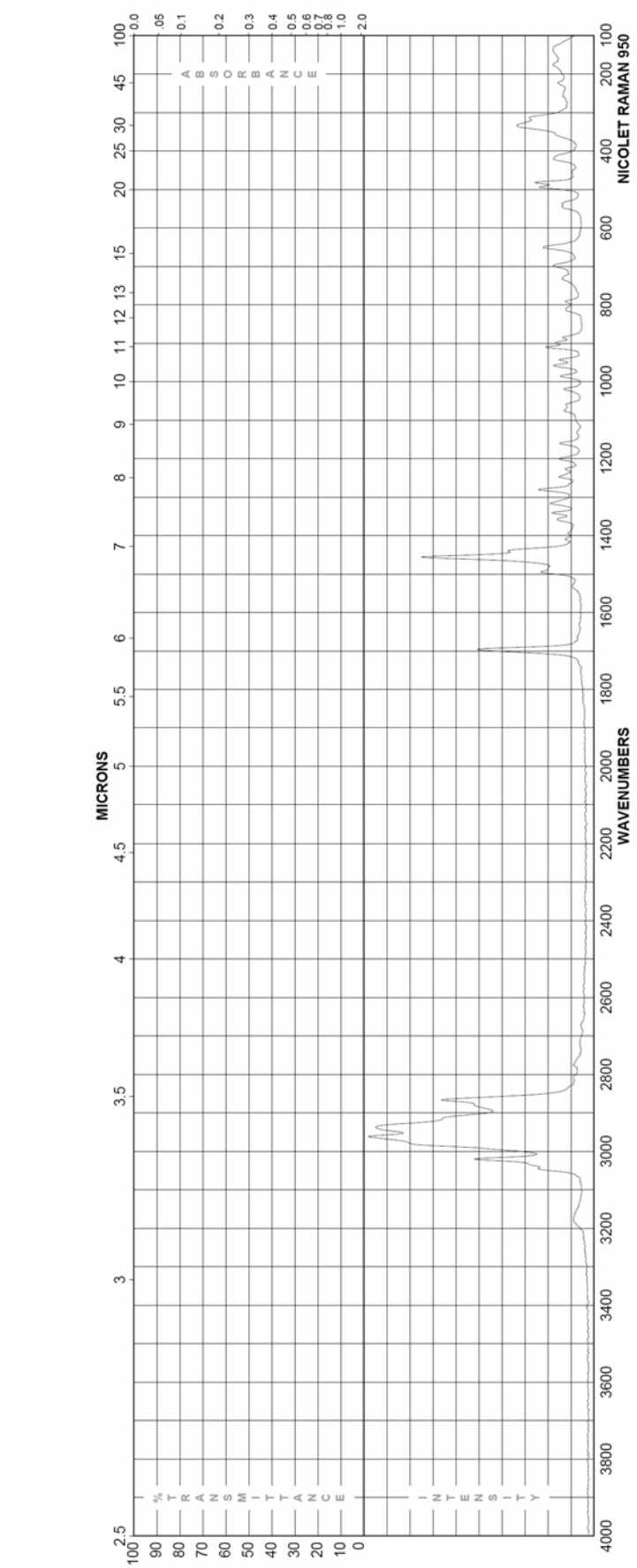

Figure C.5 FTIR-Raman spectrum for *N*-(3-Dimethylaminopropyl)-*N'*-ethylcarbodiimide hydrochloride (EDC) [63].

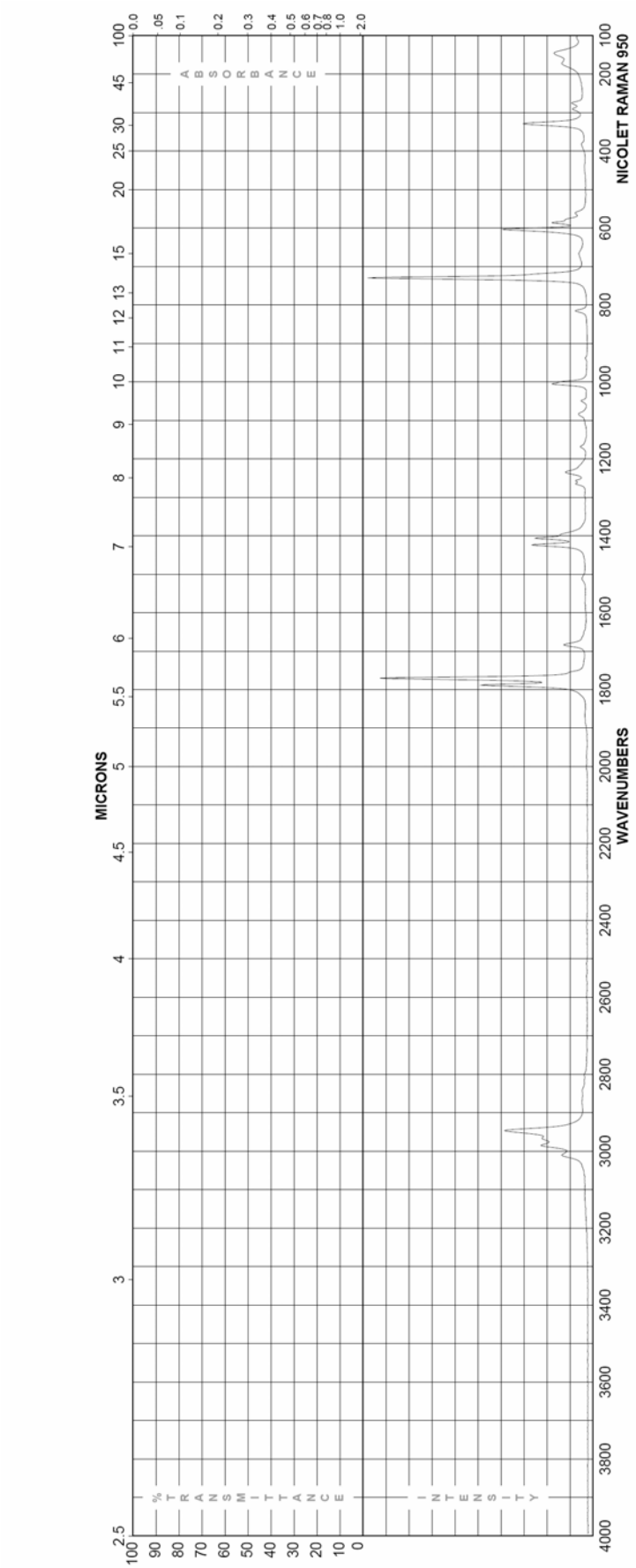

Figure C.6 FTIR-Raman spectrum for *N*-Hydroxysuccinimide (NHS) [63].

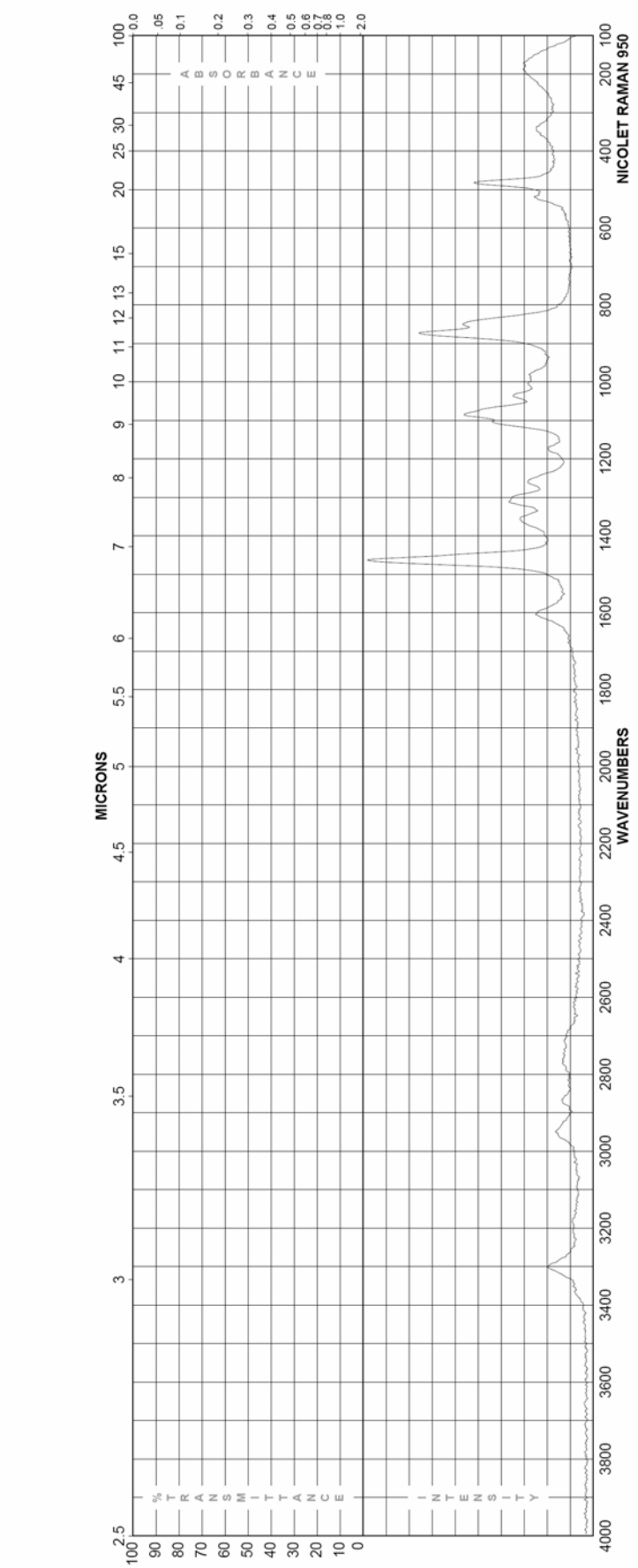

Figure C.7 FTIR-Raman spectrum for Ethanolamine [63].

C.3 Nuclear Magnetic Resonance Spectra

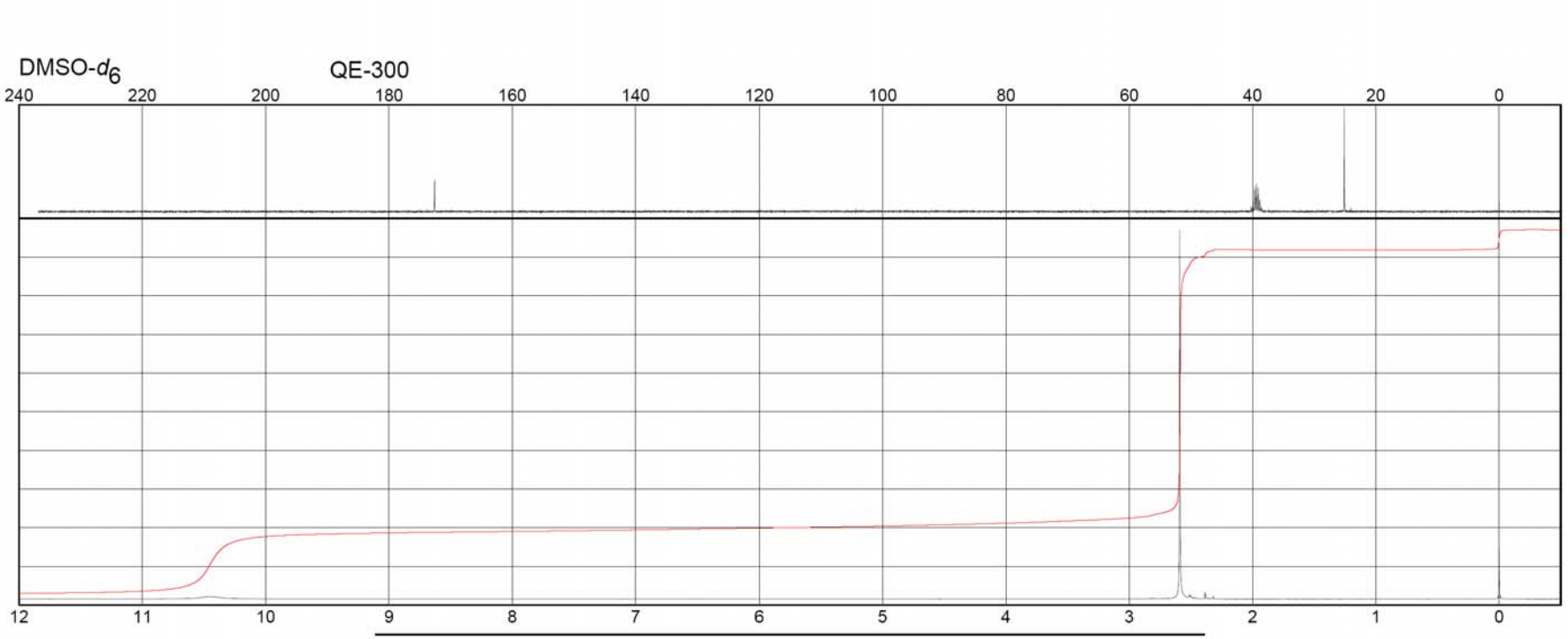

Figure C.8 NMR spectrum for *N*-Hydroxysuccinimide (NHS) [63].

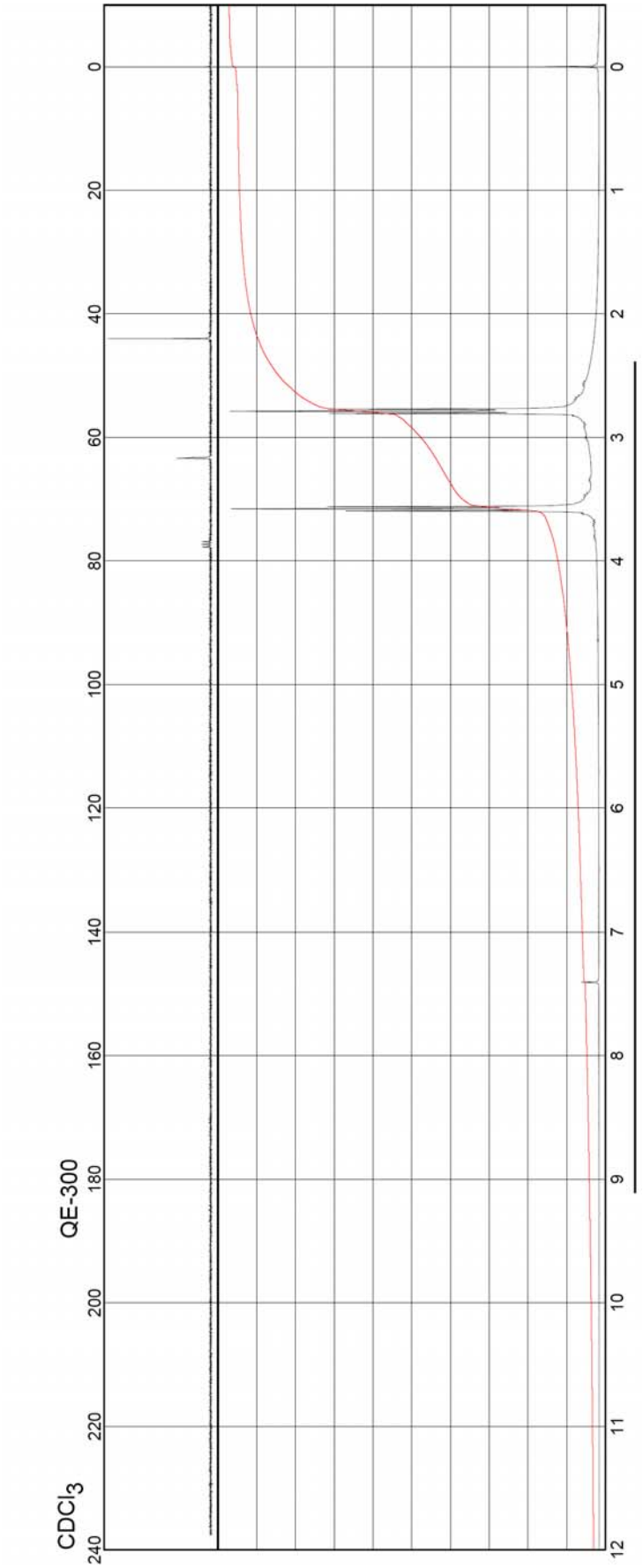

Figure C.9 NMR spectrum for Ethanolamine [63].

BIOGRAPHY

NAME	Mr.Jarupat Disrattakit
DATE OF BIRTH	May 22, 1979
PLACE OF BIRTH	Bangkok, Thailand
INSTITUTIONS ATTENDED	Srinakharinwirot University, 1997-2000: Bachelor of Science (Physics) Mahidol University, 2001-2005: Master of Science (Physics)
RESEARCH GRANT	Recipient of scholarship from the Teaching Assistant Scholarship, 2001-2004